PREDICTION OF ROTOR WAKE INDUCED FLOW ALONG THE ROCKET TRAJECTORIES OF AN ARMY AH-1G HELICOPTER

Anton J. Landgrebe, et al

United Aircraft Research Laboratories

Prepared for:

Picatinny Arsenal

March 1975

The findings in this report are not to be construed as an official Department of the Army Position.

DISPOSITION

Destroy this report when no longer needed. Do not return it to the originator.

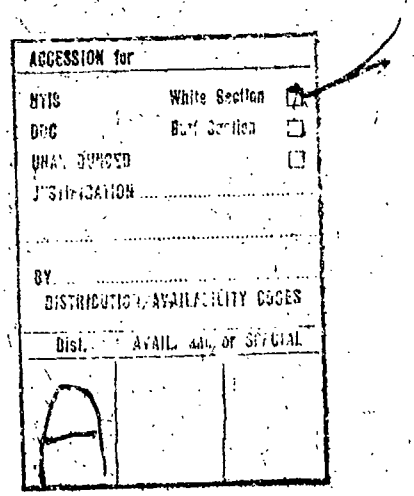

UNCLASSIFIED

SECURITY CLASSIFICATION OF THIS PAGE (When Data Entered)

REPORT DOCUMENTATION PAGE		READ INSTRUCTIONS BEFORE COMPLETING FORM
1. REPORT NUMBER TR 4797	2. GOVT ACCESSION NO.	3. RECIPIENT'S CATALOG NUMBER AD-A007 878
4. TITLE (and Subtitle) PREDICTION OF ROTOR WAKE INDUCED FLOW ALONG THE ROCKET TRAJECTORIES OF AN ARMY AH-1G HELICOPTER		5. TYPE OF REPORT & PERIOD COVERED FINAL REPORT, December 1, through February 1975. 6. PERFORMING ORG. REPORT NUMBER R911810-10
7. AUTHOR(s) Anton J. Landgrebe and T. Alan Egolf		8. CONTRACT OR GRANT NUMBER(s) DAAA21-74-C-0195 AMCMS Code No.4110.16.3643.6
9. PERFORMING ORGANIZATION NAME AND ADDRESS United Aircraft Corporation Research Laboratories 400 Main Street, East Hartford, Conn. 06108		10. PROGRAM ELEMENT, PROJECT, TASK AREA & WORK UNIT NUMBERS
11. CONTROLLING OFFICE NAME AND ADDRESS Picatinny Arsenal Dover, New Jersey 06801		12. REPORT DATE March 1975 13. NUMBER OF PAGES ~~104~~ 102
14. MONITORING AGENCY NAME & ADDRESS (if different from Controlling Office)		15. SECURITY CLASS. (of this report) UNCLASSIFIED 15a. DECLASSIFICATION DOWNGRADING SCHEDULE

16. DISTRIBUTION STATEMENT (of this Report)

Approved for public release; distribution unlimited.

17. DISTRIBUTION STATEMENT (of the abstract entered in Block 20, if different from Report)

18. SUPPLEMENTARY NOTES

19. KEY WORDS (Continue on reverse side if necessary and identify by block number)

Helicopter	2.75 in. Rocket
AH-1G Helicopter	Vortices
Rotor Wake	Induced Velocities
Rocket Trajectories	

20. ABSTRACT (Continue on reverse side if necessary and identify by block number)

An analytical investigation was conducted to predict the rotor wake induced flow velocities along the trajectories of rockets fired from an Army AH-1G helicopter. Three components of both the time-averaged and instantaneous induced velocities were predicted at selected points along the trajectories of rockets fired from four wing locations. Three flight conditions with helicopter flight speeds of 0, 15, and 30 knots were investigated. The sensitivity of the predicted induced velocities to rotor wake model, rocket launch

DD FORM 1 JAN 73 1473 EDITION OF 1 NOV 65 IS OBSOLETE

UNCLASSIFIED

SECURITY CLASSIFICATION OF THIS PAGE (When Data Entered)

20. attitude, and rocket launch position was also investigated. Velocities induced by tip vortices near the intersections of the rocket trajectories with the wake boundary were found to be similar in magnitude to the launch velocity of the 2.75 in. rocket currently in use on the AH-1G aircraft. Values of the downward induced velocity component as high as 70 fps (time-averaged) and 130 fps (instantaneous) were predicted for the hover condition, and the velocities decrease with increasing flight speed. For flight speeds greater than approximately 30 kts, the rotor wake passes behind the rocket launch position which significantly reduces the wake induced effects. The location of the rotor wake boundary relative to the rocket trajectories is a major determinant of the induced velocity distribution along the trajectories. Thus, the use of an accurate wake geometry was found to be important for accurate calculations of the induced velocities at the rockets.

SUMMARY

An analytical investigation was conducted to predict the rotor wake induced flow velocities along the trajectories of rockets fired from an Army AH-1G helicopter. The three components of both the time-averaged and instantaneous induced velocities were predicted at selected points along the trajectories of rockets fired from four wing locations. Three flight conditions with helicopter flight speeds of 0, 15, and 30 knots were investigated. The sensitivity of the predicted induced velocities to rotor wake model, rocket launch attitude, and rocket launch position was also investigated. Velocities induced by tip vortices near the intersections of the rocket trajectories with the wake boundary were found to be similar in magnitude to the launch velocity of the 2.75 in. rocket currently in use on AH-1G aircraft. Values of the downward induced velocity component as high as 70 fps (time-averaged) and 130 fps (instantaneous) were predicted for the hover condition, and the velocities decrease with increasing flight speed. For flight speeds greater than approximately 30 kts, the rotor wake passes behind the rocket launch position which significantly reduces the wake induced effects. The location of the rotor wake boundary relative to the rocket trajectories is a major determinant of the induced velocity distribution along the trajectories. Thus, the use of an accurate wake geometry was found to be important for accurate calculations of the induced velocities at the rocket.

FOREWORD

This investigation was sponsored by the U. S. Army Picatinny Arsenal, Dover, New Jersey under Contract DAAA21-74-C-0195. Efforts under this contract were initiated in December, 1973, and completed in February 1975. The Army technical representative for this contract was Mr. Saul Wasserman of the Rocket Assisted Projectile and Pyrotechnics Branch, Picatinny Arsenal. The intercommunication provided by Mr. Wasserman and Mr. Robert W. Bergman of the Army 2.75 in. Rocket Project Managers Office is gratefully acknowledged. The assistance provided by Mr. J. R. Johnson of the Bell Helicopter Company in providing the AH-1G flight condition information is also gratefully acknowledged. Direct supervision of this contract was conducted by the co-author, Mr. Anton J. Landgrebe, Supervisor, Rotary Wing Technology, United Aircraft Research Laboratories. Mr. Marvin C. Cheney, Chief of Aerodynamics, United Aircraft Research Laboratories was cognizant manager for the project.

TABLE OF CONTENTS

LIST OF ILLUSTRATIONS

LIST OF SYMBOLS

a_{1_s}	1st harmonic longitudinal flapping, positive flap up at 180 deg azimuth, deg
A_{1_s}	lateral cyclic pitch, positive pitch up at 180 deg azimuth, deg
b_{1_s}	1st harmonic lateral flapping, positive flap up at 270 deg azimuth, deg
B_{1_s}	longitudinal cyclic pitch, positive pitch up at 270 deg azimuth, deg
C_T	rotor thrust coefficient, rotor thrust/$\rho\pi R^2(\Omega R)^2$
R	rotor radius, ft
V	forward flight velocity, fps
v_i	induced velocity at a point on the blade, fps
$\bar{v}_i$	momentum induced velocity, positive upflow, fps
v_{x_T}, v_{y_T}, v_{z_T}	instantaneous induced velocity components in rocket trajectory coordinate system (x_T, y_T, z_T); sign convention is consistant with coordinate definition, fps
$v_{x_T}{}_{AVG}$, $v_{y_T}{}_{AVG}$, $v_{z_T}{}_{AVG}$	time averaged induced velocity components in rocket trajectory coordinate system (x_T, y_T, z_T); same sign convention as v_{x_T}, v_{y_T}, v_{z_T}, fps
x, y, z	hub centered axis system coordinates nondimensionalized by R, x-y plane parallel to rotor tip path plane, right handed coordinate system with positive x downstream (see Fig. 6)
x_T, y_T, z_T	rocket trajectory axis system coordinates nondimensionalized by R, centered at intersection of axis of rocket launch positions and fuselage centerline, left handed coordinate system with positive x_T in direction of rocket travel (see Fig. 1)
$\bar{y}_T$	y_T coordinate nondimensionalized by fuselage width instead of rotor radius

α_s	rotor shaft angle, angle between shaft axis and normal to V, positive nose up, deg or rad
α_{TPP}	rotor tip path plane angle, angle between rotor tip path plane and V, positive nose up, deg or rad
Γ	circulation strength of a vortex filament, ft^2/sec
θ	rocket launch attitude, positive nose up, mil
θ_o	blade collective pitch, positive pitch up, deg
μ	rotor advance ratio, component of V parallel to rotor tip path plane nondimensionalized by rotor tip speed $(V\cos\alpha_{TPP}/\Omega R)$
ρ	air density, lb/ft^3
χ	wake skew angle: angle between normal to rotor disc and wake boundary, deg or rad
ψ	blade azimuth angle measured from x axis (see Fig. 1), positive in the direction of rotation, deg or rad
Ω	rotor rotational frequency, rad/sec

INTRODUCTION

The accurate determination of the flow field around a helicopter is required when the helicopter is used as a weapons platform. Since a free-flight projectile such as a rocket, when fired from a helicopter, may initially be travelling at a speed which is of the same order of magnitude as the flow velocities, the flow field induced by the rotor wake system can have a significant effect on the rocket trajectory. This may necessitate some form of aiming compensation or special firing techniques -- particularly at the low helicopter flight speeds at which rockets are to be fired in accordance with current Army tactical concepts.

For many years the United Aircraft Research Laboratories have been engaged in analytical and experimental studies pertaining to the determination of helicopter rotor/wake flow velocities. Several of these studies, which include both the measurement and prediction of rotor wake geometries and associated induced velocities are described in References 1 through 10. References 1 through 3 represent previous efforts in this field which were supported by the Dept. of the Army and contain information which is particularly pertinent to any study of the flow environment of a helicopter when hovering or flying at low speeds. Most of the analytical methods described in these references have placed emphasis on the flow field at the rotor disc. However, with certain recognized assumptions, the methods are applicable to predicting the flow field anywhere in the vicinity of the helicopter. Refinements to the analysis, such as the provision for transient conditions (e.g., simulated gusts), inclusion of the fuselage influence, and improvements in the far wake model are currently in progress.

To assess the influence of the rotor/wake flow field on the flight path of a 2.75 inch rocket fired from the Army AH-1G helicopter when hovering or flying at low forward speeds, available UARL analyses were used to predict the induced flow velocities along the rocket trajectories. Existing UARL computer analyses which have the capability to calculate the deformed tip vortex geometry and rotor wake induced velocities was modified to calculate the flow velocities along the near rocket trajectories corresponding to rockets mounted at four wing locations. The analyses were applied to predict the time-varying (instantaneous) and time-averaged velocities for helicopter flight speeds of 0, 15, and 30 knots. A brief sensitivity study was conducted to show the sensitivity of the predicted flow velocities to variations in wake geometry, rocket launch attitude, and rocket mount location. The induced velocity results from this investigation are intended for use in Army trajectory analyses to assess the influence of the aerodynamic interference of the rotor wake on rocket trajectories.

Included in this report are (1) a brief description of the computer analyses used and inherent assumptions, (2) a description of the flight conditions, aircraft configuration and wake models used in the analyses, (3) presentation and discussion of the induced velocity results for the three flight conditions, (4) a discussion of areas for further consideration, and (5) suggested procedures for applying the induced velocity results in rocket trajectory calculations.

BRIEF DESCRIPTION OF THEORETICAL METHODS

Theoretical methods developed at the United Aircraft Research Laboratories in recent years were used during the course of this investigation. The following brief description of the theoretical methods is presented to acquaint the reader with the analyses used. More detailed information on the contents, assumptions and results of the methods is contained in Refs. 1 through 8.

The basic components of the UARL Rotor Analysis are shown in Fig. 2. Since the objective of this study was to compute induced velocities rather than rotor airloads and stresses, the UARL blade response analysis was not used and blade motions and control settings from a teetering rotor analysis were provided by the Bell Helicopter Company. A brief description of each of the other component methods making up the UARL Rotor Analysis follows.

INDUCED VELOCITY AND CIRCULATION ANALYSIS

The UARL Prescribed Wake Rotor Inflow Analysis (Deck F389) is described in Refs. 3 and 4. The function of this program is to compute the rotor time varying circulation and inflow distribution that is compatible with a prescribed set of blade section operating conditions and a prescribed wake geometry. In its simplest form the analysis generally represents an extension of the rotary-wing equivalent of the classical lifting line approach used successfully for fixed wings. Each blade is represented by a segmented lifting line, and the wake is represented by a finite number of segmented vortex filaments trailing from the blade segment boundaries. The fundamental relations of blade circulation to lift coefficient, angle of attack, blade motions, control settings, induced velocity, and wake geometry are used in this analysis. The circulation equations represent a matrix of terms, the number of which equals the square of the number of points on the rotor disc (number of azimuth positions x number of radial stations). Once the circulations are computed, the velocities induced at and away (e.g., at rocket trajectories) from the rotor disc by the bound and trailing vorticity of the rotor can be determined through application of the Biot-Savart law which can be expressed simply in the following form:

$$v_i = f\ (\Gamma,\ \text{Wake Geometry})$$

$$= \frac{1}{4\pi R} \Sigma\ (\Gamma)\ (GC) \qquad (1)$$

Here the induced velocity at a point on the blade, v_i, is a function of the circulations, Γ, and wake geometry, and is proportional to the summation of the products of the circulation strength, Γ, and the geometric influence coefficient, GC, of each element of vorticity in the rotor-wake system. The geometric coefficient is related only to the geometry between a wake element and the point at which the

induced velocity is being computed. Since the wake geometry is prescribed, the wake may vary from an undistorted wake model to a complex experimental or distorted analytical wake model with tip vortex roll-up and vortex core effects mathematically modeled.

WAKE GEOMETRY ANALYSIS

The Rotor Inflow Analysis requires that the rotor wake geometry be specified in order for circulations and induced velocities to be determined. There are several alternatives for rotor wake geometry. The least complex is a classical undistorted wake which is simply a function of the flight condition and momentum inflow velocity. The coordinates of this helical wake, which is skewed in forward flight, are easily generated in a prescribed wake type of analysis given the governing parameters which can be iterated on if desired. If analytical, realistic distorted wake geometries require more complex and operationally expensive computer analyses. Appropriate experimental wake data is certainly most desirable, but, except for hover, is not currently available for most rotor configurations and forward flight conditions. It has been established that the requirement for distortions from the classical type wake geometry is dependent on the rotorcraft configuration, flight condition, parameter of interest and accuracy required. For example, an undistorted wake geometry is generally sufficiently accurate for integrated performance calculations (thrust, torque, etc.) for conventional rotorcraft operating in high speed flight. However, for hover and low speed conditions wake distortions are very significant. Either an undistorted or distorted wake geometry may be used in the Rotor Inflow Analysis. Distorted wake geometry may be from analytical or experimental sources.

Undistorted Wake

In its simplest form, the wake from each blade can be assumed to be a classical undistorted skewed helical sheet of vorticity defined from momentum considerations (hereafter referred to as the undistorted wake). Sample undistorted wake representations are shown in Figs. 3 and 4 for hovering and forward flight conditions, respectively. In Fig. 4a, a sample computer plot of the undistorted wake (AH-1G 30 kt condition) is presented. All vortex filaments are shown*. In Fig. 4b, only the tip vortex filament is presented. The coordinates of the undistorted wake representation are obtained from the rotor advance ratio, μ, thrust coefficient, C_T, and angle of attack relative to the tip-path-plane, α_{TPP}. For example, the top view of the tip vortex filaments in Fig. 4b is obtained directly from the helicoidal path of the blade tip as it translates at the velocity $V\cos\alpha_{TPP}$ and rotates at the velocity ΩR. The side view is dependent on the wake skew angle, χ (angle between normal to the rotor disc and wake boundary), which is defined in the following manner:

---

* As used for this study, the five outboard filaments were not separate as shown, but combined at 15 deg behind each blade to simulate each rolled up tip vortex.

$$\tan \chi = \frac{\text{ROTOR FORWARD VELOCITY COMPONENT IN PLANE OF ROTOR DISC}}{\text{MEAN ROTOR INFLOW VELOCITY NORMAL TO ROTOR DISC}}$$

or (2)

$$\chi = \tan^{-1} \left\{ - \frac{V \cos \alpha_{TPP}}{V \sin \alpha_{TPP} - v_i} \right\}$$

Distorted Wake

To eliminate the necessity for prescribing an undistorted wake goemetry, an analytical method for computing more realistic wake geometries was developed at UARL. The basic approach of this method, entitled the UARL Rotor Wake Geometry Analysis (UARL Deck F506), involves the following. First, an undistorted wake model is defined along with the distribution of circulation strengths of the various vortex elements comprising the wake. The classical Biot-Savart law is then applied to determine the velocities induced by each vortex wake element at numerous points in the wake. These distorting velocities are then numerically integrated over a small time increment to obtain new wake element positions. The process of alternately computing new velocities and positions is continued until a converged, periodic distorted wake geometry is attained. Further details of the procedures used to compute wake geometries and results are given in Refs. 1 through 4. Sample computer plots of the distorted tip vortex geometry (AH-1G at 30 kt) are presented in Fig. 5. The inboard wake filaments are not shown for clarity.

For hovering conditions, systematic model rotor wake geometry data have been acquired experimentally at UARL. The data have been generalized in Ref. 1 to facilitate the rapid estimation of wake geometry for a wide range of rotor designs and operating conditions and have been used to accurately predict the hover performance for a wide range of full-scale helicopters. A special computer subroutine has been prepared to model the hovering rotor wake in accordance with the generalized data. A comparison of the experimental hovering wake representation with the undistorted wake representation is presented in Fig. 3.

It will be mentioned that, for this investigation, the wake geometry analysis was used to generate wakes for the forward flight conditions, and the generalized experimental wake geometry was used for the hover condition.

DESCRIPTION OF FLIGHT CONDITIONS AND AIRCRAFT CONFIGURATION USED IN THE ANALYSES

Induced velocities were calculated for the Army AH-1G helicopter, commonly referred to as the Cobra. A schematic of the AH-1G helicopter is shown in Fig. 1. The teetering type rotor of this helicopter has a radius of 22 ft. Each of its two blades has a nominal chord of 2.25 ft, a linear twist of -10 deg, a modified 0009 airfoil section, and a preconing of 2.75 deg.

The calculations were performed for a helicopter gross weight of 9500 lbs and a center-of-gravity position at 198.5 in. from the nose of the aircraft. Three flight conditions were investigated corresponding to flight speeds of 0 (hover), 15, and 30 kts. Considering the rotor tip speed of 746 fps, these flight speeds result in rotor advance ratios, μ, of 0, 0.034, and 0.068, respectively. The respective rotor control, flapping, and disc angles used in the analyses are listed below in Table I:

Table I: ROTOR CONTROL, FLAPPING, AND DISC ANGLES

	Flight Speed, kts		
	0	15	30
Collective Pitch, θ_o, deg	16.2	15.6	14.6
Lateral Cyclic Pitch, A_{1_s}, deg	-2.0	-2.4	-2.4
Longitudinal Cyclic Pitch, B_{1_s}, deg	1.4	1.5	1.6
1st Harmonic Longitudinal Flapping, a_{1_s}, deg	-1.3	-0.9	-0.5
1st Harmonic Lateral Flapping, b_{1_s}, deg	-1.9	-0.9	-0.1
Rotor Shaft Angle, α_s, deg	1.5	0.9	0.1
Rotor Tip Path Plane Angle, α_{TPP}, deg	0.2	0.0	-0.4

Due to the unavailability of accurate measured flight test angles, the above values were calculated by the Bell Helicopter Company using the C-81 Rotorcraft Performance Analysis.

Induced velocity calculations were performed for the four rockets mounted at the following locations relative to the center of the rotor hub and parallel or normal to the fuselage waterline (see Table II and Fig. 1):

Table II. ROCKET LOCATIONS

		ROCKET 1	ROCKET 2	ROCKET 3	ROCKET 4
Distance Below the Rotor Hub:	in. -	103	103	103	103
	÷ R -	0.39	0.39	0.39	0.39
Lateral Distance From Rotor Hub:	in. -	-59	-42.5	42.5	59
	÷ R -	-0.22	-0.16	0.16	0.22
Distance Forward of Rotor Hub:	in. -	9	9	9	9
	÷ R -	0.034	0.034	0.034	0.034

The rocket launch attitudes were all specified at an elevation of 126 mils (7 degrees) relative to the fuselage waterline except in a sensitivity study where 160 and 195 mils were used. It is noted that each rocket was assumed to be concentrated at a point (center-of-gravity) when determining the launch point. Induced velocities were calculated at increments of 0.1 R along the rocket trajectories from the launch point. The trajectories from the launch point to a distance of one rotor diameter (extent of calculation) were assumed to be straight lines. The coordinate system (x_T, y_T, z_T) used for the predicted induced velocities is referenced to the rocket launch point and the axes are parallel and normal to the rocket trajectories as shown in Fig. 1. Positive directions are also shown in Fig. 1.

DESCRIPTION OF WAKE GEOMETRIES USED IN THE ANALYSES

The wake representation used in the analyses consisted of 10 finite vortex filaments trailing from each blade. These vortex filaments were divided into straight vortex elements at azimuth intervals corresponding to 15 degrees of blade rotation. The extent of the filament geometry was prescribed by 6 wake revolutions from the rotor except for the hover condition for which it was 8 revolutions. This resulted in wake truncation at a sufficiently far distance to be insignificant for velocities at the rocket trajectory. The five outer vortex filaments which emanated from the outer 20 percent of the blade were combined beyond a 75 degree azimuth distance from the blade to simulate the roll-up of the tip vortex. Both undistorted and distorted wake models, described previously, were used to show the sensitivity of the results to wake geometry. For the undistorted vortex filaments, the vortex elements were positioned in a direction normal to the rotor disc in accordance with the mean induced velocity as determined from momentum theory at the rotor disc. The values of this momentum induced velocity for the 0, 15, and 30 kt flight conditions are -36.3, -31.6, and -22.9 fps, respectively. These values when used in equation (2) in combination with the rotor thrust coefficient, advance ratio, tip speed, and tip path plane angle, result in wake skew angles, χ, of 0, 39, and 65 degrees.

The undistorted and distorted tip vortex geometries for the 0, 15, and 30 kt conditions are presented in Figs. 6 through 11. For the hover condition, the entire distorted wake model was obtained from the generalized wake equations of Ref. 1. Thus for the hover condition, both the inboard wake (inboard vortex sheets) and the tip vortex geometry are based on experimental data. Due to the current lack of generalized experimental wake geometry data for forward flight, the distorted tip vortex geometry for the 15 and 30 kt conditions was calculated using the UARL Rotor Wake Geometry Analysis. It is noted that only distortions of the tip vortices were calculated for the two forward flight conditions and an undistorted inboard wake model was assumed. Although it is physically inaccurate and compromises the results somewhat, the latter assumption may be justified considering the relatively higher circulation strength of the rolled up tip vortices compared to that of the inboard vortex filaments.

The primary difference between the undistorted and distorted wakes (Figs. 6 and 7) for the hover conditions is the wake contraction. In addition, as shown in Fig. 3, the inboard wake is transported downward with a nonuniform radially varying axial velocity which causes the outer portion to travel faster than the inner portion. At 15 kts, the tip vortex distortions (Fig. 9) result in a contraction of the forward boundary of the wake relative to the undistorted wake boundary (Fig. 8). A similar contraction occurs at 30 kts (Figs. 10 and 11). This contraction of the wake has a predominant effect on the induced velocity distribution along the rocket trajectories in that it moves the intersection point of each trajectory with the wake boundary rearward, and thus decreases the duration of time that the rocket is inside the rotor wake. The contraction will be shown to be particularly significant for the 30 kt condition.

DISCUSSION OF INDUCED VELOCITY RESULTS

The three components of induced velocity, v_{x_T}, v_{y_T}, and v_{z_T}, were calculated along each rocket trajectory at points corresponding to an interval in x_T of 0.1 R. The calculations were performed from the rocket launch point to a point on each trajectory 2.0 R from the launch point. Thus, velocities were computed at 21 field points for each trajectory. The four rockets and their trajectories were numbered in order, 1 through 4, as shown in Fig. 1.

Since the orientation of the rotor blades and wake relative to a point on a rocket trajectory varies with time, the instantaneous velocity components induced at that point also vary with time. Since steady flight conditions were selected for this investigation, the positions of the blade and wake and the resulting velocities are periodic. The period is the time corresponding to the blade passage interval, which for the 2-bladed AH-1G rotor is the time required for a blade to travel 180 degrees. Thus, time was expressed in terms of increments of rotor rotation designated by rotor position and the corresponding azimuth angles of the two blades. The calculations were performed using an azimuth increment of 15 degrees, which resulted in 12 rotor positions per blade passage interval*. In addition to the instantaneous velocities at each rotor position, the time-averaged velocities were calculated.

The major variables for this investigation and the notation to be used for the plotted results are summarized below in Table III:

Table III. MAJOR VARIABLES

Flight Conditions	V = 0, 15, 30 kt
Wake Models	Distorted, Undistorted
Instantaneous Velocity Components	v_{x_T}, v_{y_T}, v_{z_T}
Time-Averaged Velocity Components	$v_{x_{T_{AVG}}}$, $v_{y_{T_{AVG}}}$, $v_{z_{T_{AVG}}}$
Rotor Positions (Time Step)	1, 2, 3, ..., 12
Blade Azimuths, ψ, deg	0,180; 15,195; 30,210; ... 165,345
Rocket Number	1, 2, 3, 4
Rocket Lateral Position	y_T = -0.2235, -0.161, 0.161, 0.2235
Position Along Rocket Trajectory	x_T = 0, 0.1, 0.2, ..., 2.0

* Using the AH-1G rotor tip speed of 746 fps and the rotor radius of 22 ft, the time interval corresponding to 15 degrees of blade azimuth travel is 0.0077 seconds. For a rocket velocity of 100 fps, the time interval corresponding to an interval in x_T of one rotor radius is 0.22 seconds. At the speed of 100 fps, a rocket travels a distance of 0.42 R during a blade passage interval (one-half rotor revolution), and it takes the time corresponding to 1.19 rotor revolutions (429 degrees) to travel a distance of one rotor radius.

In addition to all combinations of these variables, a few computer cases were run to investigate the sensitivity of the results to rocket launch attitude and launch position. That is, for the hover condition, rocket launch attitude relative to the fuselage waterline was varied in 2 degree increments from the reference 7 degrees (126 mils elevation) to 9 and 11 degrees (160 mils and 195 mils). For the 30 kt condition, a variation of rocket launch position of 0.05 R in the x and z directions was investigated.

In total, six base cases (3 flight conditions x 2 wake models) plus three sensitivity variations were run. Considering the 3 velocity components, 4 rockets, 21 rocket trajectory points and the 12 rotor positions plus the time-average velocities, a total of 3276 velocity values were computed for each of the 9 cases. Tabulations of these values have been provided separately to the Army. Since inclusion of plots of all these results was beyond the scope of this effort, a judicious selection was made of combinations of variables for which data are to be presented. In this selection, emphasis was placed on the results based on the more realistic distorted wake model over those of the undistorted wake. The v_{z_T} velocity component was emphasized over the v_{x_T} and v_{y_T} components because the magnitude of the v_{z_T} velocity is generally significantly greater. Rocket number 4 was arbitrarily selected for emphasis. It will be shown that rocket lateral position is generally the least significant variable. For consistency, rotor positions 1, 4, 7, and 10 corresponding to reference blade azimuths of 0, 45, 90, and 135 degrees were selected. Where the selection of specific points along the rocket trajectory were required, points 1 ($x_T = 0.0$), 21 ($x_T = 2.0$) and points in the immediate vicinity of the wake boundary were generally selected.

The following results are grouped by flight condition and presented in order of flight speed -- 0, 15, and then 30 kt. Results based on both distorted and undistorted wake models are presented for each flight condition. Following these results, the results showing the sensitivity of the induced velocities to variations in rotor launch attitude and position are presented.

HOVER CONDITION (V = 0)

The variation of the time-averaged v_{z_T} velocity along the rocket trajectories of all four rockets, based on the distorted wake model, is presented in Fig. 12. This velocity component normal to each trajectory, increases from approximately 30 to 70 fps (downward) going from the rocket launch position ($x_T = 0$) to the intersection of each trajectory with the wake boundary shown in the top view in Fig. 7 (e.g., at $x_T = 0.77$ for rocket 4). This increase is consistent with the fact that the rocket launch position is near the center of the wake in hover, and the wake vertical transport velocity has been observed experimentally to increase with increasing radial position (Ref. 1). It is interesting that the mean induced velocity as the rocket passes through the wake is approximately the 50 fps used by the Army in previous calculations of the rocket trajectory. Moving from inside to outside of the wake boundary an abrupt change in velocity occurs in both magnitude and direction (downflow to upflow). The upflow is not as severe as the downflow because the contributions of the tip vortices and the inboard wake are opposing

outside of the wake, whereas they are additive just inside the wake. As the rocket moves away from the wake, the velocity decreases as expected, and at 2.0 R from the launch point the upward velocity is less than 2 fps. It is also shown in Fig. 12 that the influence of the different lateral positions of the four rocket trajectories on this average velocity component is small.

In Fig. 13, the instantaneous v_{z_T} velocity component is presented for the four rocket trajectories and rotor position 1 where the blades are positioned at 0 and 180 degrees. These instantaneous velocity results are similar to the averaged values of Fig. 12 (generally within ±5 fps) except near the wake boundary. Near the wake boundary the instantaneous velocities vary significantly with rotor position as shown in Fig. 14 for rocket 4 and four selected rotor positions at azimuth increments of 45 degrees. This time variation is clearly shown in Fig. 15 where the v_{z_T} velocity is plotted versus rotor position for selected trajectory points both near and far from the wake boundary. For the rocket launch point ($x_T = 0$), the variation with rotor position is relatively small. At the farthest point calculated ($x_T = 2.0$), the 2 fps velocity is probably negligible, considering its effect on the rocket, and its variation is insignificant. The variation is generally small for points in the wake up to the region of $x_T = 0.7$ as shown in Fig. 15 by the abrupt change in the peak-to-peak values between $x_T = 0.6$ and 0.7. At $x_T = 0.7$ the velocity component ranges from 36 to 130 fps in the downward direction. It is noted that the 130 fps flow velocity exceeds the initial rocket launch velocity which is approximately 100 fps. The cyclic nature of the induced flow at a frequency of once-per-blade passage is a direct result of the passage of the tip vortex, and to a lesser extent the inboard vortex sheet, past the trajectory point. The peak downward velocity of 130 fps occurs when the tip vortex is closest to the point. The magnitude of the velocity is low (36 fps) at rotor position 1, because as shown in Fig. 7, the trajectory passes approximately mid-way between the tip vortices at this rotor position. Looking back to Fig. 13, it can thus be stated that the low values in the vicinity of the vortex are due to the selected rotor position. Greater differences between the values for different rockets near the wake boundary were noted in the tabulations for other rotor positions.

Results for the v_{x_T} velocity component are presented in Figs. 16, 17, and 18. The time-averaged velocity is shown in Fig. 16 to be in a direction opposite to that of the rocket travel, and the peak value of 23 fps near the wake boundary is significantly less than the 70 fps of the v_{z_T} velocity component. The instantaneous v_{x_T} is shown in Fig. 17 for the 4 rockets and rotor position 1. In Fig. 18, the variation with rotor position for rocket 4 at selected trajectory points is presented. It is shown that the instantaneous v_{x_T} velocity changes direction in the vicinity of the wake boundary, and values as high as 60 fps are indicated. Similar plots for the v_{y_T} velocity component are presented in Figs. 19, 20, and 21. It is shown that this component, which is in a direction to influence the lateral motion of the rockets, has the lowest magnitude of the three. The time-averaged velocity does not exceed 10 fps, and the instantaneous velocity does not exceed 25 fps.

The effect of wake model, distorted versus undistorted, on the induced velocity components may be noted by comparing Figs. 22 through 27 for the undistorted wake with the appropriate figures presented previously for the distorted wake model. The predominant difference observed from the time-averaged velocity plots (Fig. 22 vs. Fig. 12, Fig. 24 vs. Fig. 16, and Fig. 26 vs. Fig. 19) is the shift of the point at which the velocity components change abruptly. This outward shift for the undistorted wake corresponds to the outward shift of the uncontracted wake boundary shown by comparing Fig. 6 to Fig. 7. Thus, it is important to have a realistic wake model to accurately predict the point along the rocket trajectory up to which the velocities increase and then change abruptly.

The predominant effect of wake model on the instantaneous velocity components also occurs in the region of the wake boundary, and consists of a shift in the time (rotor position) at which the peak velocities occur at rocket trajectory points in this region. Studying the time variations of each component (Fig. 23 and Fig. 15 for v_{z_T}, Fig. 25 and Fig. 18 for v_{x_T}, Fig. 27 and Fig. 21 for v_{y_T}), it is noted that the peak velocities for the x_T position inside and nearest to the wake boundary occur at times associated with approximately the following azimuth positions of the reference blade (generalized to within approximately ±30 degrees):

	DISTORTED WAKE	UNDISTORTED WAKE
APPROXIMATE AZIMUTH OF THE MORE NEGATIVE VELOCITY PEAK	90 deg.	0 deg.
APPROXIMATE AZIMUTH OF THE MORE POSITIVE VELOCITY PEAK	0 deg.	90 deg.

The time variation of the velocity components is mostly due to the periodic passage of the tip vortices past the point on the rocket trajectory. The relation between the phasing of the peak velocities and the relative positioning of the tip vortex geometry with the points where the rocket trajectories intersect the forward wake boundary may be clearly seen by relating the azimuth locations of the peak velocities to the orientations shown in Fig. 28. The more negative peak values generally occur when a tip vortex passes closest to the point, and the more positive peak values generally occur when the point is approximately midway between two successive tip vortices. The greatest magnitudes of velocity correspond to the more negative peak values of the point just inside the wake boundary produced by the presence of the tip vortex. It is also shown in this figure that, for this flight condition, the wake model variation from distorted to undistorted results in a phase shift of approximately 90 degrees in the tip vortex passage time (see Fig. 28(b) and 28(c)) which produces the phase shift noted between the velocities of the two wake models. This indicates the importance of accurately representing the wake if the time variation of the instantaneous velocities at the rocket trajectory are of interest.

15 KT FLIGHT CONDITION

At the 15 kt flight condition, the wake boundary is skewed back toward the rocket launch point as shown in Fig. 9. The rocket trajectory intersects the distorted wake boundary between an x_T of 0.3 and 0.4. This results in the occurrence of the maximum downward velocity component (v_{z_T}) in that region as shown in Figs. 29 to 31. Thus, the rapid change in the skew angle of the wake with the small change in flight speed from 0 to 15 kts leads to a significant decrease in the distance from the launch point that the rocket is inside the rotor wake ($x_T \simeq 0.35$ at 15 kts vs. 0.77 at 0 kt). The maximum time-averaged downward velocity ($v_{z_{T_{AVG}}}$) at the four rocket trajectories ranges between approximately 40 and 60 fps (Fig. 29) compared to the 70 fps at 0 kts (Fig. 12). Greater variations of the instantaneous v_{z_T} velocity for different rockets are also indicated at this flight condition for points in the wake (Fig. 30 vs. Fig. 13). However, this is mainly a timewise phasing variation in that the results in these figures are limited to rotor position 1 and similar high and low velocities occur for each rocket at other rotor positions. The sensitivity of the v_{z_T}velocity component to rotor position is shown in Figs. 31 and 32 for the trajectory of rocket 4. Similar to the results for 0 kt, the downward velocity exceeds 100 fps near the wake boundary. Unlike the results for 0 kt, a large upward velocity (approximately 90 fps) is predicted in addition to the large downward velocity for the point just inside the wake boundary (trajectory point 4). This is due to the predicted close passage of tip vortex filaments on both sides of the trajectory point at different rotor positions. A phasing difference between the rotor positions corresponding to the peak velocities for 15 kt vs. 0 kt is also noted in Figs. 32 and 15.

The time-averaged and instantaneous v_{x_T} velocity variations are presented in Figs. 33 and 34, respectively. The magnitudes of this velocity component are shown to be generally greater at 15 kt than at 0 kt, and the phase difference with rotor position occurs. As shown in Figs. 35 and 36, similar to the results for 0 kt, the lateral velocity component v_{y_T} at 15 kt is small in magnitude.

The difference between the distorted and undistorted wake geometries for the 15 kt flight condition was shown in Figs. 8 and 9. It is shown by comparing the results for the undistorted wake presented in Figs. 37 through 42 with those just presented for the distorted wake that the predominant effects of wake model variation are similar to those at 0 kt. That is, the tip vortex distortion contracts the wake to a position closer to the rocket launch point and causes the peak velocities to also occur closer. Also, the phasing of the instantaneous velocities is different. Thus, again the importance of accurately representing the wake geometry is demonstrated.

30 KT FLIGHT CONDITION

It is shown in Fig. 11 that the predicted distorted wake is skewed just enough at 30 kt for the tip vortices to pass behind the rocket launch point*. This placement of the rocket trajectories outside of the wake results in relatively low magnitudes (less than ±10 fps) of all velocity components as noted in Figs. 43 through 50. Also, only minor variations of the velocity components are predicted between the four rocket trajectories and the various rotor positions. It thus appears that beyond a flight speed of approximately 30 kt the AH-1G rotor wake is swept behind the rocket trajectories, and the wake induced effects at the rockets are probably insignificant.

In Fig. 10, it is shown that the use of an undistorted wake model places the rocket launch point right at the wake boundary. The velocity components based on this undistorted wake representation are presented in Figs. 51 through 56. The close proximity of the tip vortices to the launch point results in large instantaneous velocities at certain rotor positions. Thus it is at this 30 kt flight condition where the sensitivity to wake model is the greatest. Depending upon the placement of the launch point inside, at, or outside the wake boundary results in an extreme difference in the predicted induced velocities.

VARIATIONS OF ROCKET LAUNCH ATTITUDE AND POSITION

In order to show the sensitivity of the induced velocity component to small variations in rocket launch attitude, the launch attitude relative to the fuselage waterline was changed in 2 degree increments for the hovering flight condition. As shown in Fig. 57(a), the resulting attitudes were changed from 7 degrees (126 mils elevation) to 9 and 11 degrees (160 and 195 mils). Since the flight condition and distorted wake geometry were unchanged, the time-averaged velocity components did not change significantly with the small reorientation of the rocket to the time-averaged wake geometry. However, the instantaneous velocity components in the vicinity of the wake boundary experienced a phase shift with rotor position due to the reorientation of the rocket trajectory to the tip vortices at a specific rotor position. This phase shift is shown in Fig. 58 for the three rocket attitudes. For the 126 mils elevation, the peak velocity for rocket 4 near the wake boundary ($x_T = 0.7$) occurs at rotor position 6. Increasing the elevation to 160 mils and 195 mils shifts the occurrence of the peak velocity to rotor positions 5 and 3, respectively. Thus, a 4 degree change in attitude results in approximately a 45 degree change in rotor rotation for the occurrence of the peak v_{z_T} velocity component. This effect is similar to that noted earlier for the change from the distorted to the undistorted wake model where the reorientation of the tip vortices to the rocket trajectory resulted generally in a 90 degree phase shift.

---

* Although a tip vortex filament appears to be very close to the rocket launch point in the side view in Fig. 11, it is shown in the top view that the lateral displacement of the launch points place them forward of the vortex filament.

What is the significance of the phase shift, and is it important for establishing improved rocket firing techniques? Considering that a rocket passes through the wake boundary at one instant of time, the rocket at such a point along its trajectory, such as that of Fig. 58, will experience the wake induced effects associated with just one rotor position. Since the downward v_{z_T} component varies from approximately 40 to 130 fps with rotor position, the time (rotor position) at which the rocket crosses the wake boundary may be very significant. If so, a means of synchronizing the rocket firing time with rotor position could be considered which would cause the rocket to cross the wake boundary at the rotor position for minimum induced velocity. This would result in minimizing the aerodynamic interference at the rocket. Although the phase difference produced by varying rocket attitude is not relevant to current firing techniques where the rockets are fired without regard to rotor position, the phase difference would be important to know if a firing synchronization technique were used.

To show an example of the sensitivity of the induced velocity components to a change in rocket launch position, the launch position was moved forward and down by 0.05 R for the 30 kt flight condition (see Fig. 57(b)). The selection of this example was based on the intent to show the potential for significantly reducing the induced effects at the rocket by moving the launch point outside the wake. It was previously shown that at 30 kt the rocket launch point moved from outside the wake to inside the wake in changing from a distorted to an undistorted wake model. A significant increase in aerodynamic interference resulted. As shown in Fig. 59, moving the launch point outside the undistorted wake by the 0.05 R movements mentioned above, results in a significant decrease in interference similar to that attained through use of the distorted wake model. This emphasizes the importance of the location of the wake boundary relative to the rocket launch point. It is noted that similar changes in the relative position of the rocket launch point to the wake boundary could be produced by changes in any of the factors determining the wake skew angle (flight speed, aircraft gross weight, and rotor attitude as determined by the aircraft center of gravity location or maneuver condition).

AREAS FOR FURTHER CONSIDERATION

Several assumptions were made in the computer analyses and procedures used to determine the induced velocities presented. The fact that some of these assumptions could have a significant effect on the wake interference at the rockets should be recognized when making use of the results presented herein, and they should be subject to further consideration.

The distorted wake geometry used in the calculations for the hovering flight condition, although determined from experimental information, is accurate only in the region directly beneath the rotor (the near wake). It was assumed in the analysis that following the contraction of the wake boundary, the far wake continued at the same vertical transport velocity and retained its symmetry and stability. In reality, the wake becomes unsteady at some point beneath the rotor and viscous dissipation occurs. This is explained in Refs. 1 and 2 based on observations from both experimental flow visualization data and analytical wake geometry results. It is shown in these references that the unsteadiness of a tip vortex from a hovering, two-bladed rotor is initiated at approximately 2 vortex revolutions from the blade. For the AH-1G rotor wake shown in Fig. 7, this would place the onset of the unsteady wake at approximately 0.6 R below the rotor hub. Since the rocket trajectories intersect the tip vortices (wake boundary) at approximately 0.3 R below the rotor hub, it appears that the rocket trajectories are completely within the steady near wake region. Some inaccuracy in the results presented herein are produced by differences in the induced effect of the unsteady far wake. The extent of this inaccuracy remains to be assessed. However, it is known that the wake in the local vicinity of the rocket trajectory is significantly more effective, and since this near wake has been modelled accurately the results presented herein should be sufficiently accurate for providing an improved understanding of the wake interference at the rockets and for initial rocket trajectory calculations.

At the 15 and 30 kt flight conditions, the unsteadiness of the wake could also have a significant effect. Although experimental flow visualization data are more limited for low flight speeds, some evidence of wake unsteadiness does exist. This unsteadiness has also been predicted analytically in that a completely converged far wake geometry was not achieved in the calculations leading to the distorted wake geometries presented in Figs. 9 and 11. Although this lack of complete convergence of the far wake could be partially attributed to the finite vortex filament and finite time step wake model, it is noted that the analysis has predicted the onset of the unsteadiness accurately for hovering conditions (Ref. 1). However, it should also be recognized that the most complex wake patterns occur at low forward speeds where the tip vortices at the upstream region of the rotor pass up through the rotor disc before returning below the rotor, and tend to roll-up into two concentrated vortices downstream from the sides of the rotor disc. The interaction of these complex tip vortex patterns with the blades results in the "transition roughness" experienced on some aircraft as increased vibrations and control sensitivity at low speeds. The occurrence of this on the AH-1G aircraft could be an additional factor leading to rocket inaccuracy.

Some inaccuracy in the predicted velocity components is produced by the use of finite time and spatial increments in the calculations along with an approximate vortex core representation. The use of time steps corresponding to 15 deg increments of rotor rotation and positions along the rocket trajectory of 0.1 R leads to some inaccuracy in establishing the peak induced velocities. Since the peak velocities generally occur when the rocket is in close proximity to the tip vortices, these intervals may be too coarse to establish the actual peak values. If the rocket trajectory passes extremely close to a tip vortex, the vortex core diameter assumed becomes important, for it is at the boundary of the core that the peak velocity would occur. A vortex core diameter of one-fifth of the blade chord was assumed for the calculations performed in this study. Also, any dissipation of the vortex circulation strength neglected in the analysis could be significant.

Another assumption made in this initial study is that the rocket trajectories are a straight line in the vicinity of the aircraft. That is, the induced velocity components were calculated along straight lines from each rocket launch point to a point 2.0 R from the launch point. In reality, the rockets veer somewhat from a straight course. In fact, the computation of the induced velocities are directed toward the objective of determining the true rocket trajectories. Thus, when the sensitivity of the rocket paths to the induced effects is determined, the requirement for performing iterations to include induced velocities calculated along the actual rocket trajectories should be considered.

Fuselage and wing aerodynamic interference effects were neglected in the study reported herein. However, to roughly determine the order of magnitude of the effect of the fuselage on the flow at the rockets, the velocities at the rocket trajectories were calculated using an existing general fuselage representation in an analysis developed at the Sikorsky Division of the United Aircraft Corporation. This analysis is described in Ref. 10 and is a potential flow analysis based on vortex lattice techniques. This analysis is shown in Ref. 10 to accurately predict fuselage loads. An isometric view of a general fuselage modelled for this analysis is shown in Fig. 60. To construct the geometry of the AH-1G fuselage was beyond the scope of this investigation, and thus the general fuselage representation was used. To scale the rocket trajectory lateral positions from the AH-1G to the general fuselage, the AH-1G values in percent fuselage width were used as shown in the schematic of the configuration in Fig. 61. It should be noted that the general fuselage used has a fineness ratio (length/width) of 6 compared to the AH-1G value of 14. Thus, the results to be presented should be considered as preliminary and in a relative rather than absolute sense.

The fuselage induced increments of the three components of induced velocity at points along the rocket trajectories are shown in Figs. 62 and 63. Since the velocities scale with the forward velocity of the aircraft, the induced velocities have been nondimensionalized by this quantity. In these figures, it is shown that the peak velocity components occur at a distance from the rocket launch point which is in the vicinity of 0.5 R. For the rockets closest to the fuselage (at 65 percent of the fuselage width, Fig. 62), the peak induced velocity components are of the

order of 10 percent of the forward flight speed. For the further rockets (at 108 percent of the fuselage width, Fig. 63) the peak velocities are decreased to approximately one-half of the values at the closer location. At the low speeds of this investigation (0 to 30 kt), these results indicate that the direct fuselage effect is quite small. For example, at the 30 kt condition, the peak velocity component is approximately 6 fps. The downward component, v_{z_F}, which was greatest for the rotor induced flow is least for the fuselage induced flow, and it's peak is only about 2 fps at 30 kt. It should be noted, however, that the analysis used does not account for the influence of the fuselage on the rotor wake and rotor induced velocities nor the effect of the wing. These effects are probably greater than the direct fuselage effect at low speeds, particularly near the rocket launch points at the wings.

Although the above factors should be considered for future studies, in that they could have a significant effect on the detailed quantitative results, the results presented herein are believed to be generally accurate. The degree of accuracy required of the induced effects for rocket trajectory calculations should be established when applying the results presented herein. The specific areas for future consideration should be decided by the degree of accuracy required.

SUGGESTED PROCEDURES FOR APPLYING INDUCED VELOCITY RESULTS

At each point in time along their trajectories, the rockets are affected by the instantaneous induced velocity components associated with the particular rotor position at that instant of time. Thus, to be accurate when performing the rocket trajectory calculations, the procedure should be to determine the rotor position for each point along a trajectory and use the corresponding induced velocity components. However, the problem arises that the rotor positions are not known due to the fact that the firing time is currently determined by the gunner irrespective of rotor position. Without rotor position synchronization, the correspondence of rocket position with rotor position is unknown. However, to evaluate the impact of this problem, the following procedures are suggested for the rocket trajectory calculations:

1. Perform the rocket trajectory calculations using the time-averaged induced velocity components at each point.

2. Perform the calculations assuming that the rockets pass in close proximity to a tip vortex. In accordance with this assumption, select the rotor position which produces the maximum velocity components (emphasize v_{z_T} in the selection) at the trajectory point nearest and inside the wake boundary. Using an assumed rocket velocity (e.g., the launch velocity of approximately 100 fps), determine the time increment and corresponding rotor rotation interval between points along the trajectory. Based on the rotor rotation interval, determine the rotor positions for each point along the trajectory and interpolate the tabulated results provided to obtain the velocity components at each point to be used in the calculation of the rocket trajectory.

3. Perform the calculations using instantaneous velocities corresponding to a few other selected rotor position sequences. Include in this selection the rotor position at the wake boundary which produces the minimum induced velocity components.

Using the above procedures, the maximum and minimum deviations of the rocket trajectories based on the instantaneous induced velocities relative to the trajectories based on the time-averaged velocities should generally result. With these results, the range of possible trajectories produced at indiscriminate firing times would be established, as well as whether or not the provision of a mechanism for firing synchronization in the aircraft instrumentation is desirable.

CONCLUSIONS

The following conclusions apply to the AH-1G helicopter operating at hover and low speed flight conditions:

1. Although the effect of the aerodynamic interference of the rotor wake on the rocket trajectories remains to be determined, the magnitudes of the predicted induced velocity components at the trajectories appear to be significant considering that they can exceed the rocket launch velocity. Values of the downward induced velocity component as high as 70 fps (time-averaged) and 130 fps (instantaneous) were predicted.

2. Of the three velocity components, the greatest induced velocities were predicted for the downward component normal to the rocket trajectory. The component along the rocket trajectory was generally next in order of magnitude, and the smallest velocity magnitudes were predicted for the lateral component.

3. As the rocket moves from its launch position, the downward velocity component increases as the wake boundary is approached. As the rocket moves to the outside of the rotor wake the magnitude of the downward velocity decreases abruptly, and becomes insignificant within a distance of one rotor diameter from the launch position.

4. The position of the intersection of a rocket trajectory with the wake boundary is most influential for it determines the length of time that the rocket remains in the higher induced velocity region inside the wake. It also determines the location where the close proximity to a tip vortex can result in a high induced velocity. The importance of the wake boundary location establishes the importance of accurately determining the items which establish the wake skew angle -- flight speed, rotor and aircraft attitude, and aircraft gross weight (rotor thrust).

5. Considering the variation of the predicted induced velocities with flight speed, the influence of the wake aerodynamic interference on the rocket trajectories is expected to decrease with increasing flight speed. In hover, the predicted velocities are the highest, and the rocket remains in the wake for the longest period of time. For flight speeds greater than approximately 30 kts, the rotor wake generally passes behind the rocket launch position which significantly reduces the wake induced effects.

6. Large induced velocity variations with time occur at points on the rocket trajectory near the wake boundary. These variations are caused by the passage of the tip vortices. If the high impulsive type velocities induced by the close passage of a tip vortex are found to significantly alter the flight path of the rocket, a mechansim for synchronizing the rocket firing time with the rotor position for minimum tip vortex interference may be desireable.

7. The variation of the predicted time-averaged induced velocity components between the four rockets of the AH-1G helicopter is within ±10 fps at similar points along the trajectories.

8. It is necessary to use an accurate rotor wake model in calculations directed toward predicting induced velocities at rocket trajectories. The use of an undistorted wake model rather than a realistic distorted wake model results in significant differences in predicted induced velocities.

9. Small variations (4 degrees) in rocket launch attitude produce small induced velocity changes at the rocket trajectories except near the wake boundary where the variations produce a difference in the phasing of the velocities associated with the relation between rotor position and the passage of a tip vortex. This is generally also true for small variations in rocket launch point. However, vertical and/or longitudinal variations in launch point produce significant variations in induced velocities near the launch point at approximately 30 kts due to the movement of the point from inside to outside of the rotor wake or vice versa. The relative position of the rocket launch point to the wake boundary could also be varied by changes in any of the factors which determine the wake boundary (flight speed, aircraft gross weight, and rotor/fuselage attitude).

RECOMMENDATIONS

1. Several factors which were approximated or neglected in the analytical calculations, should be considered. These are wake instability and dissipation, vortex core size, the selection of the finite spatial and temporal increments used in the analyses, and wing and fuselage interference effects. Also, the possible requirement for iterating between the induced velocities and the rocket trajectory should be considered.

2. The effect of the rotor wake induced velocities determined in this investigation on the rocket trajectories should be calculated using the Army rocket dynamic response analysis and the procedures described herein*. Using these procedures, the deviations of the rocket trajectories can be determined, and the degree of accuracy required of the induced effects for rocket trajectory calculations would be established.

3. The rotor wake effects for flight conditions other than those investigated herein should be determined. In particular, calculations for specific flight conditions for which flight test rocket trajectory data become available should be performed for correlation purposes. Also, the sensitivity of the results to variations of the significant parameters in actual aircraft operation which influence the wake strength and wake/rocket positioning should be investigated.

4. Model helicopter tests should be conducted to acquire systematic experimental data on this rocket aerodynamic interference problem. Model hovering and wind tunnel facilities and experimental flow measurement visualization techniques, such as those available at the United Aircraft Research Laboratories, should be used to measure the wake boundaries and flow velocities in the regions of the rocket trajectories. Combined model rotor-fuselage-wing testing (as discribed in Ref. 6), application of flow visualization techniques (such as those reported in References 1, 2, 8 and 9), and application of laser velocimeter techniques (as reported in Reference 11) to measure flow velocities, should be conducted. The results of such an experimental program would provide data for correlation with theory and for a systematic determination of the total and separate influence of each of the aircraft components (rotor, fuselage and wing) and significant parameters (flight speed, gross weight, aircraft attitude, etc.). In addition, the determination of the velocity field at potential locations for wind sensors mounted on the aircraft would assist in solving the problem of accurately measuring the low aircraft flight speeds required in accordance with current rocket firing tactics.

* These calculations are currently in progress at the Army Picatinny Arsenal.

LITERATURE CITED

1. Landgrebe, A. J., An Analytical and Experimental Investigation of Helicopter Rotor Hover Performance and Wake Geometry Characteristics, USAAMRDL Technical Report 71-24, Prepared by the United Aircraft Research Laboratories for the Eustis Directorate, U. S. Army Air Mobility Research and Development Laboratory, Fort Eustis, Va., June 1971.

2. Landgrebe, A. J., The Wake Geometry of a Hovering Helicopter Rotor and Its Influence on Rotor Performance, Jl. American Helicopter Society, Vol. 17, No. 4 October 1972.

3. Landgrebe, A. J. and E. D. Bellinger, An Investigation of the Quantitative Applicability of Model Helicopter Wake Patterns Obtained from a Water Tunnel, USAAMRDL Technical Report 71-69, Prepared by the United Aircraft Research Laboratories for the Eustis Directorate, U. S. Army Air Mobility Research and Development Laboratory, Fort Eustis, Va., December 1971.

4. Landgrebe, A. J., An Analytical Method for Predicting Rotor Wake Geometry, Jl. American Helicopter Society, Vol. 14, No. 4, October 1969.

5. Jenney, D. J., J. R. Olson, and A. J. Landgrebe, A Reassessment of Rotor Hovering Performance Prediction Methods, Jl. American Helicopter Society, Vol. 13, No. 2, April 1968.

6. Bain, L. J. and A. J. Landgrebe, Investigation of Compound Helicopter Aerodynamic Interference Effects, USAAVLABS Technical Report 67-44, Prepared by the United Aircraft Corporation for the U. S. Army Aviation Materiel Laboratories, Fort Eustis, Va., November 1967.

7. Clark, D. R. and A. J. Landgrebe, Wake and Boundary Layer Effects in Helicopter Rotor Aerodynamics, AIAA Paper No. 71-581, AIAA 4th Fluid and Plasma Dynamics Conference, June 1971.

8. Landgrebe, A. J. and M. C. Cheney, Rotor Wakes - Key to Performance Prediction, AGARD-CP-111, AGARD Conference Proceedings No. 111 on Aerodynamics of Rotary Wings, Fluid Dynamics Panel Specialists Meeting, September 1972. (Also, paper presented at the Symposium on Status of Testing and Modeling Techniques for V/STOL Aircraft, Mideast Region of the American Helicopter Society, October 1972.)

9. Landgrebe, A. J. and E. D. Bellinger, Experimental Investigation of Model Variable-Geometry and Ogee Tip Rotors, NASA CR-2275, Prepared by the United Aircraft Research Laboratories for the Langley Research Center, NASA, February 1974. (Paper with Same Title: AHS Paper No. 703, 29th Annual National Forum of the American Helicopter Society, May 1973.)

10. Sheehy, T. W., A Simplified Approach to Generalized Helicopter Configuration Modeling and the Prediction of Fuselage Surface Pressures, Proceedings of the National Symposium on Helicopter Aerodynamic Efficiency, American Helicopter Society, March 1975.

11. Landgrebe, A. J. and B. V. Johnson, Measurement of Model Helicopter Rotor Flow Velocities with a Laser Doppler Velocimeter, Jl. American Helicopter Society, Vol. 19, No. 3, July 1974.

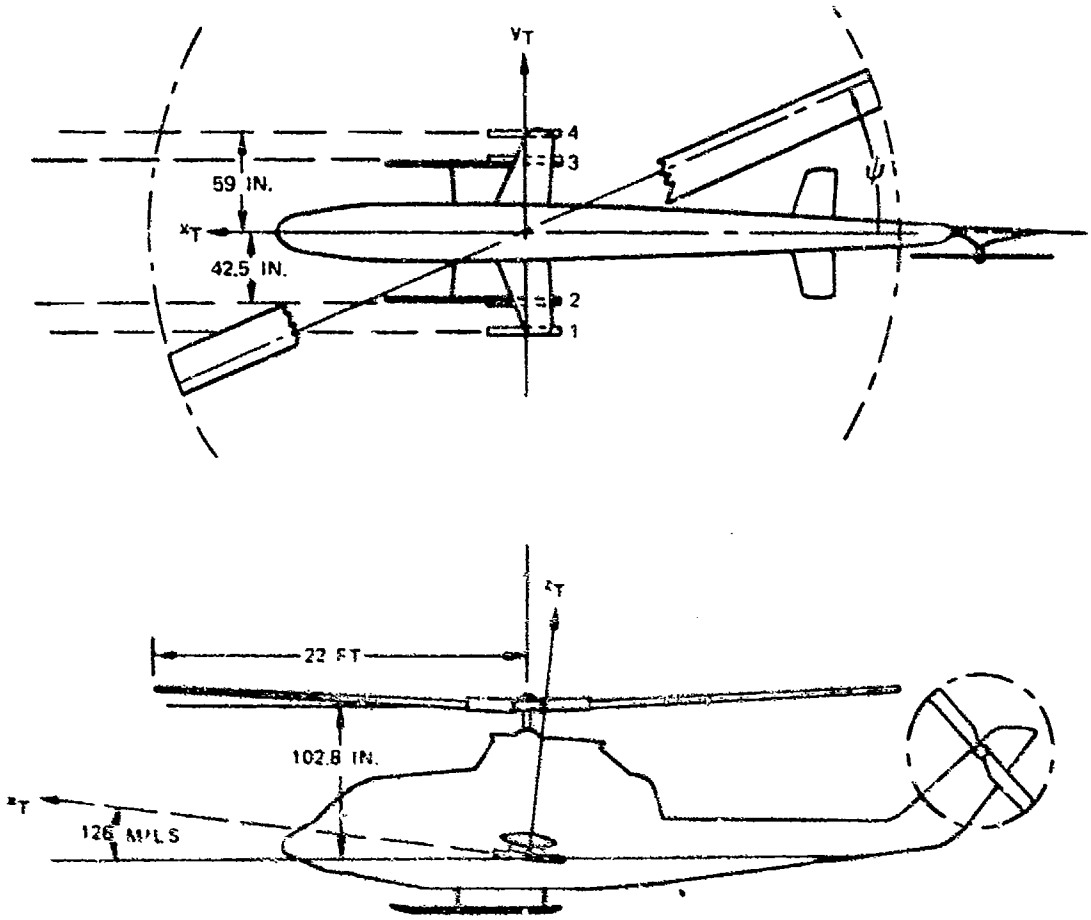

Figure 1. Schematic of AH-1G Helicopter Showing Assumed Rocket Trajectories and Coordinate System.

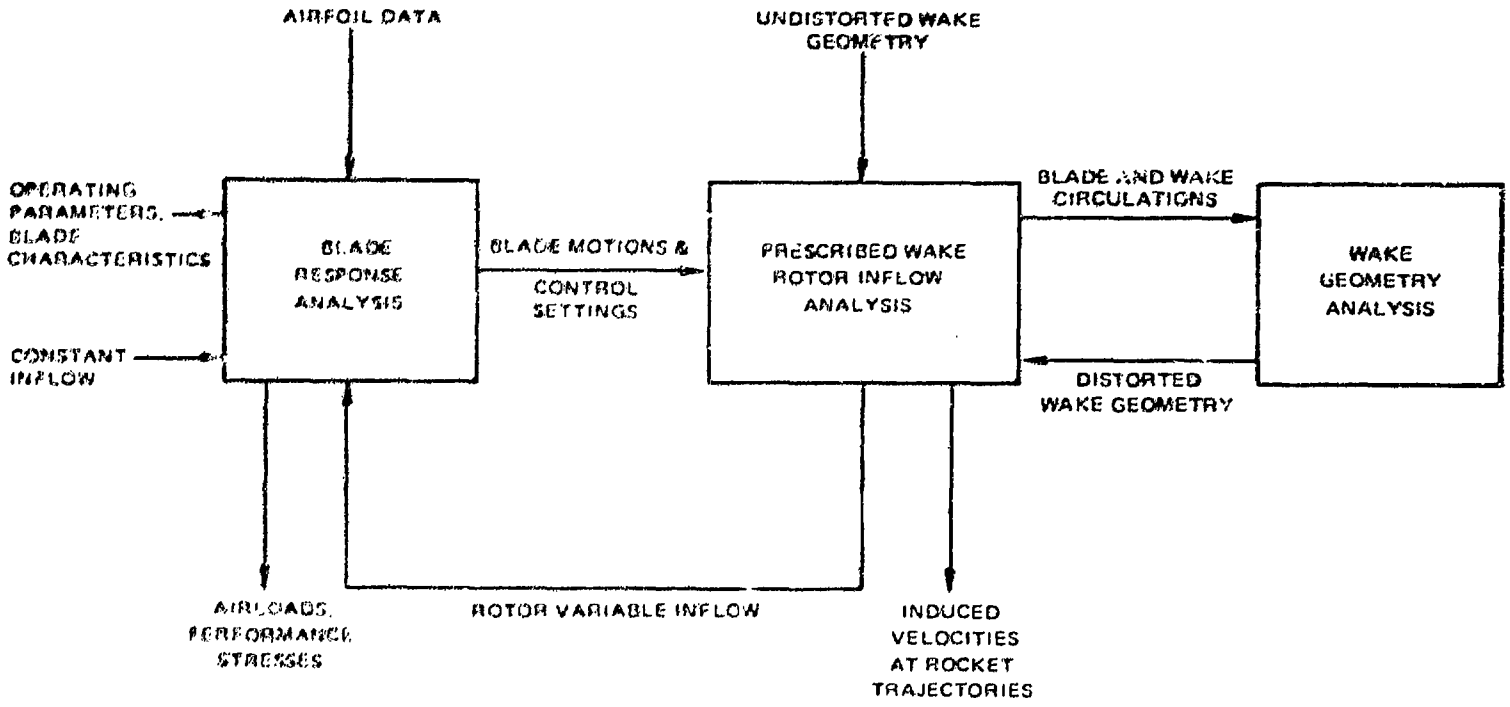

Figure 2. Components of the UARL Rotor Analysis.

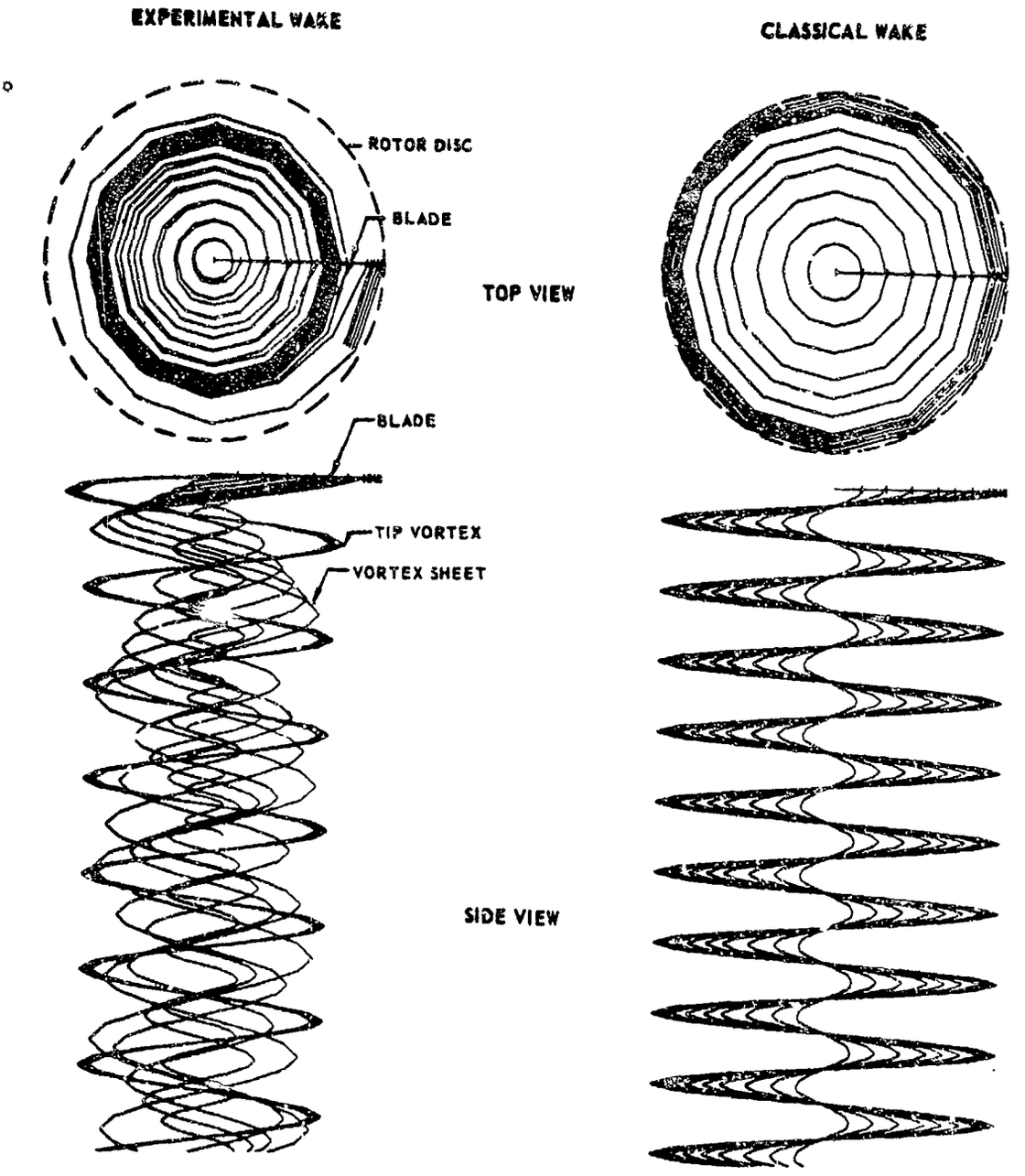

Figure 3. Computer Wake Trajectories For One Blade of a Hovering Rotor.

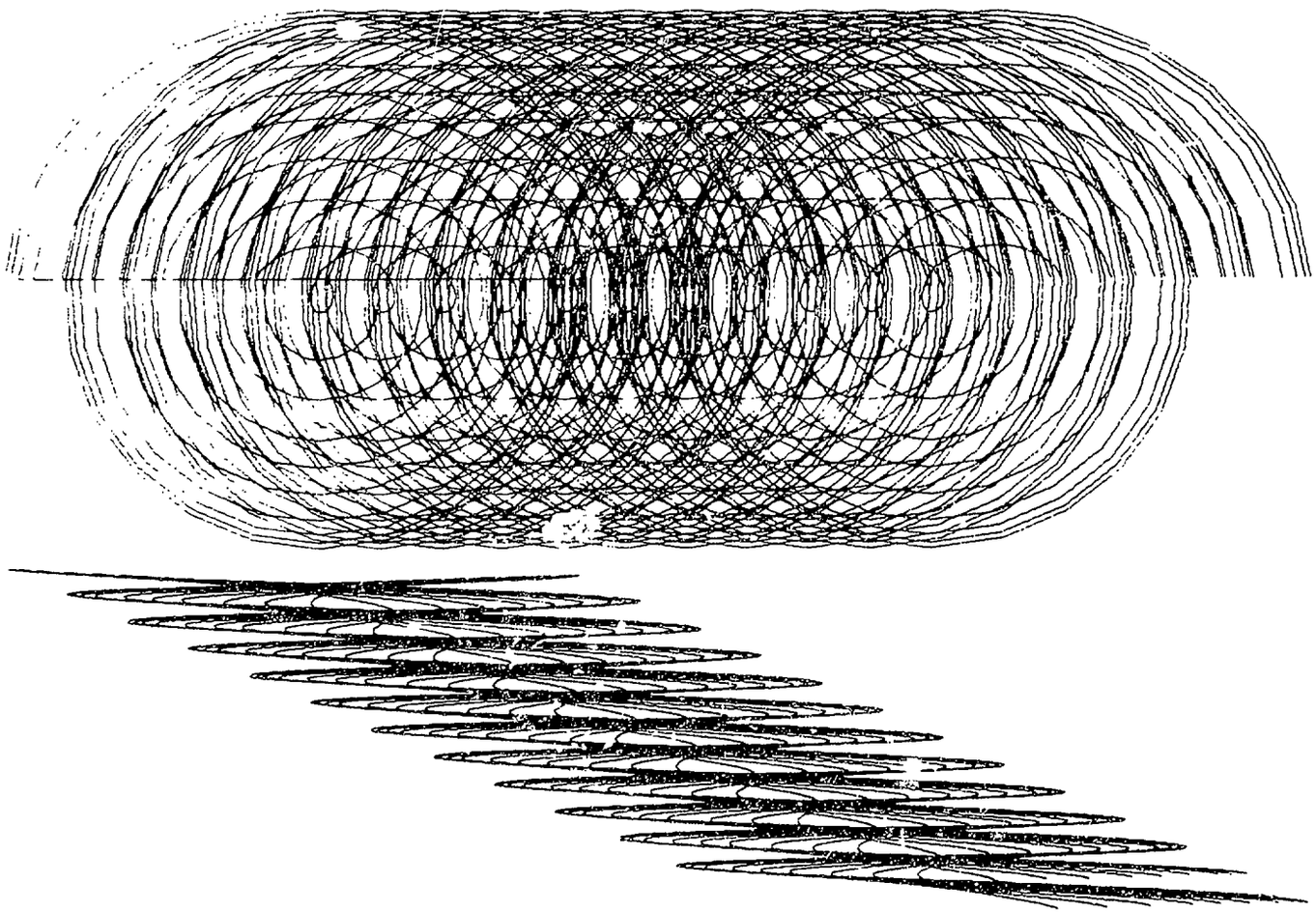

Figure 4(a). Computer Wake Representation for a Forward Flight Condition -- Undistorted Wake Model, All Filaments Shown.

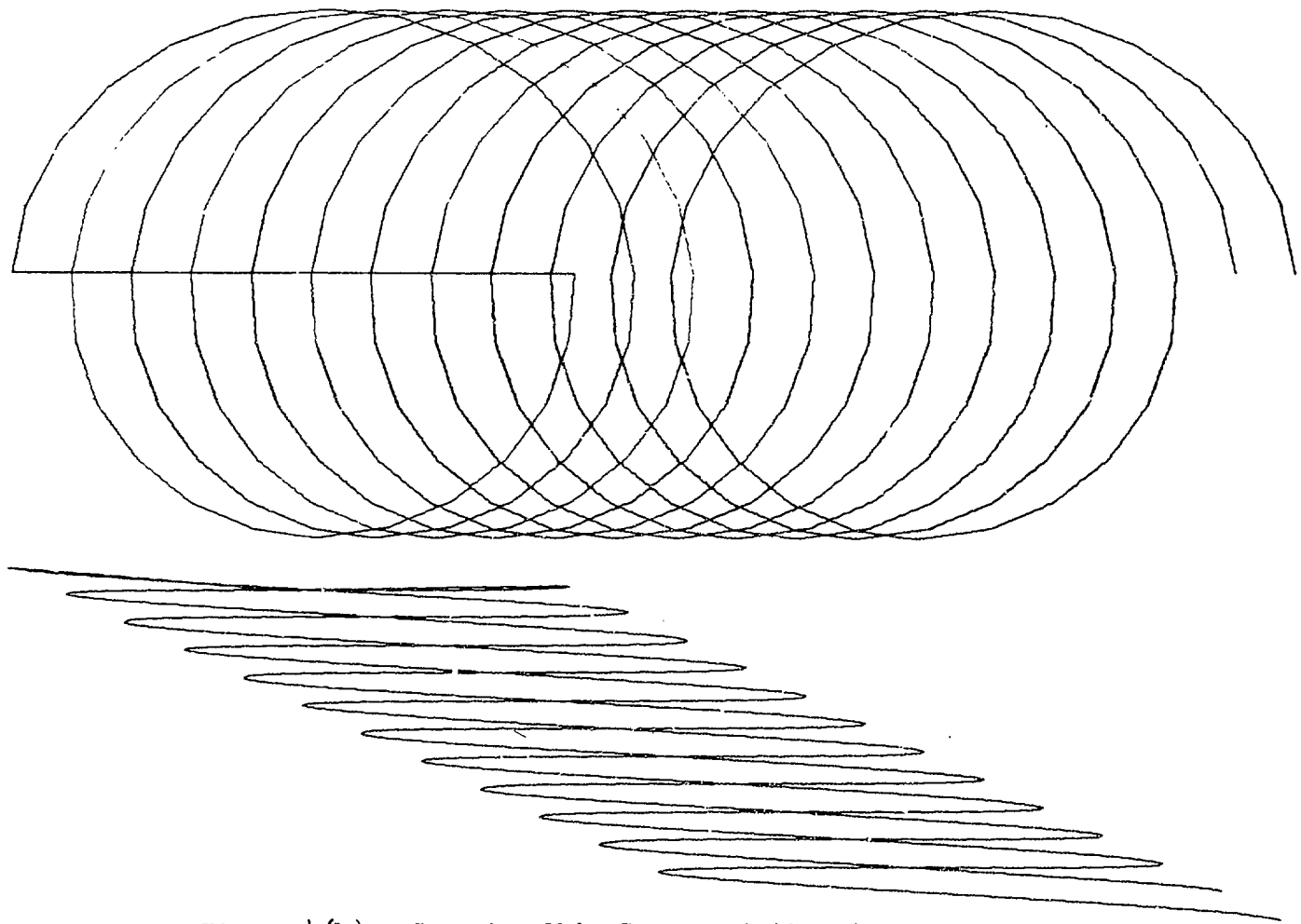

Figure 4(b). Computer Wake Representation for a Forward Flight Condition -- Undistorted Wake Model, Tip Filaments Only.

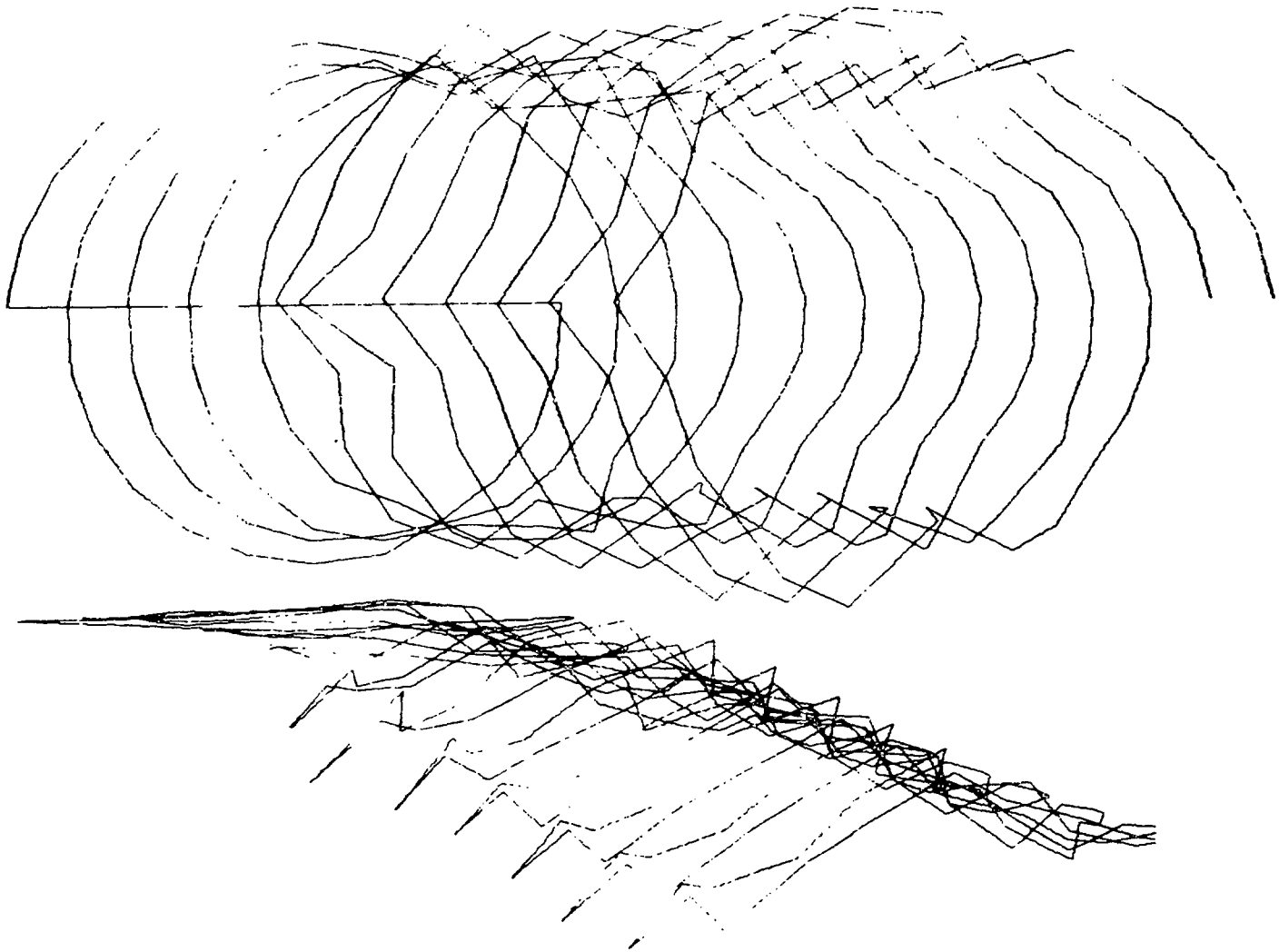

Figure 5. Computer Wake Representation for a Forward Flight Condition -- Distorted Wake Model.

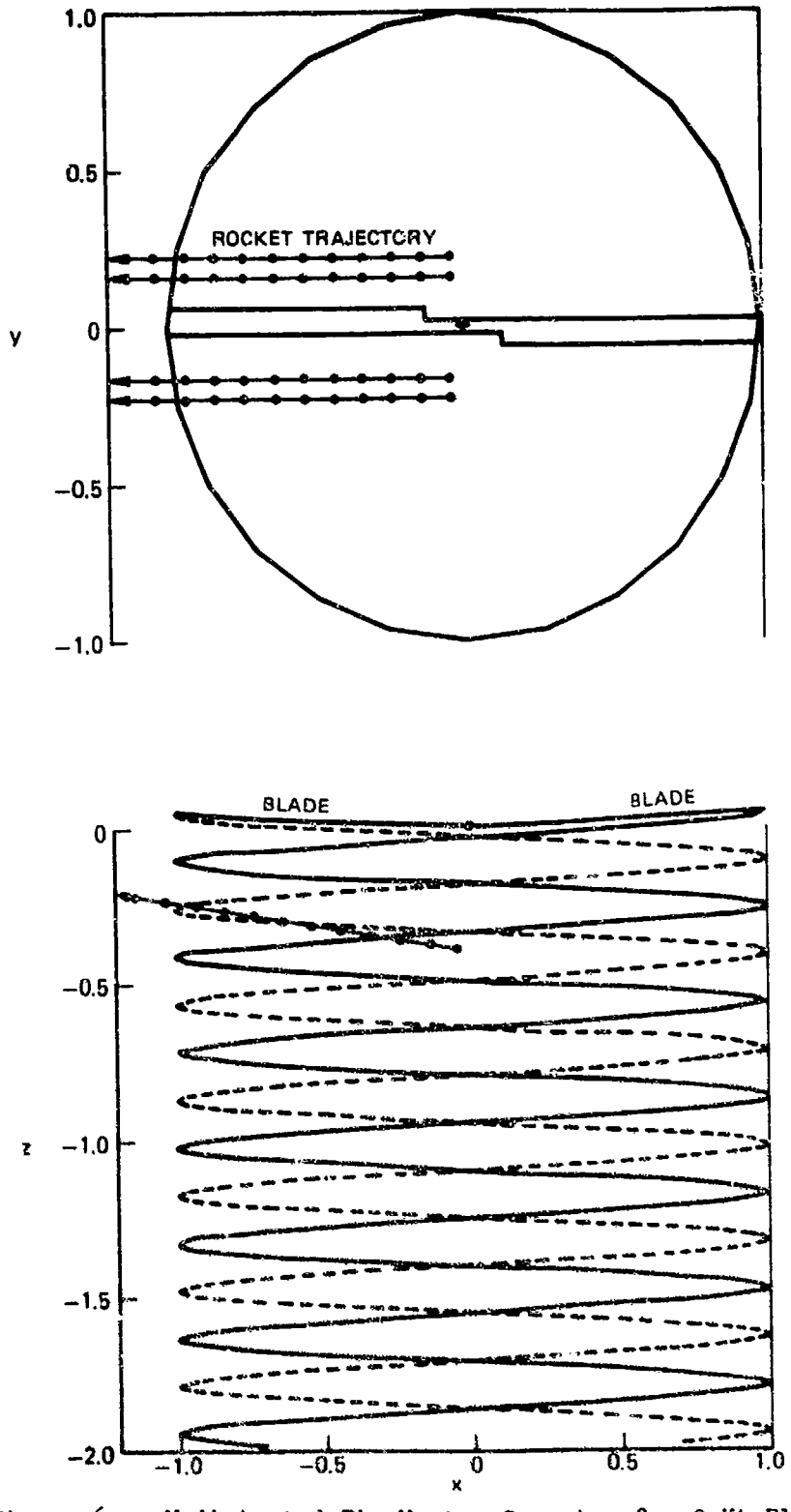

Figure 6. Undistorted Tip Vortex Geometry for 0 Kt Flight Condition and Rotor Position 1.

R02-58-3

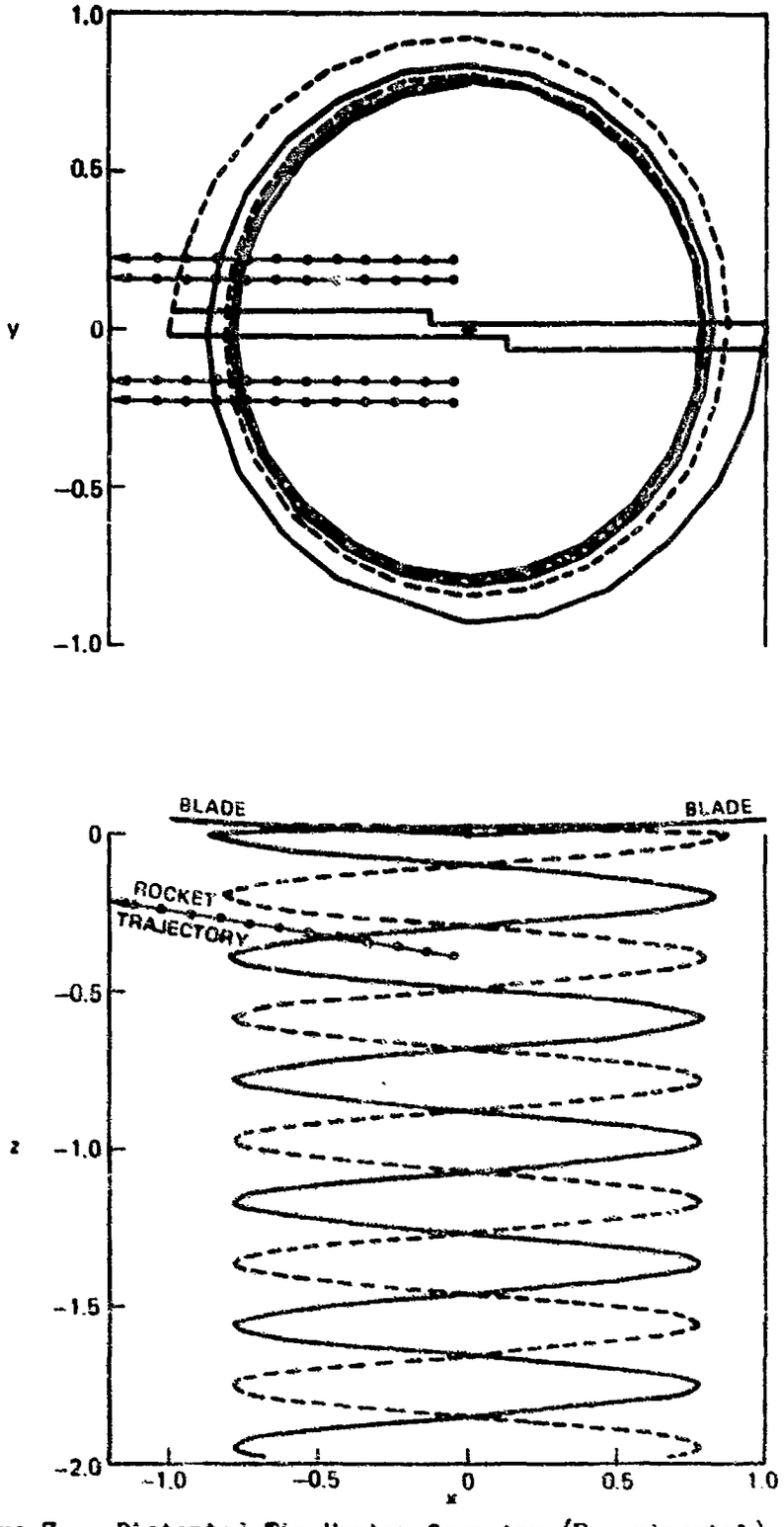

Figure 7 Distorted Tip Vortex Geometry (Experimental) for 0 Kt Flight Condition and Rotor Position 1.

RO2-58-1

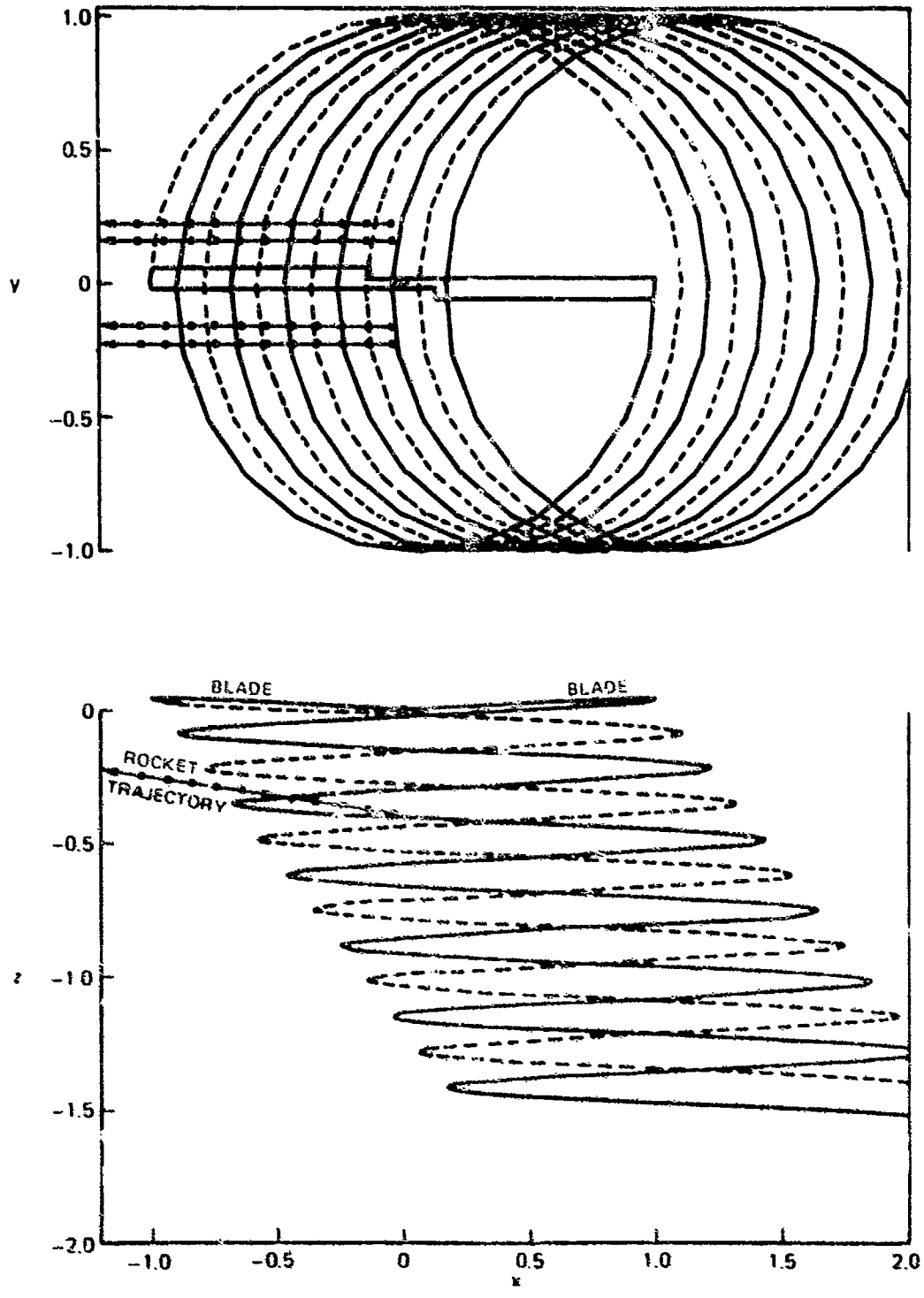

Figure 6. Undistorted Tip Vortex Geometry for 15 Kt Flight Condition and Rotor Position 1.

RO2-58-4

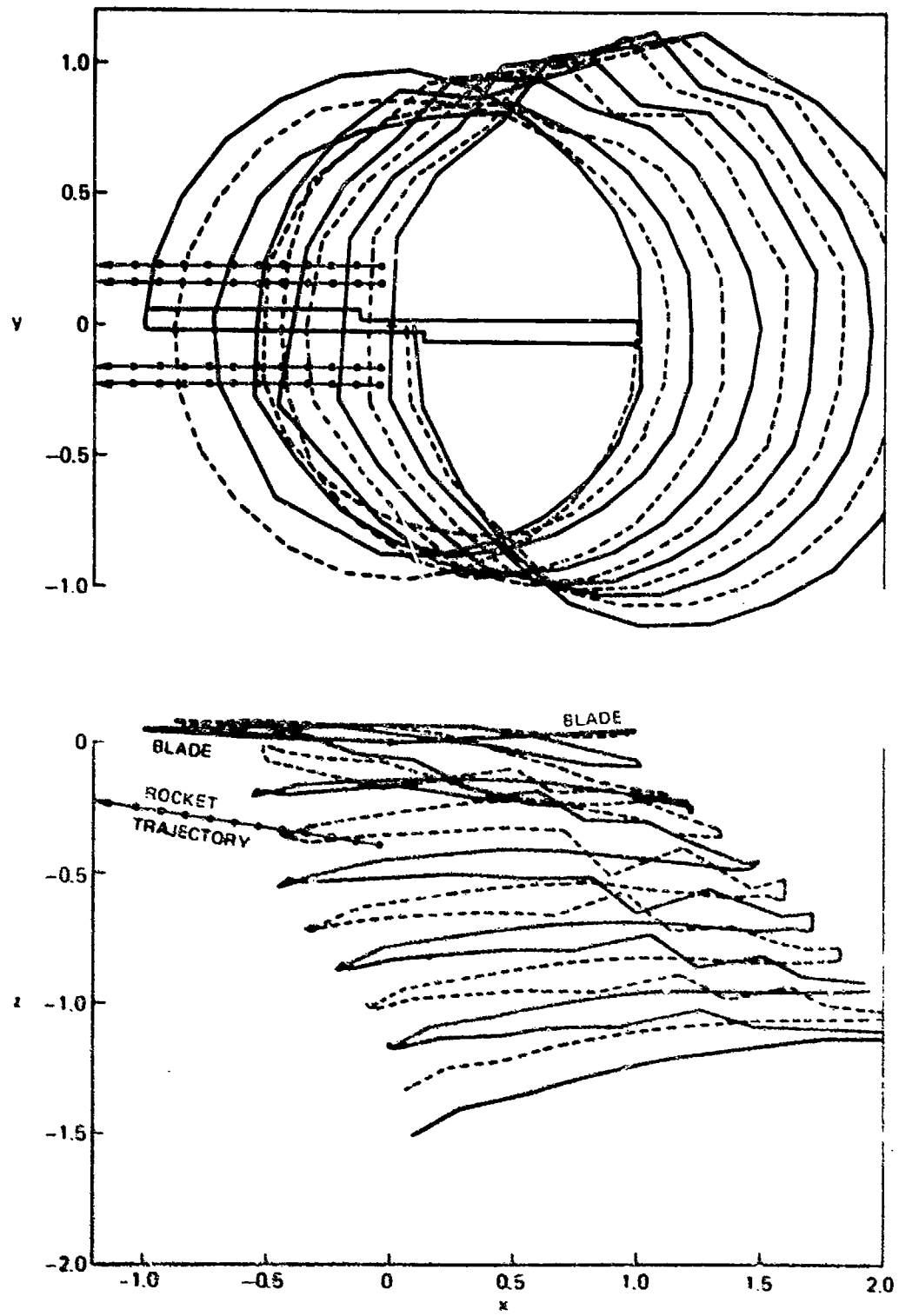

Figure 9. Distorted Tip Vortex Geometry (Analytical) for 15 Kt Flight Condition and Rotor Position 1.

RO2-58-5

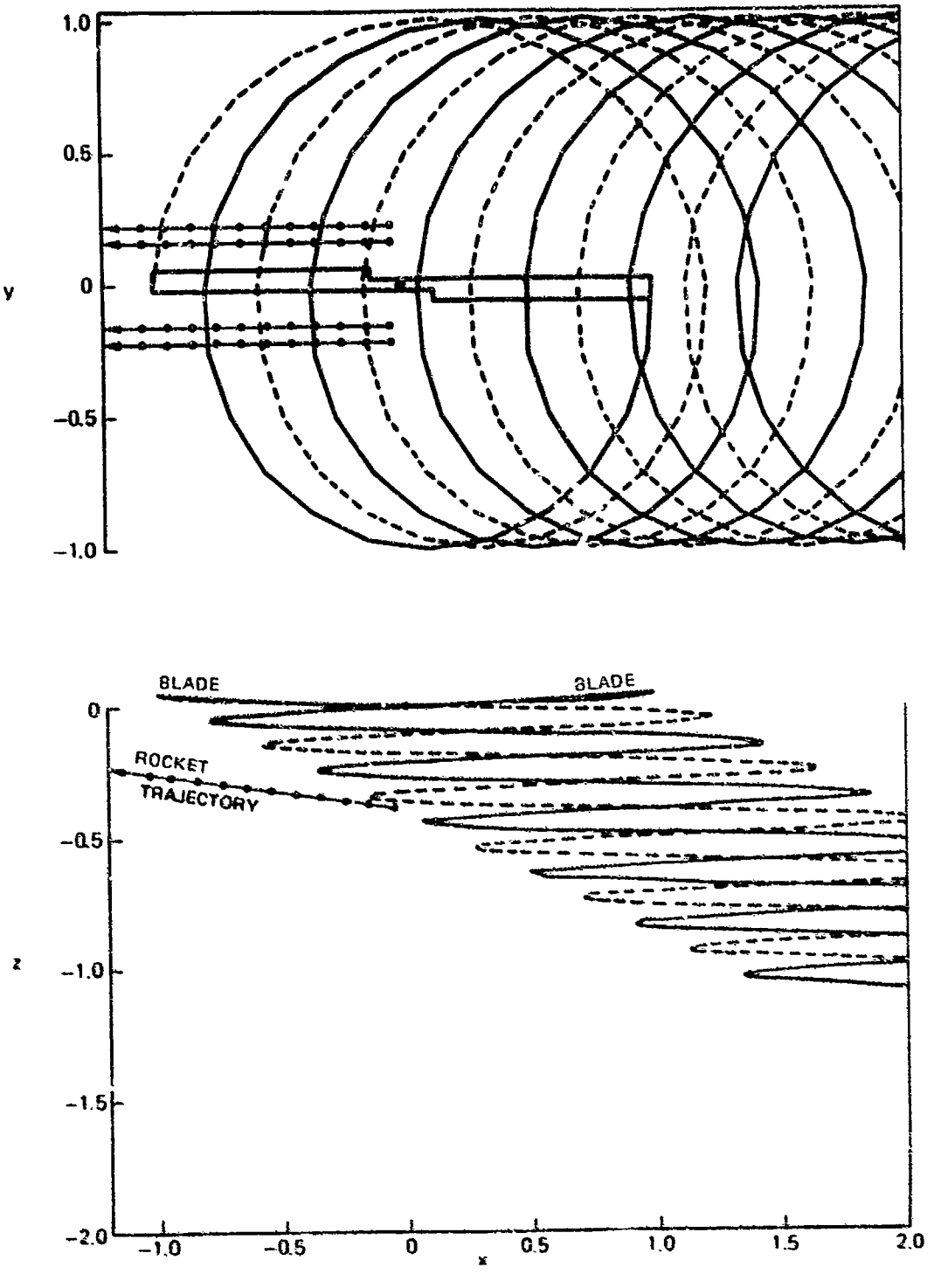

Figure 10. Undistorted Tip Vortex Geometry for 30 Kt Flight Condition and Rotor Position 1.

R02-58-6

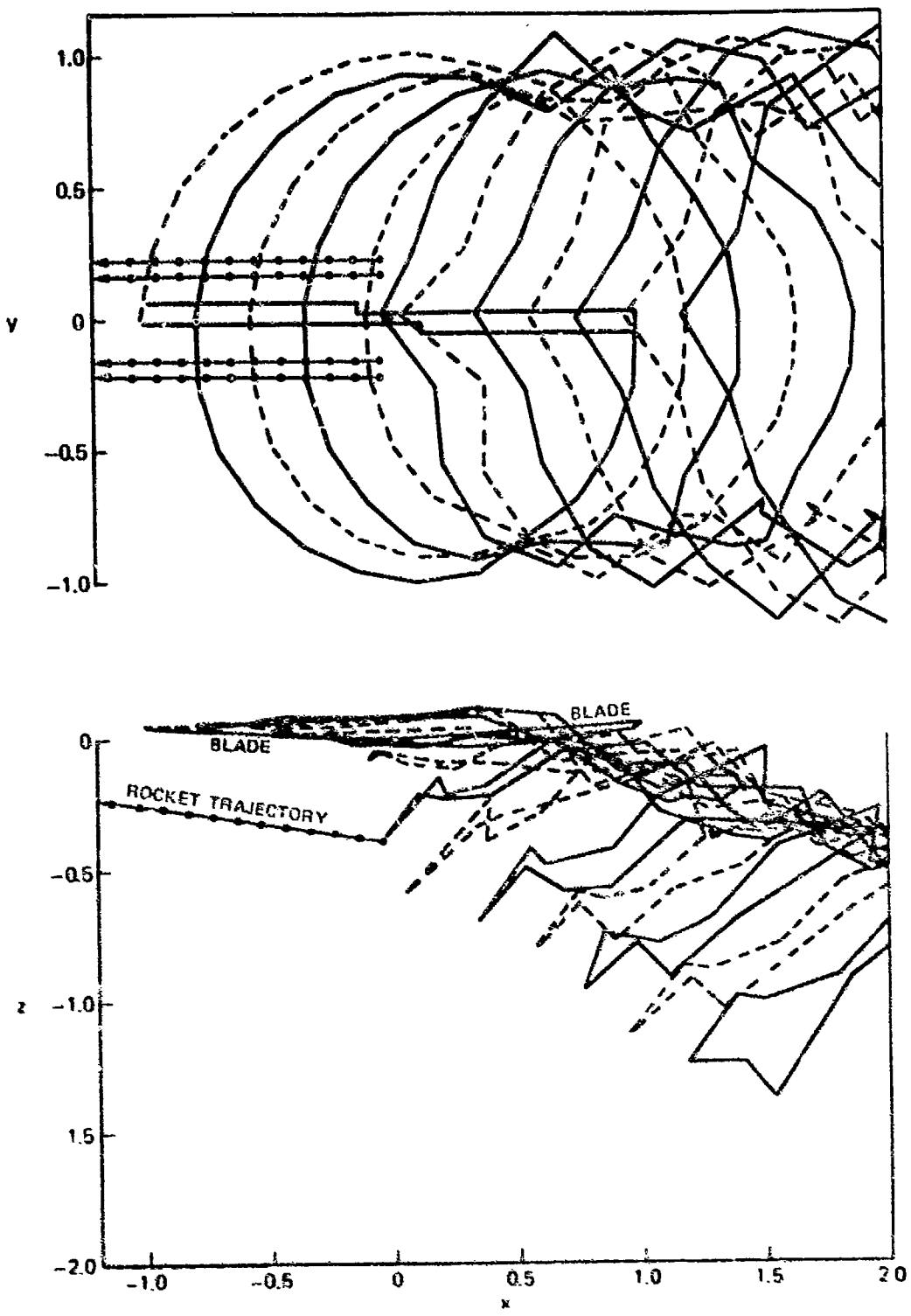

Figure 11. Distorted Tip Vortex Geometry (Anslytical) for 30 Kt Flight Condition and Rotor Position 1.

RO2-58 7

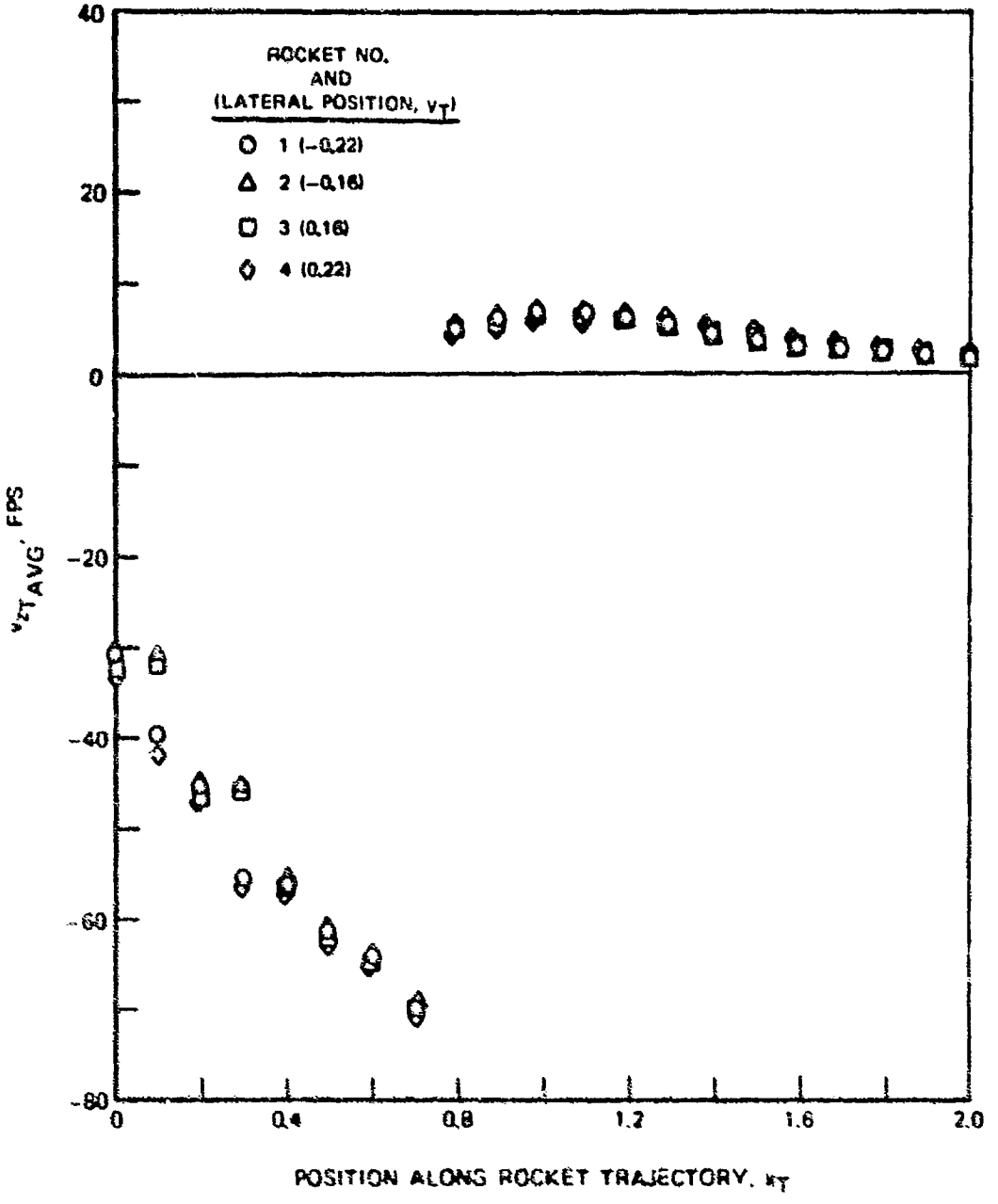

Figure 12. Variation of Time-Averaged v_{z_T} Velocity Component Along the Four Rocket Trajectories -- 0 Kt, Distorted Wake.

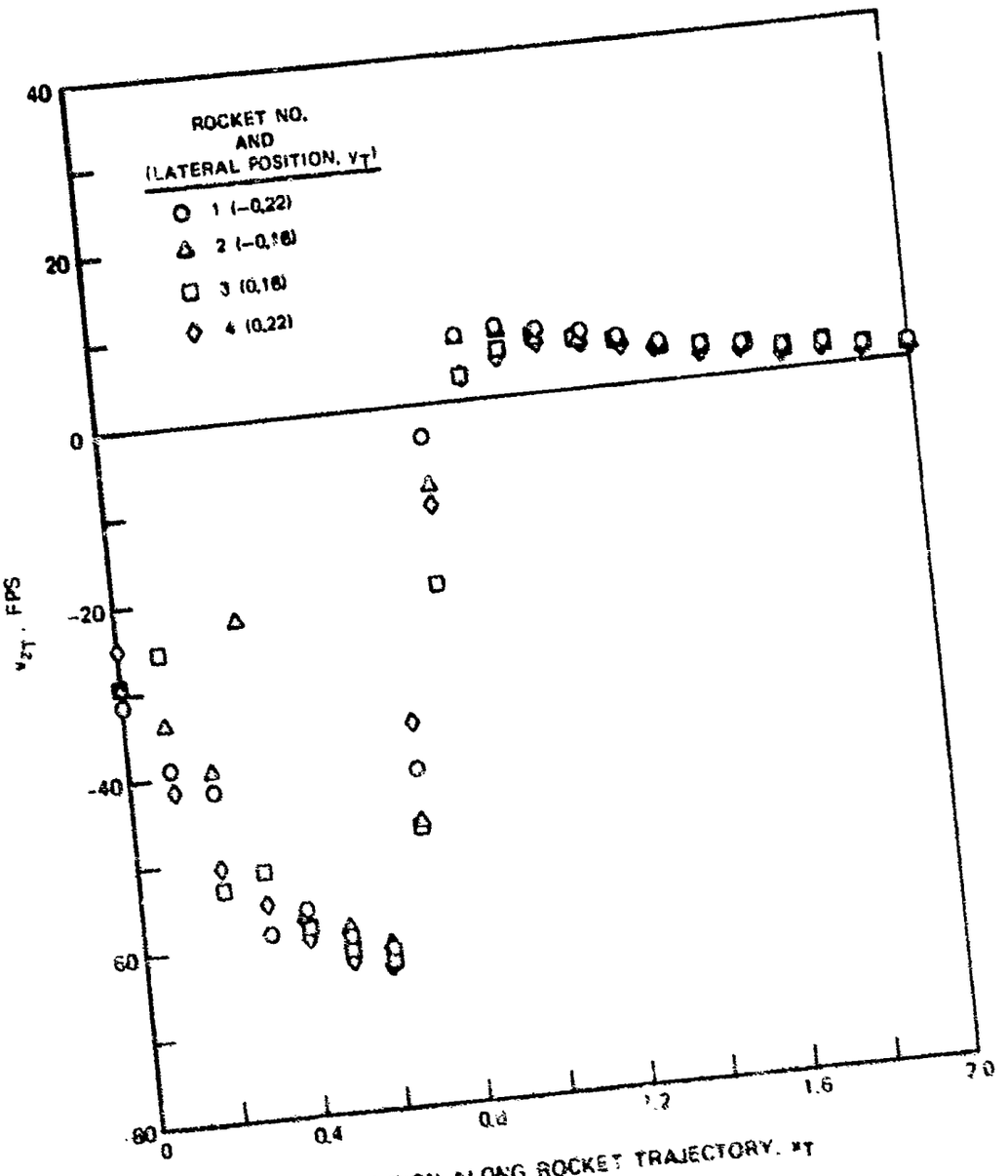

Figure 13. Variation of Instantaneous Vortex Velocity Component Along the Four Rocket Trajectories for One Rotor Position -- 0 Kt, Distorted Wake, Rotor Position 1 (Ψ = 0, 180 Deg).

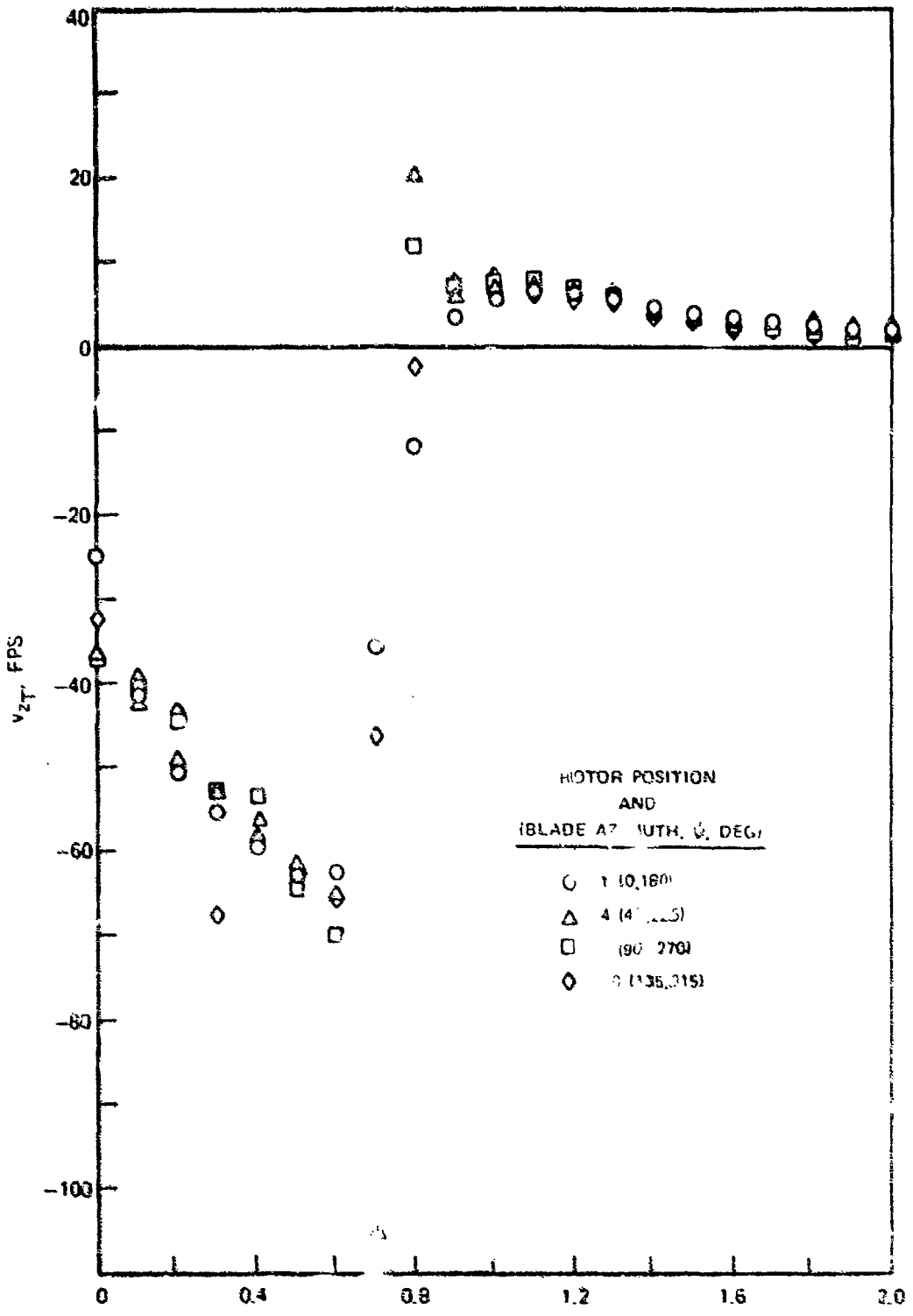

Figure 14. Variation of Instantaneous v_{z_T} Velocity Component Along One Rocket Trajectory for Selected Rotor Positions -- 0 Kt, Distorted Wake, Rocket No. 4 (y_T = 0.22).

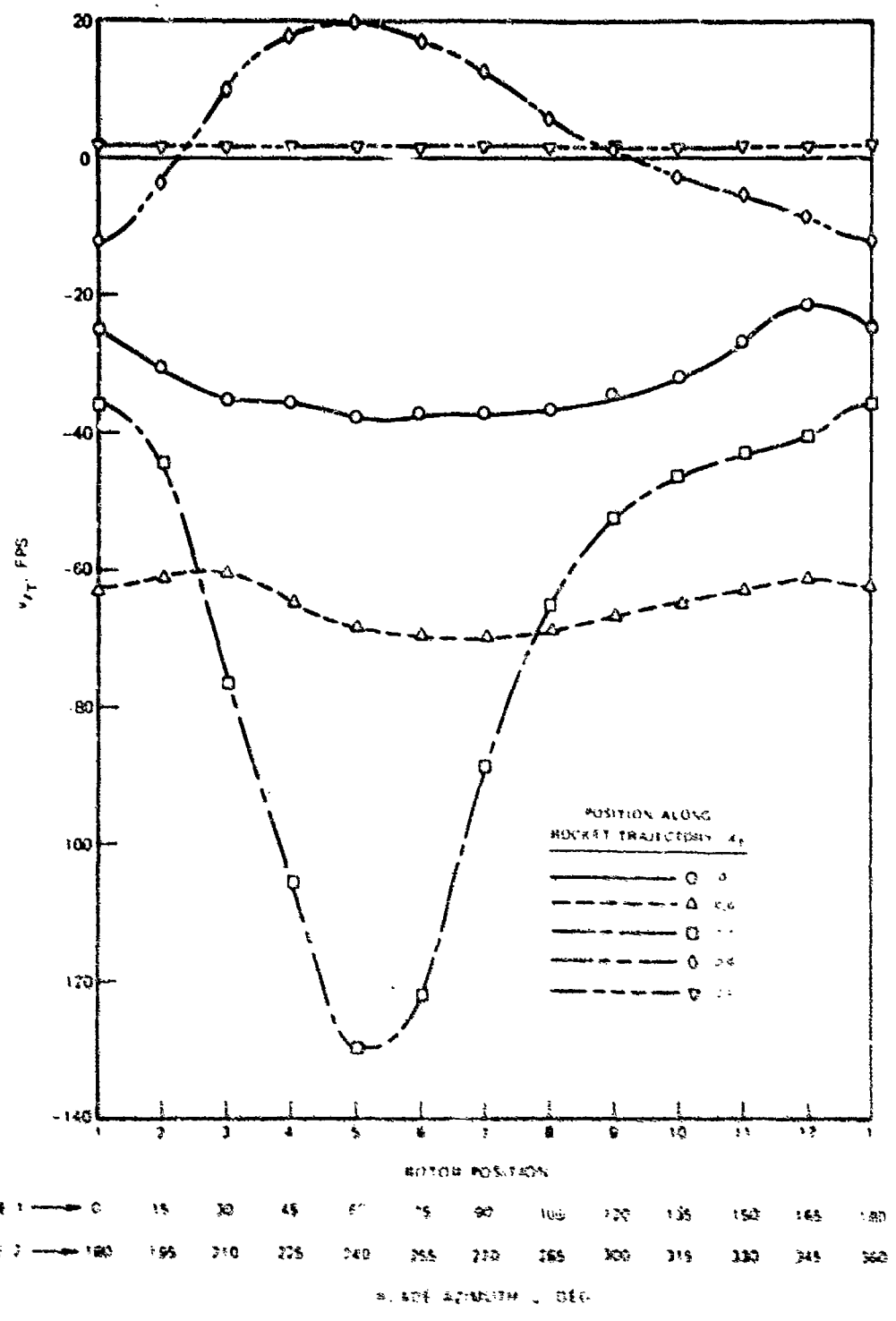

Figure 15. Variation of Instantaneous v_{rT} Velocity Component With Rotor Position for Selected Points on One Rocket Trajectory -- 0 Kt, Distorted Wake, Rocket No. 6 ($\bar{V}_T$ = 0.22).

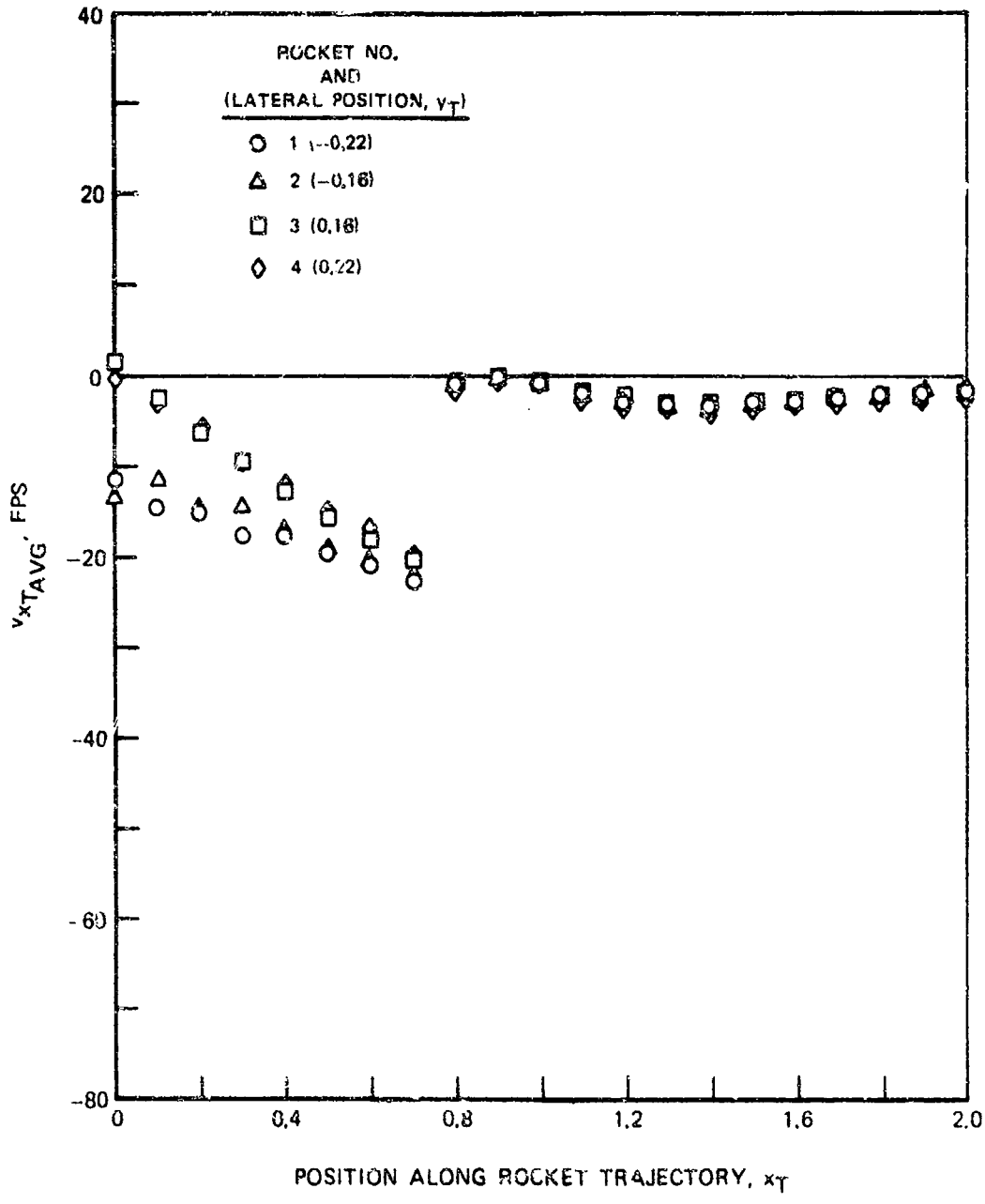

Figure 16. Variation of Time-Averaged v_{xT} Velocity Component Along the Four Rocket Trajectories -- 0 Kt, Distorted Wake.

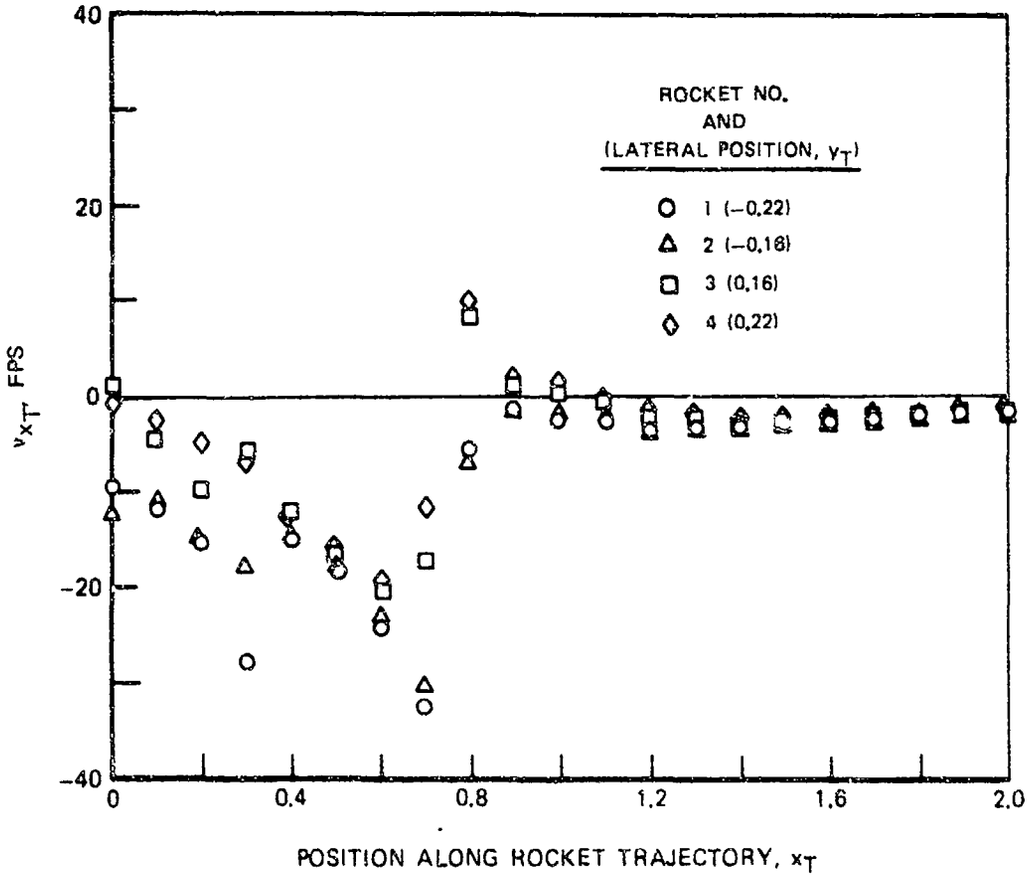

Figure 17. Variation of Instantaneous v_{xT} Velocity Component Along the Four Rocket Trajectories for One Rotor Position -- 0 Kt, Distorted Wake, Rotor Position 1 (Ψ = 0, 180 Deg).

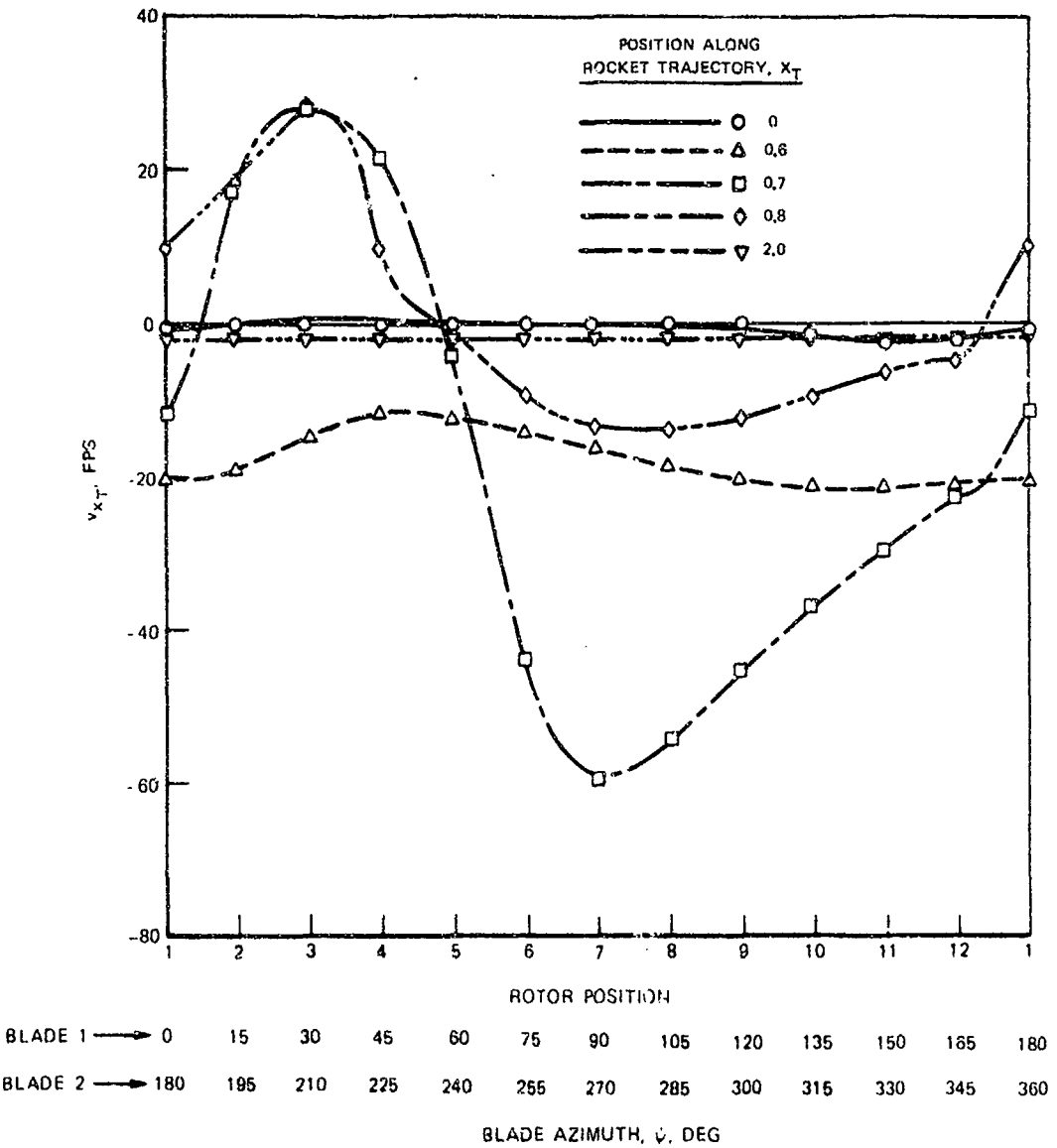

Figure 18. Variation of Instantaneous v_{X_T} Velocity Component With Rotor Position for Selected Points on One Rocket Trajectory -- 0 Kt, Distorted Wake, Rocket No. 4 (μ_T = 0.22).

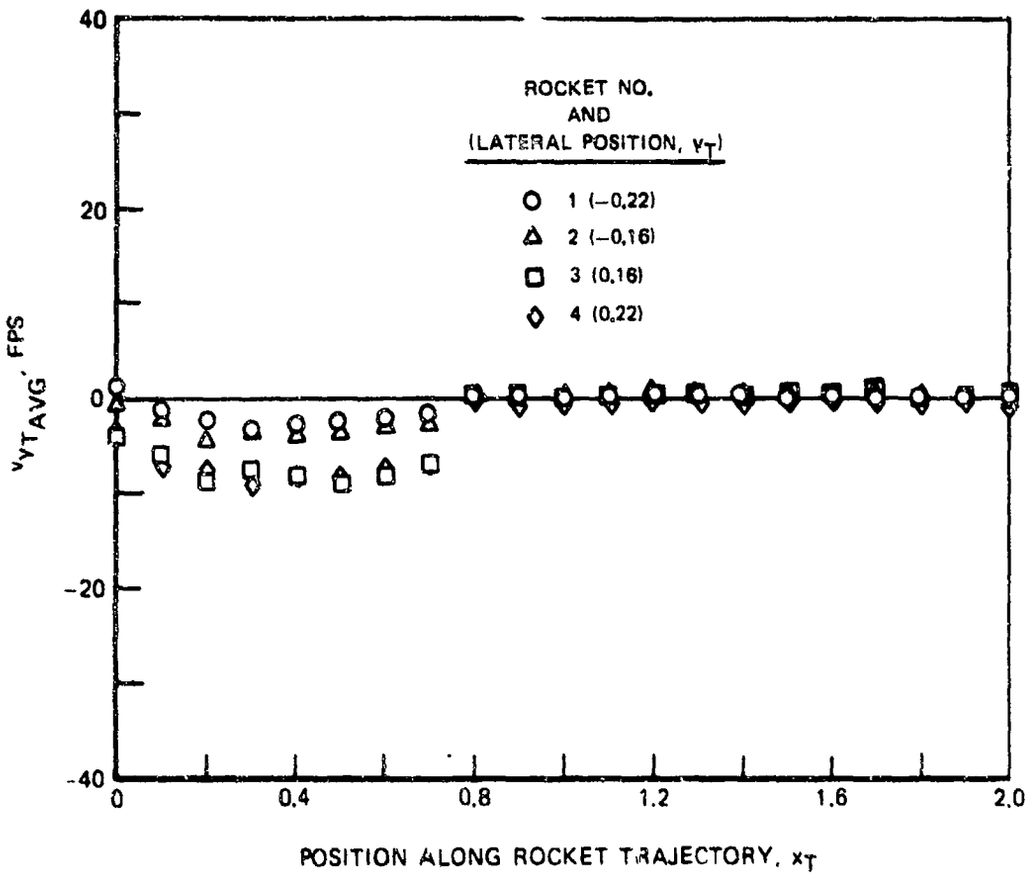

Figure 19. Variation of Time-Averaged v_{yT} Velocity Component Along the Four Rocket Trajectories -- 0 Kt, Distorted Wake.

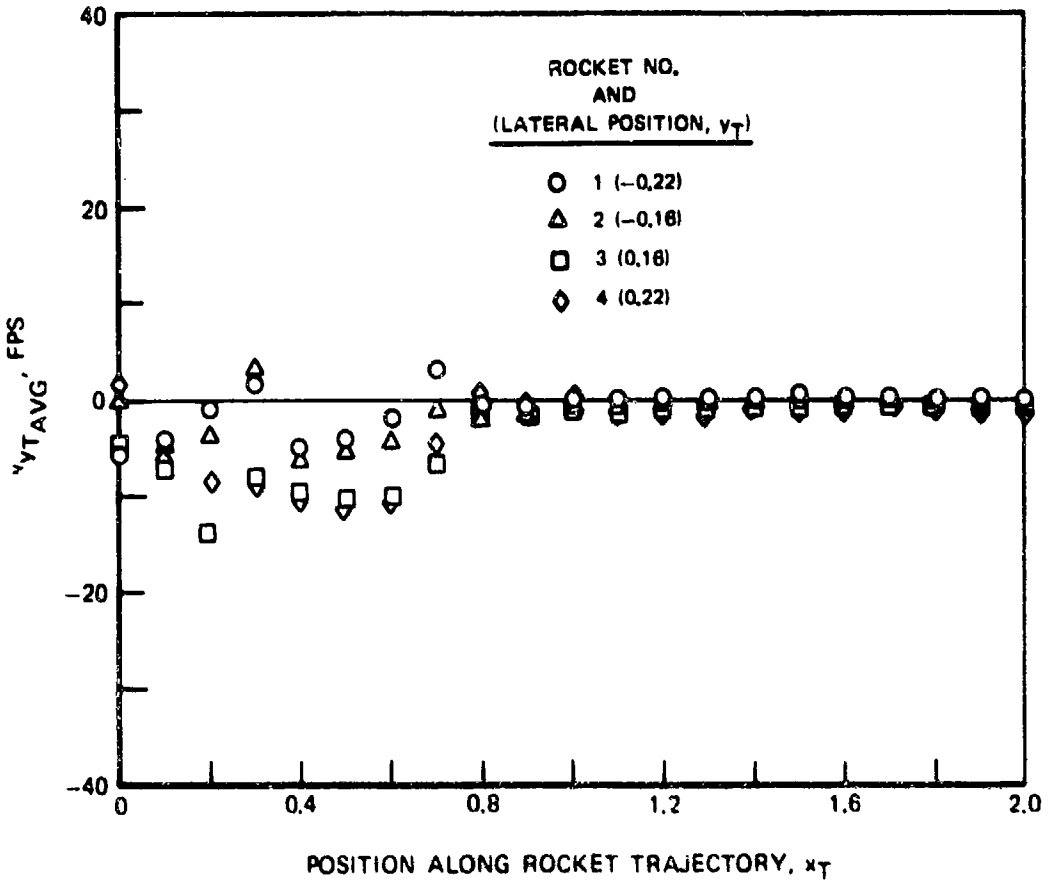

Figure 20. Variation of Instantaneous v_{y_T} Velocity Component Along the Four Rocket Trajectories for One Rotor Position -- 0 Kt, Distorted Wake, Rotor Position 1 (Ψ = 0, 180 Deg).

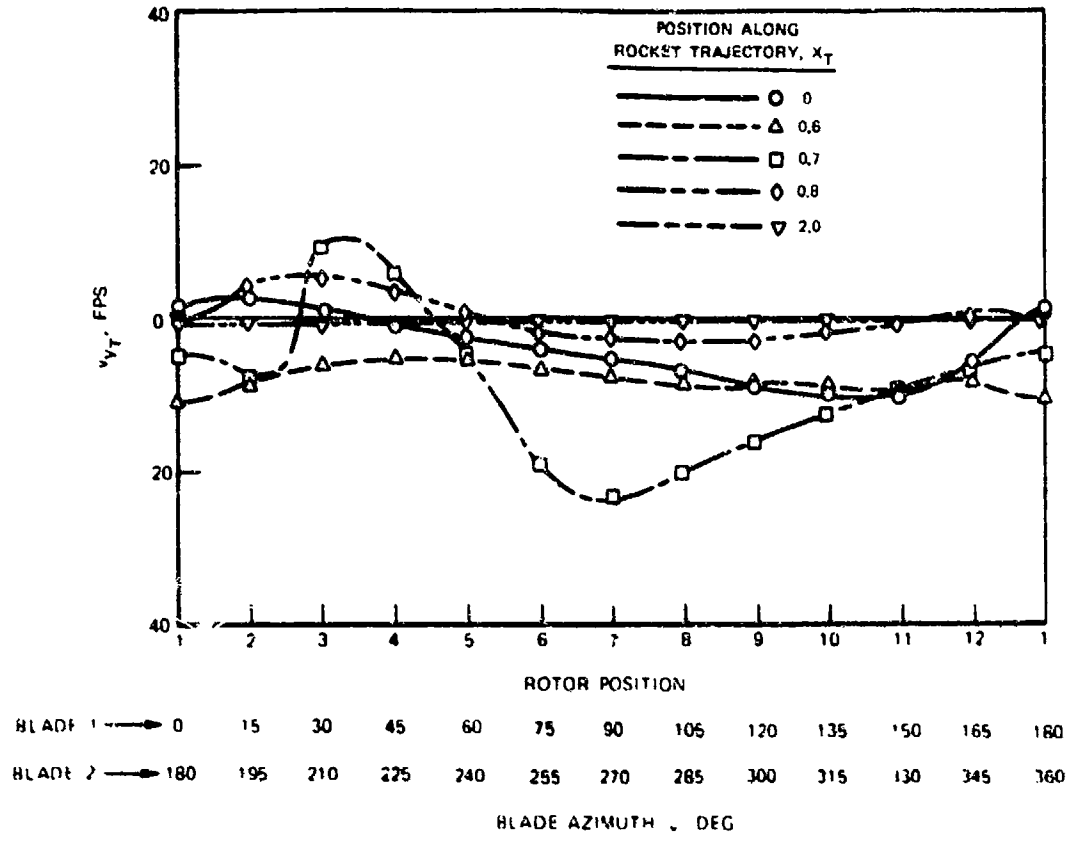

Figure 21. Variation of Instantaneous v_{y_T} Velocity Component With Rotor Position for Selected Points on One Rocket Trajectory -- 0 Kt, Distorted Wake, Rocket No. 4 (y_T = 0.22).

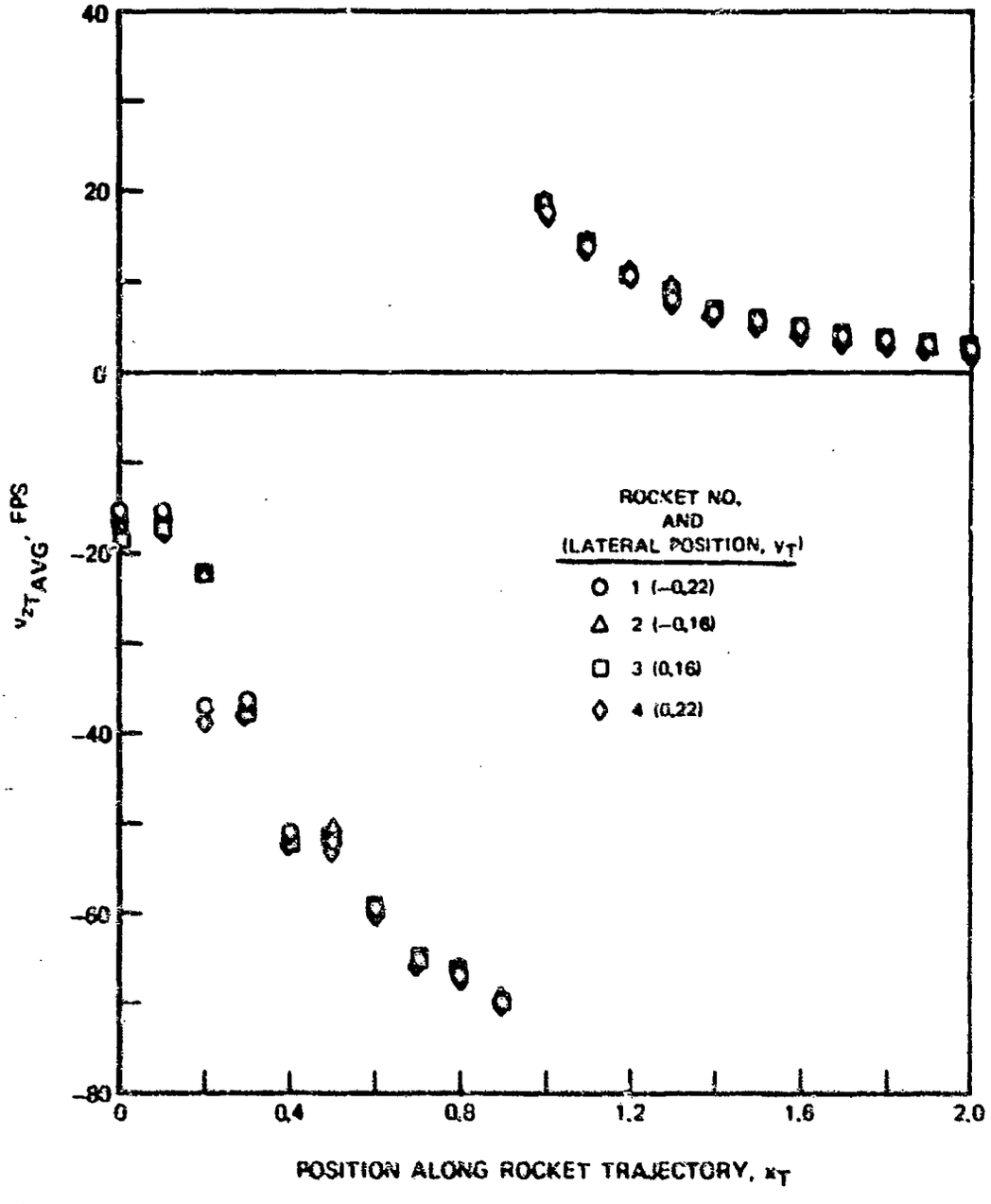

Figure 22. Variation of Time-Averaged v_{z_T} Velocity Component Along the Four Rocket Trajectories -- 0 Kt, Undistorted Wake.

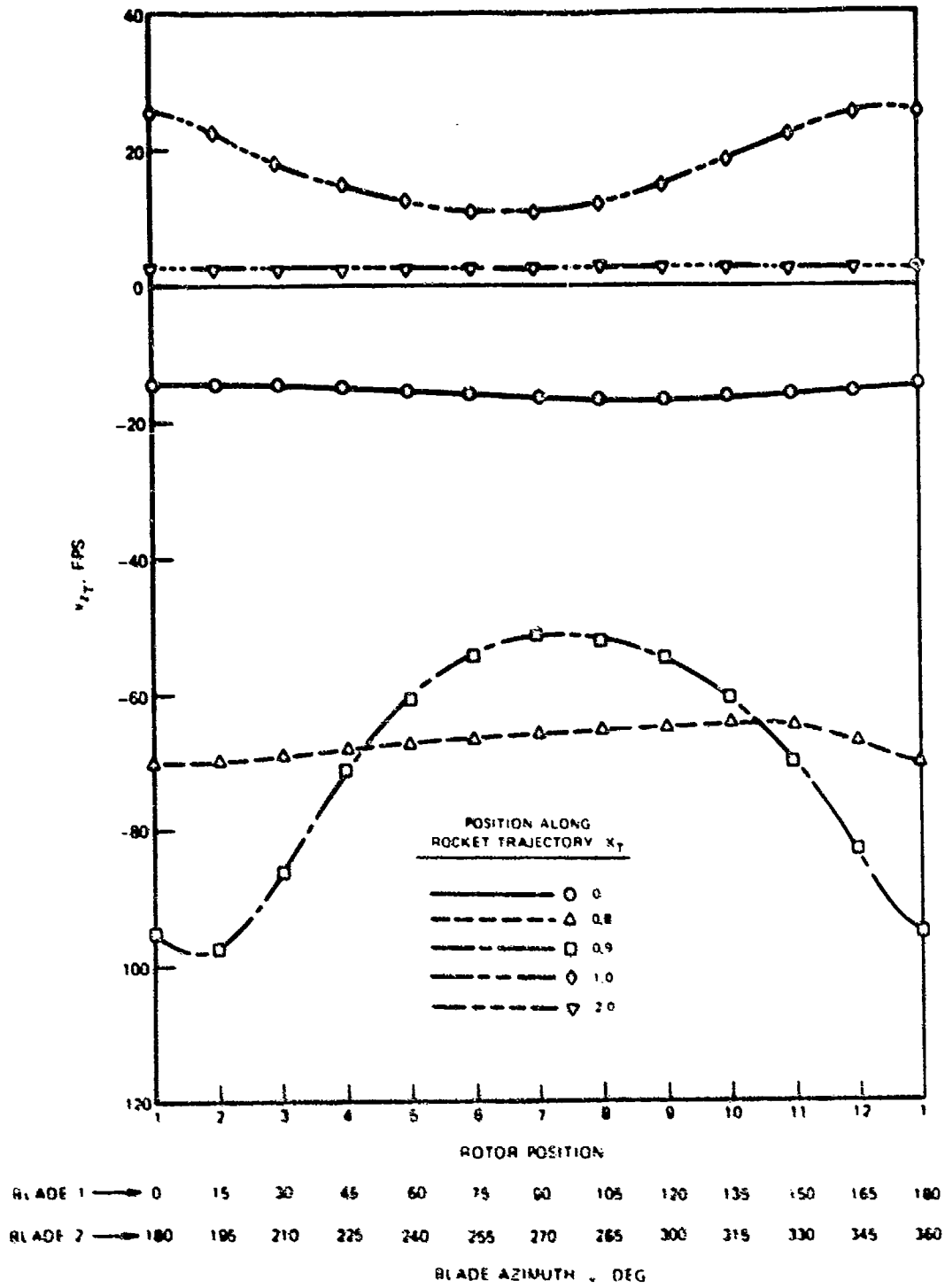

Figure 23. Variation of Instantaneous v_{zT} Velocity Component With Rotor Position for Selected Points on One Rocket Trajectory -- 0 Kt, Undistorted Wake, Rocket No. 4 (y_T = 0.22).

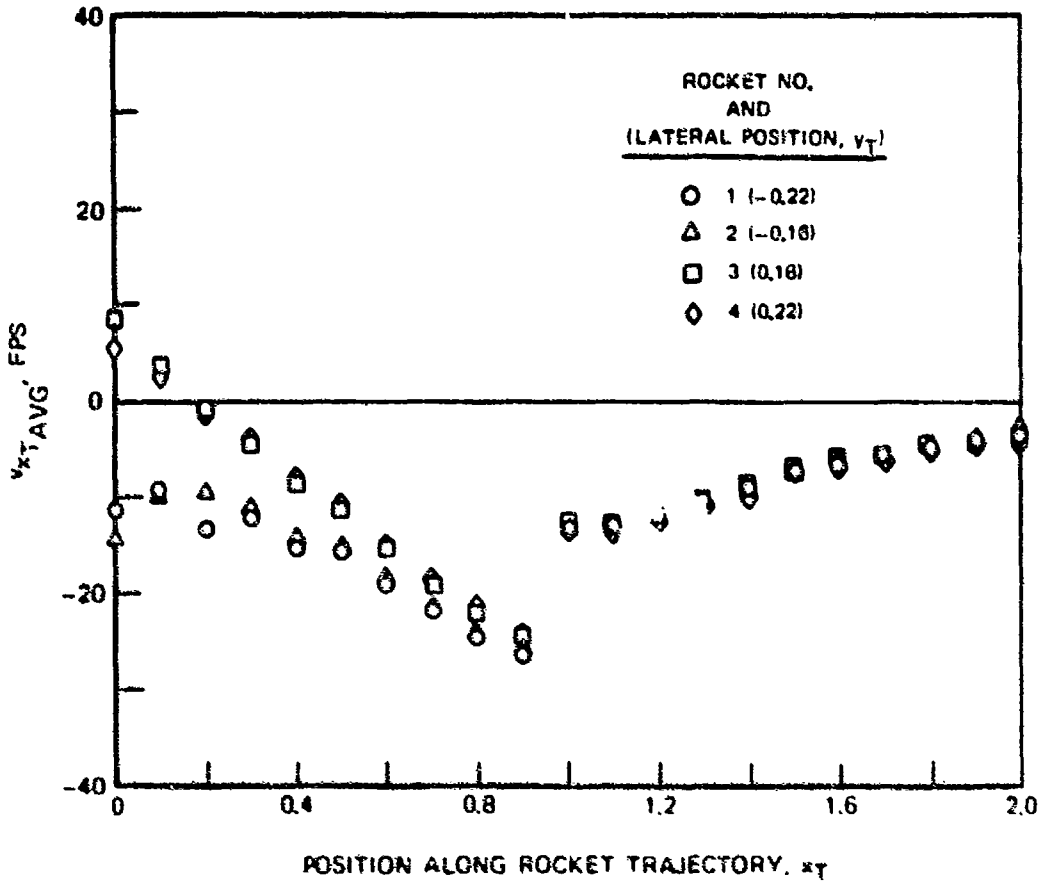

Figure 24. Variation of Time-Averaged v_{x_T} Velocity Component Along the Four Rocket Trajectories -- 0 Kt, Undistorted Wake.

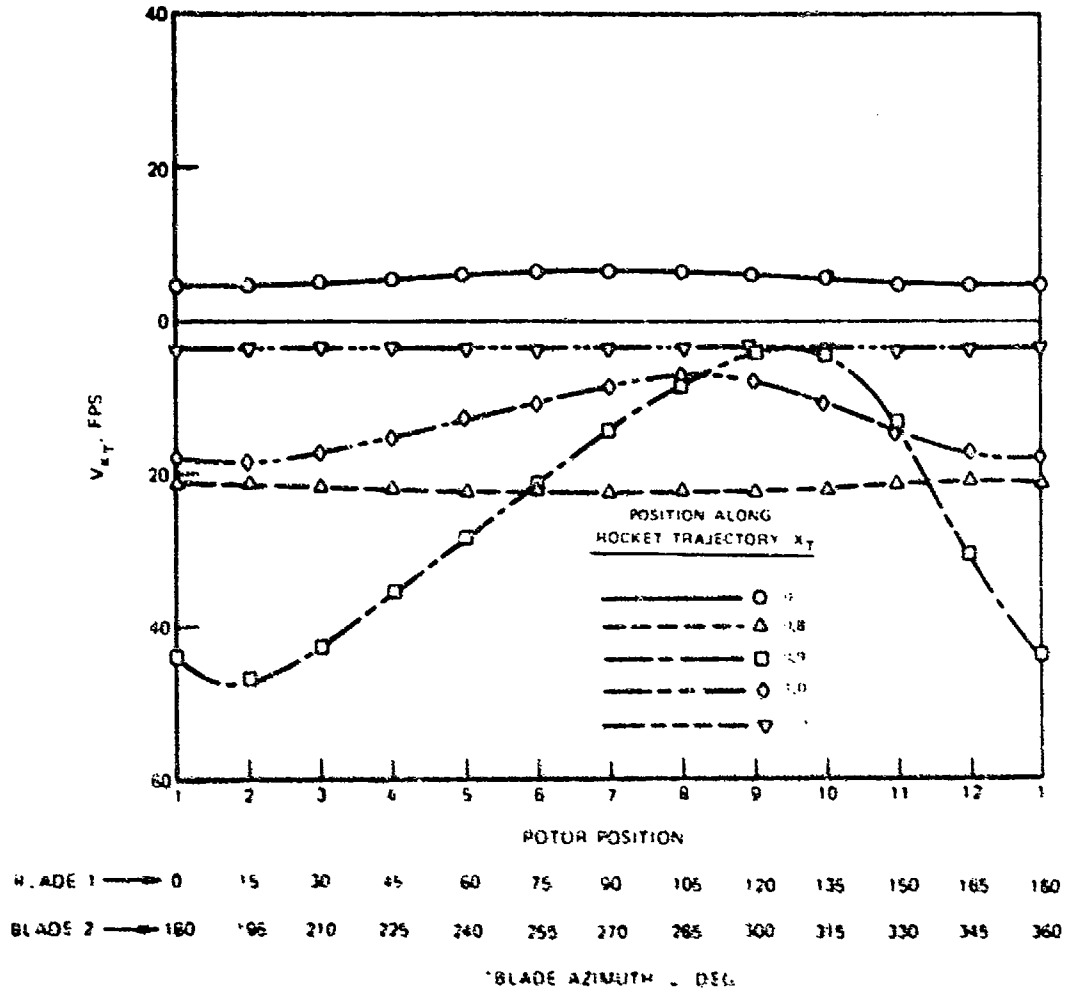

Figure 25. Variation of Instantaneous v_{xT} Velocity Component With Rotor Position for Selected Points on One Rocket Trajectory -- 0 Kt, Undistorted Wake, Rocket No. 4 (y_T = 0.22).

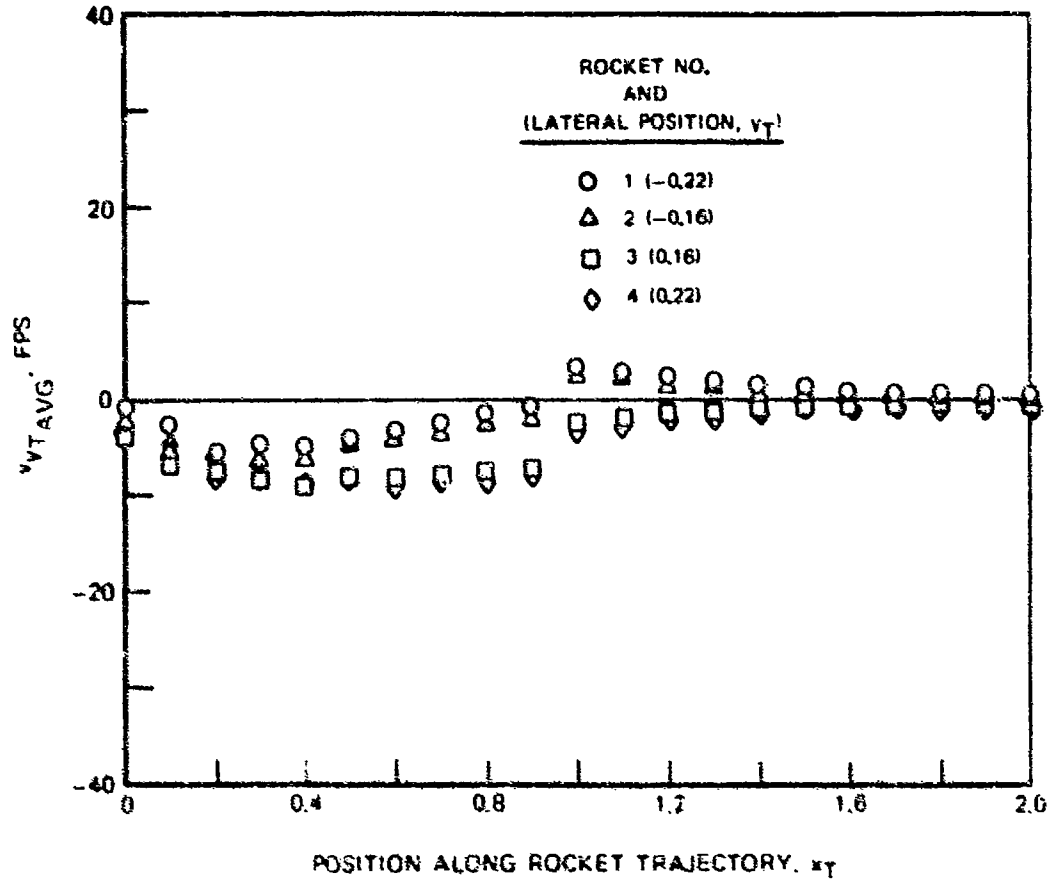

Figure 26. Variation of Time-Averaged v_{y_T} Velocity Component Along the Four Rocket Trajectories -- 0 Kt, Undistorted Wake.

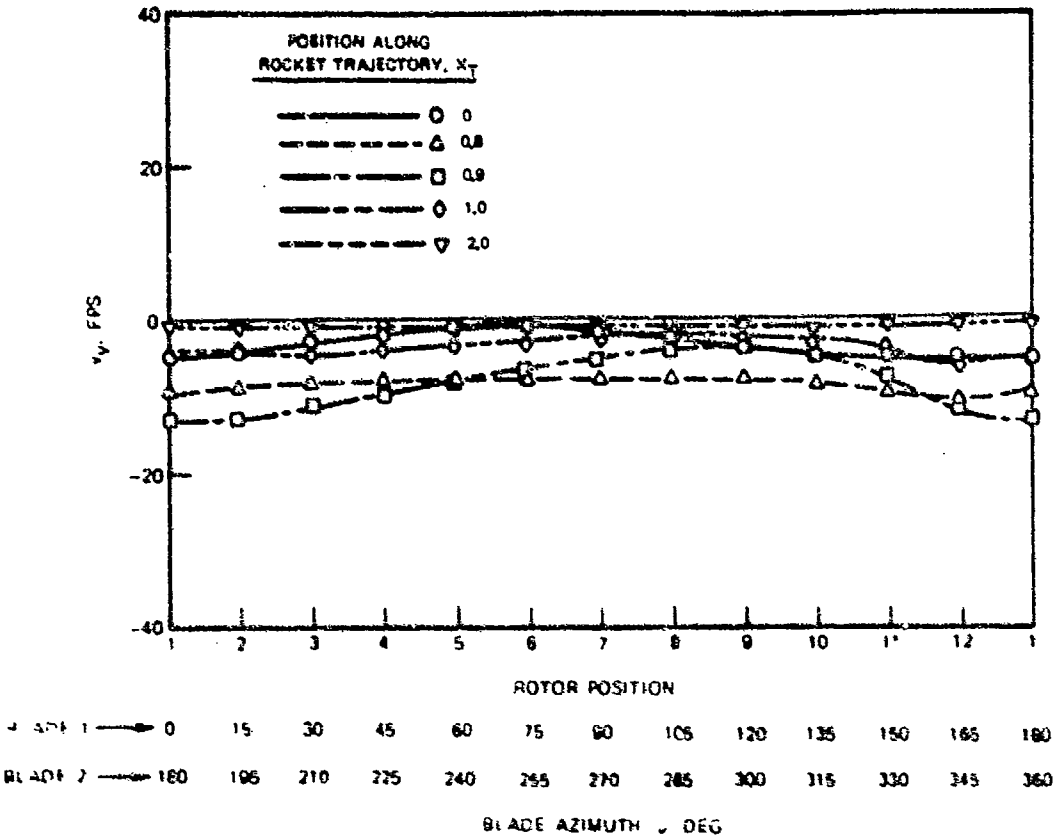

Figure 27. Variation of Instantaneous v_T Velocity Component With Rotor Position for Selected Points on One Rocket Trajectory -- 0 Kt, Undistorted Wake, Rocket No. 4 (y_T = 0.22).

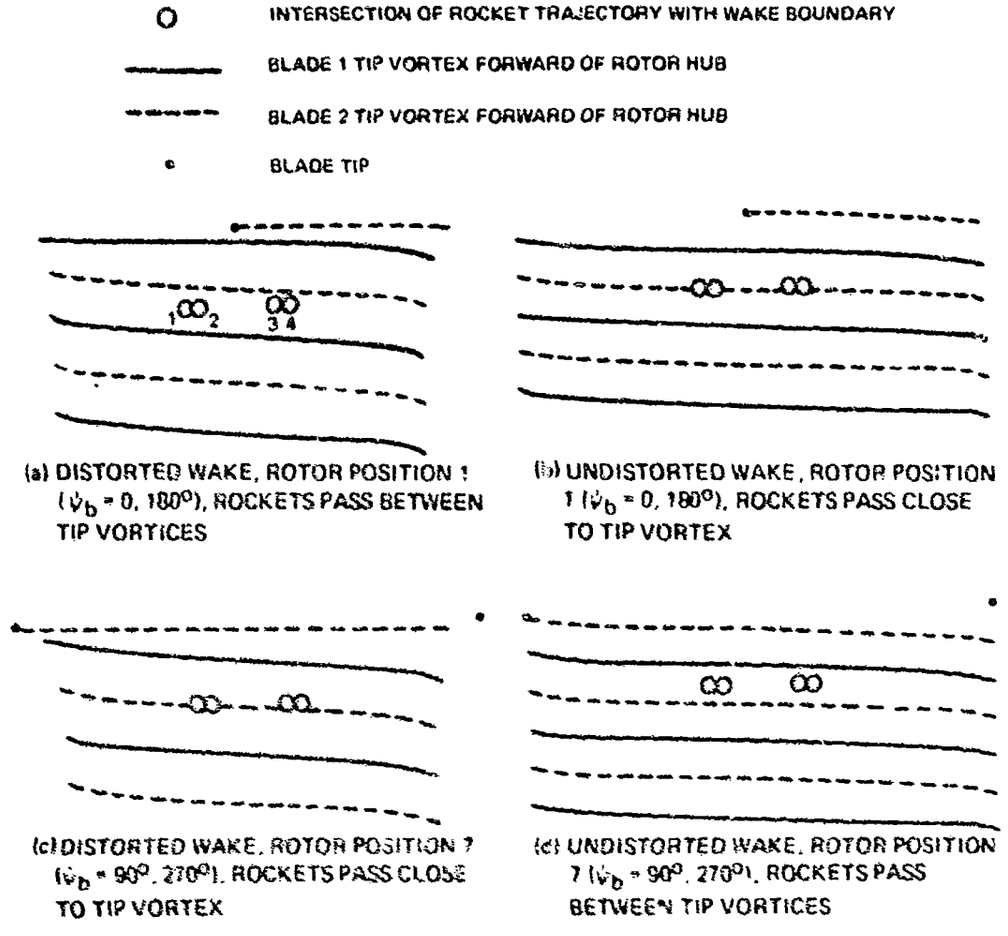

Figure 26. Relative Positions of Rocket Trajectories to Tip Vortices at Intersections With Forward Wake Boundary.

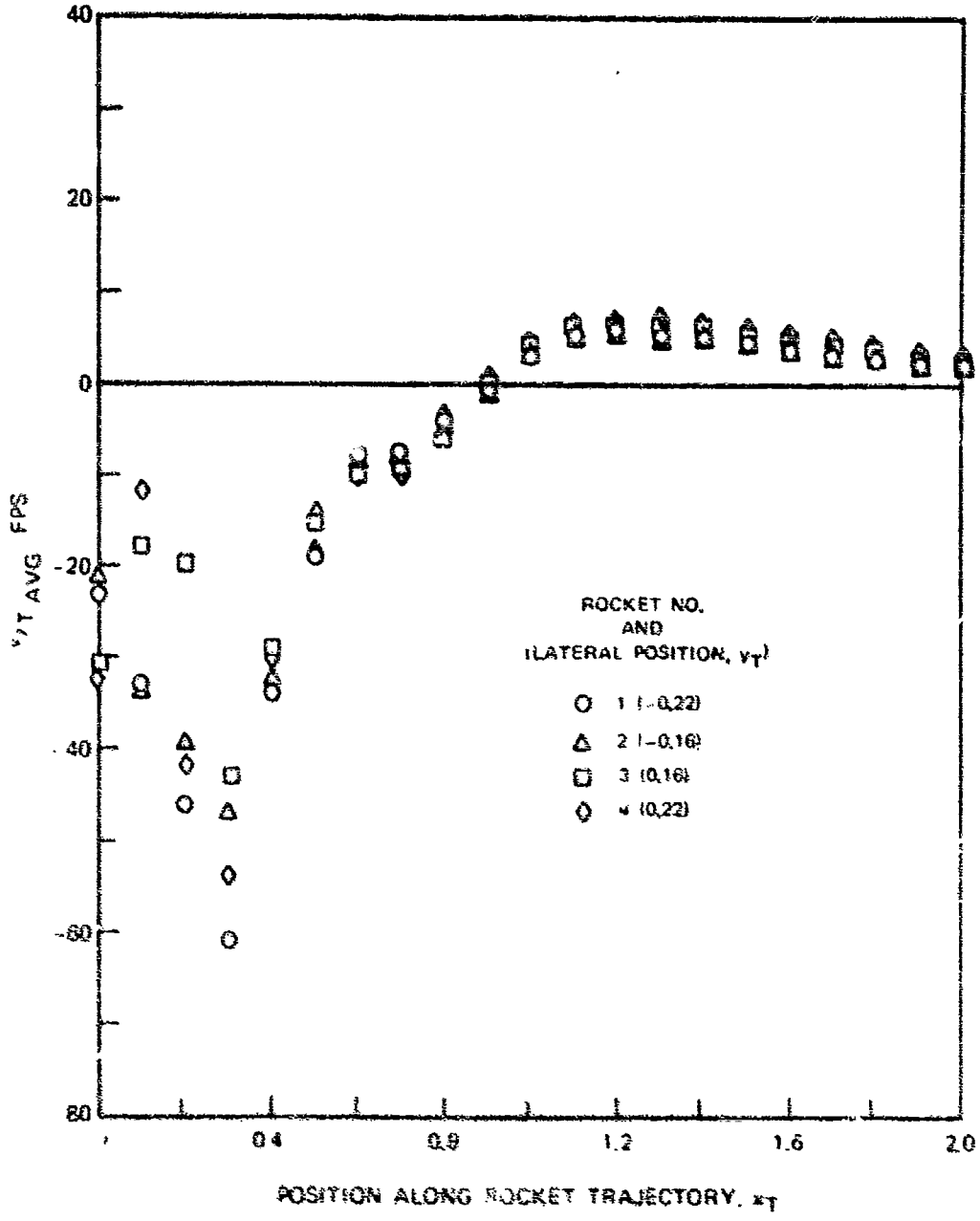

Figure 29. Variation of Time-Averaged v_T Velocity Component Along the Four Rocket Trajectories -- 15 Kt, Distorted Wake.

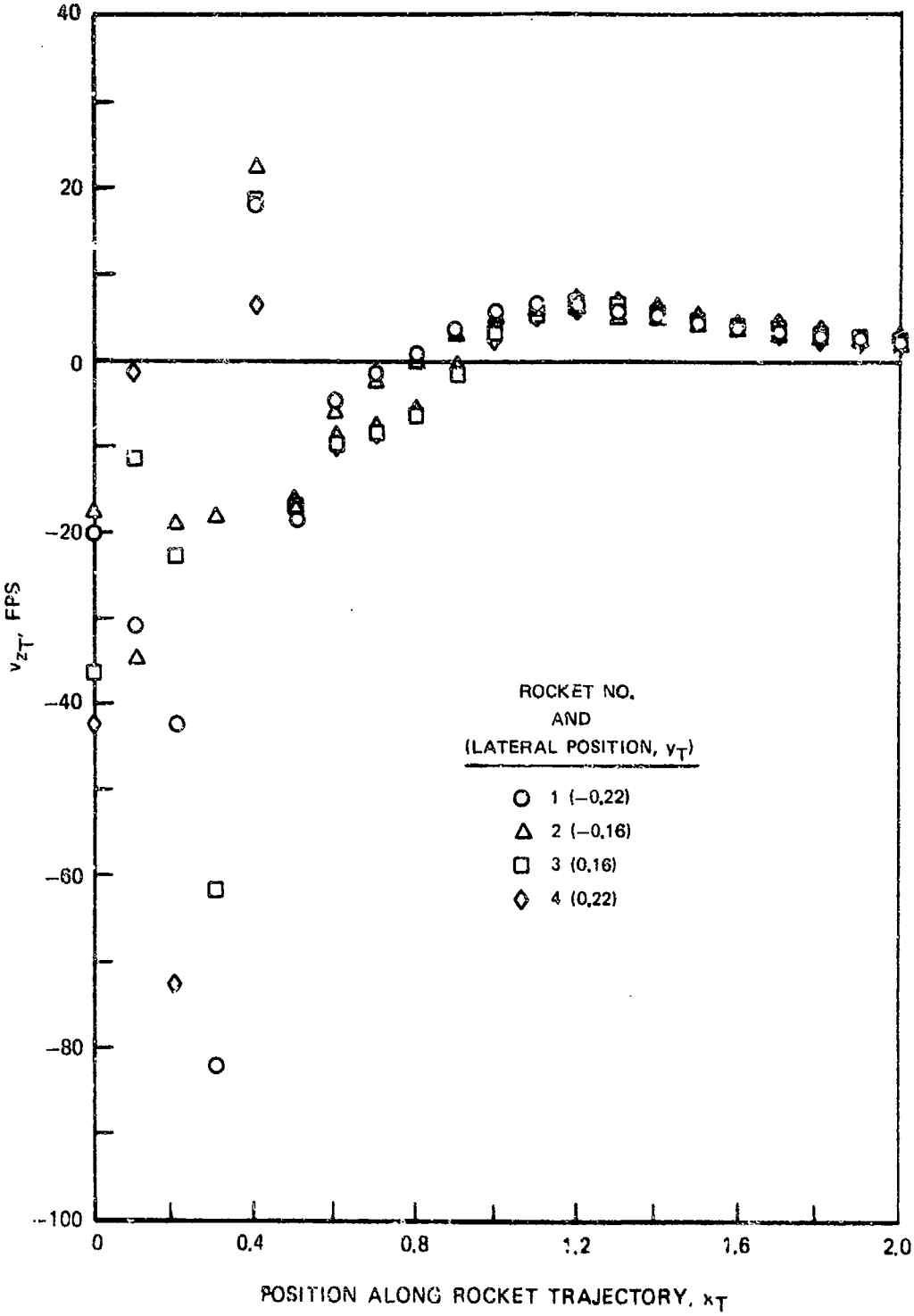

Figure 30. Variation of Instantaneous v_{Z_T} Velocity Component Along the Four Rocket Trajectories for One Rotor Position -- 15 Kt, Distorted Wake, Rotor Position 1 (Ψ = 0, 180 Deg).

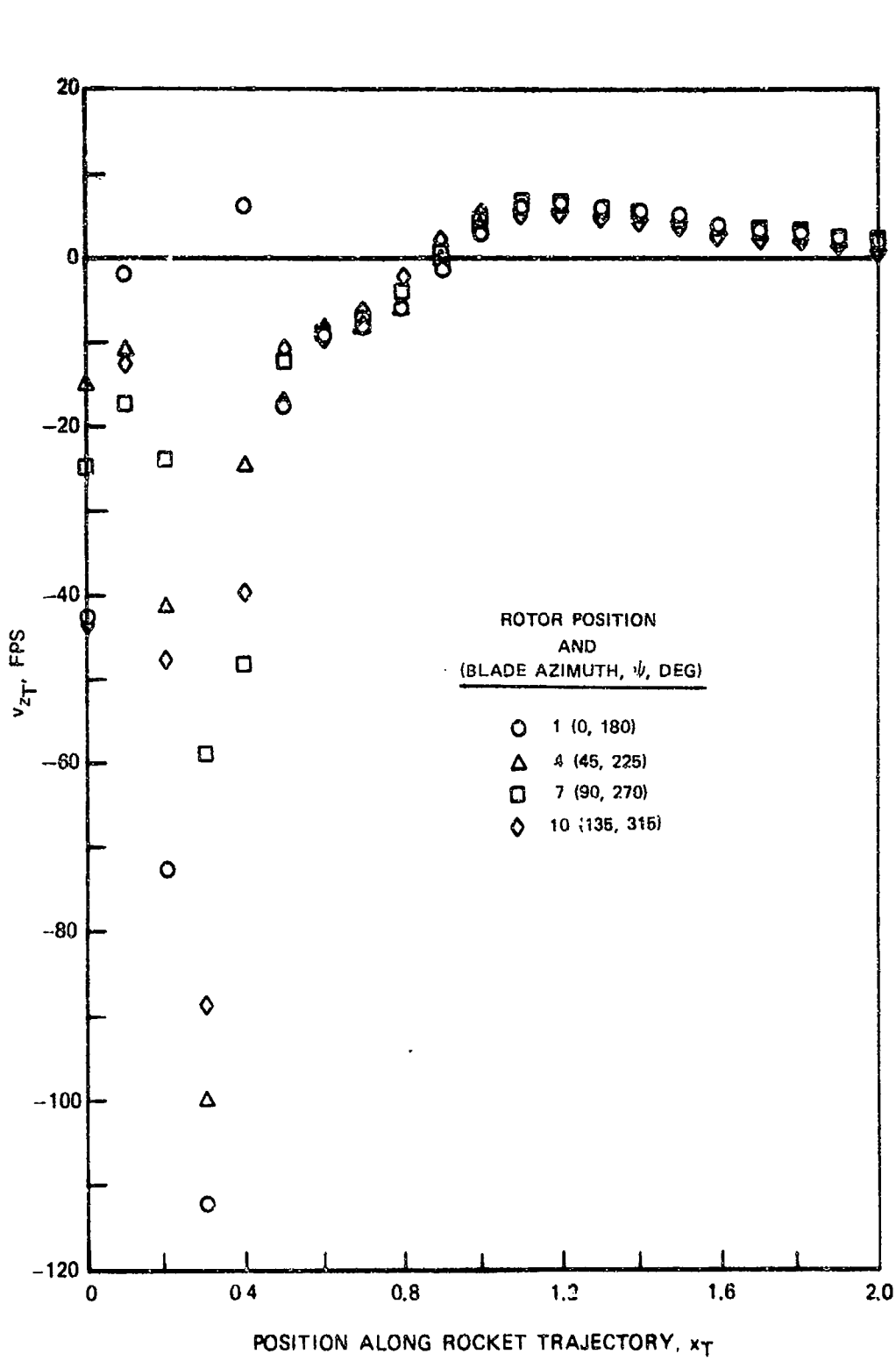

Figure 31. Variation of Instantaneous v_{z_T} Velocity Component Along One Rocket Trajectory for Selected Rotor Positions -- 15 Kt, Distorted Wake, Rocket No. 4 (y_T = 0.22).

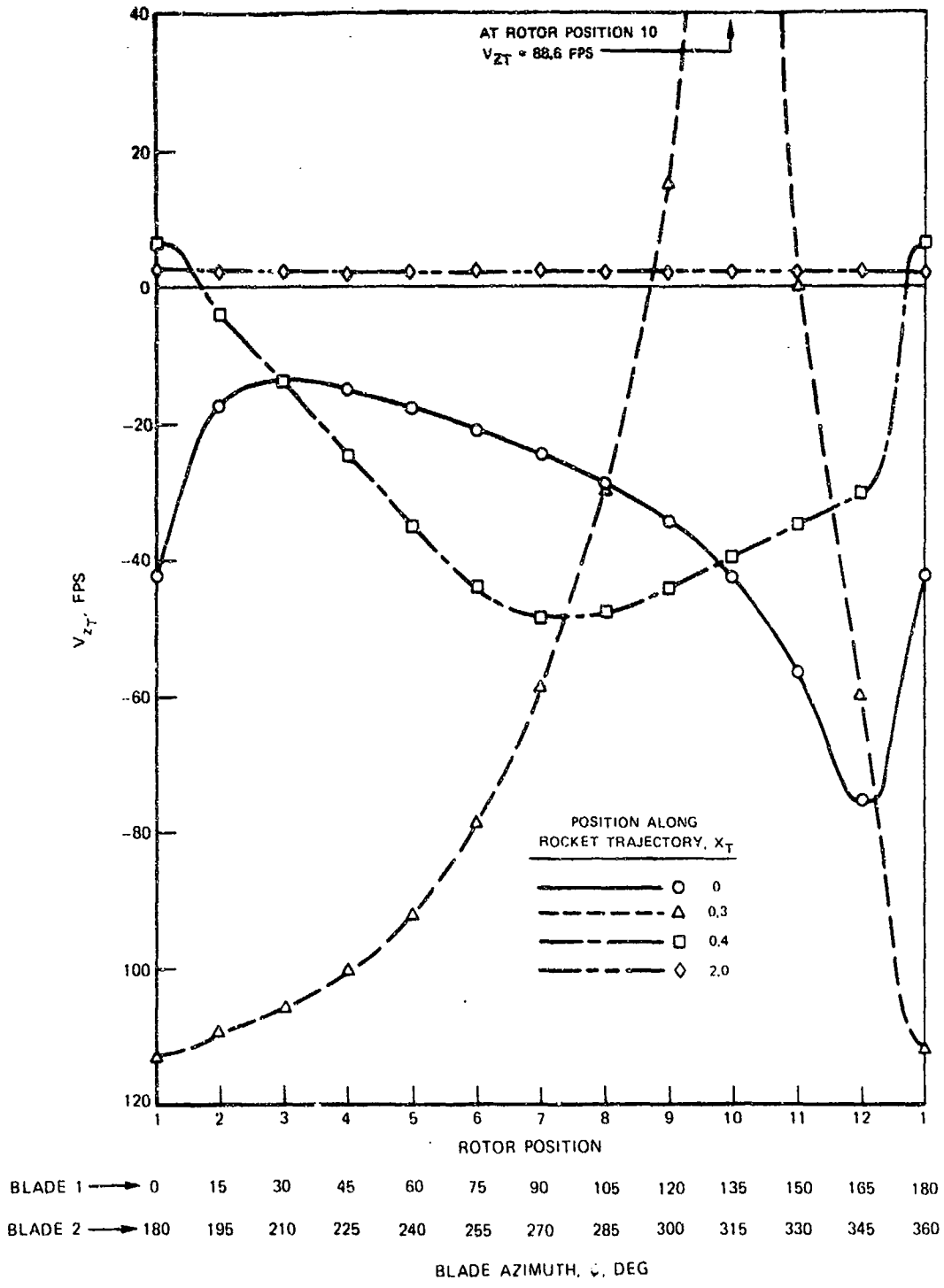

Figure 32. Variation of Instantaneous v_{z_T} Velocity Component With Rotor Position for Selected Points on One Rocket Trajectory -- 15 Kt, Distorted Wake, Rocket No. 4 (y_T = 0.22).

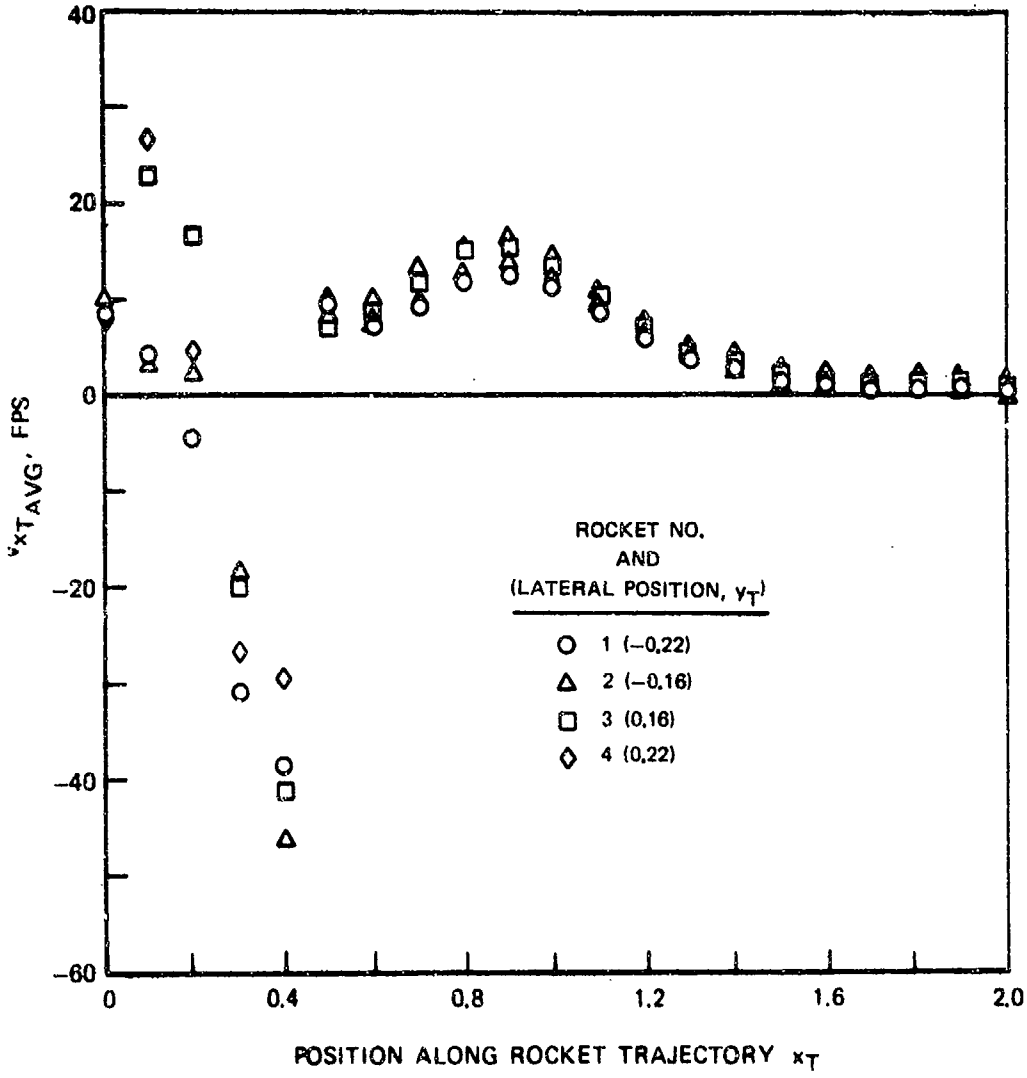

Figure 33. Variation of Time-Averaged v_{x_T} Velocity Component Along the Four Rocket Trajectories -- 15 Kt, Distorted Wake.

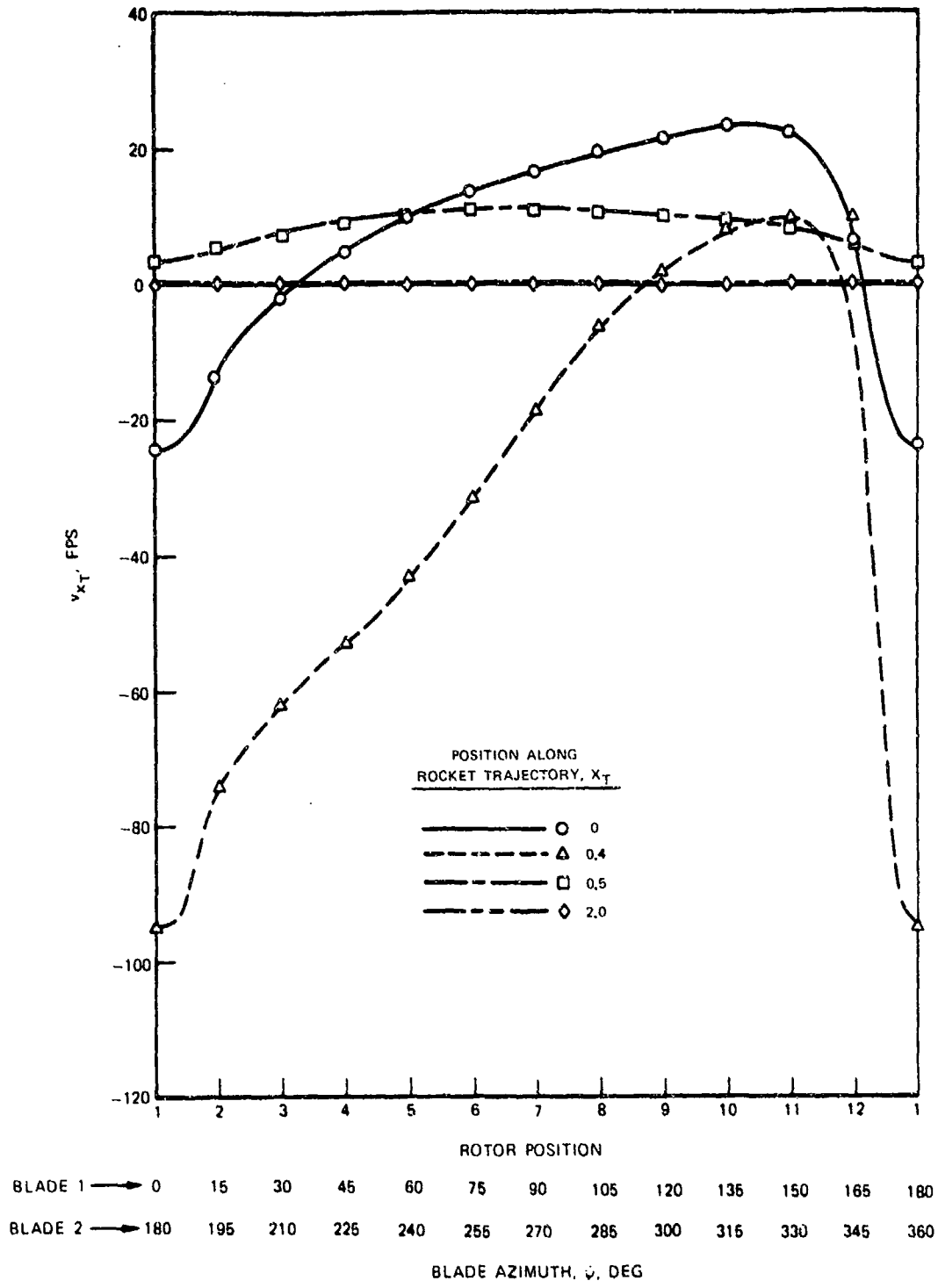

Figure 34. Variation of Instantaneous v_{X_T} Velocity Component With Rotor Position for Selected Points on One Rocket Trajectory -- 15 Kt, Distorted Wake, Rocket No. 4 (y_T = 0.22).

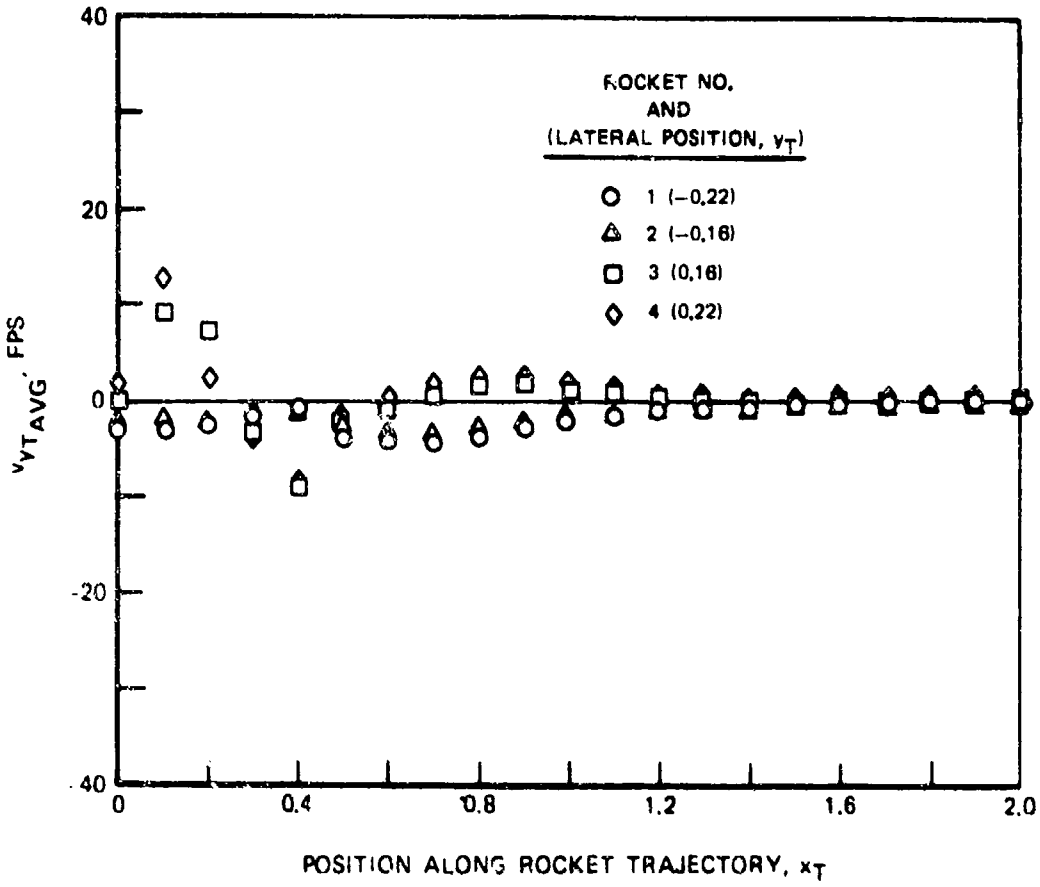

Figure 35. Variation of Time-Averaged v_{y_T} Velocity Component Along the Four Rocket Trajectories -- 15 Kt, Distorted Wake.

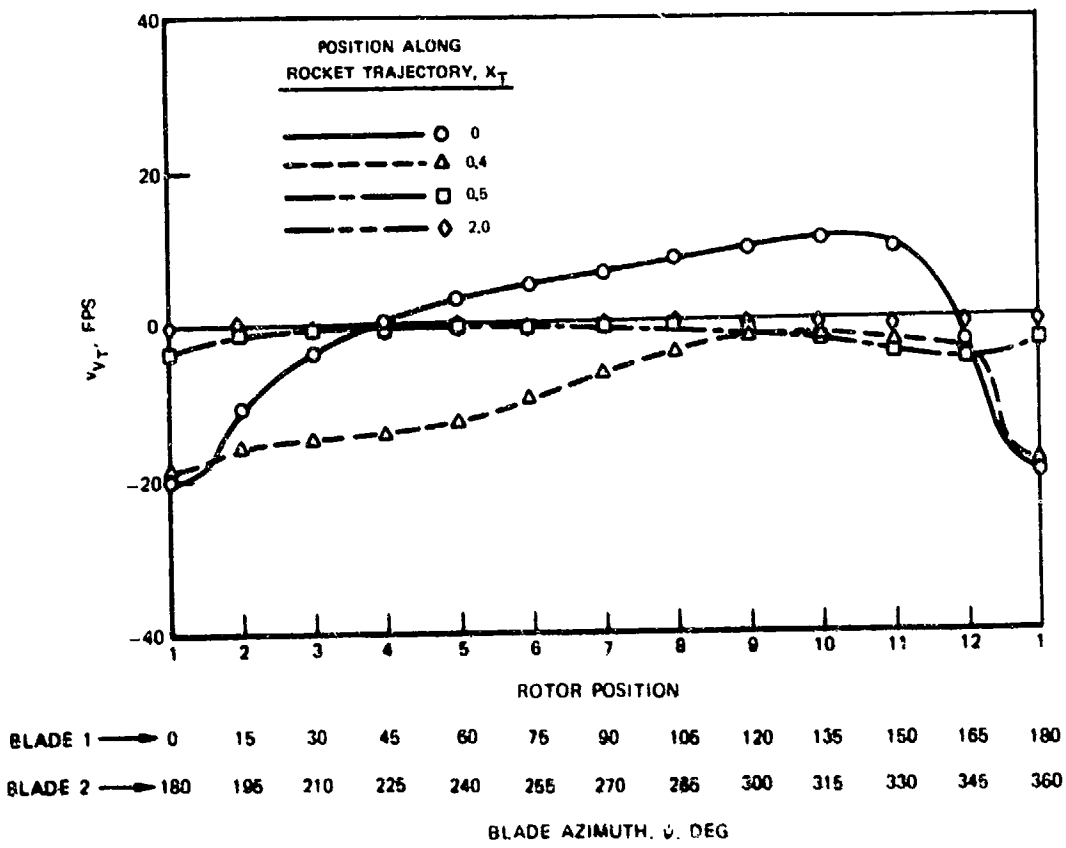

Figure 36. Variation of Instantaneous v_{y_T} Velocity Component With Rotor Position for Selected Points on One Rocket Trajectory -- 15 Kt, Distorted Wake, Rocket No. 4 (y_T = 0.22).

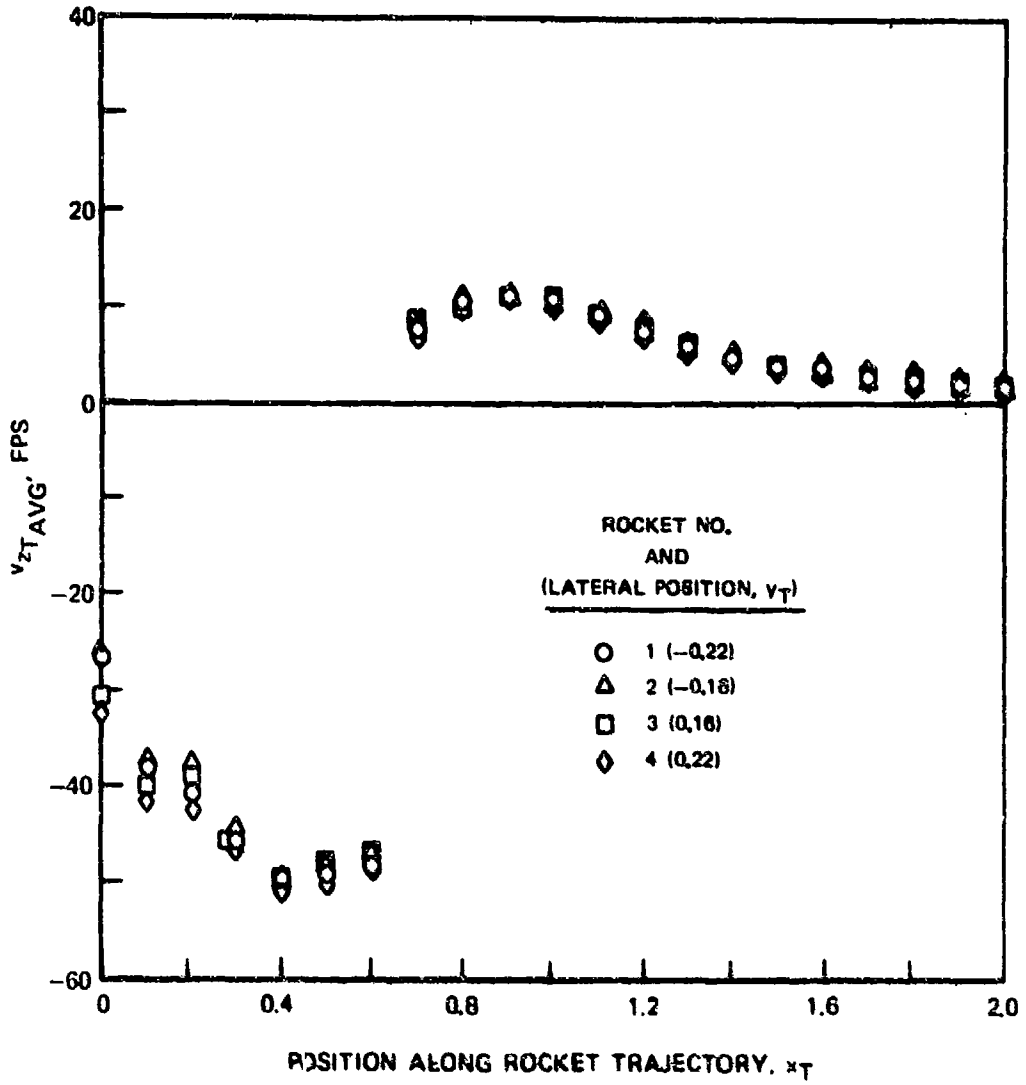

Figure 37. Variation of Time-Averaged v_{zT} Velocity Component Along the Four Rocket Trajectories -- 15 Kt, Undistorted Wake.

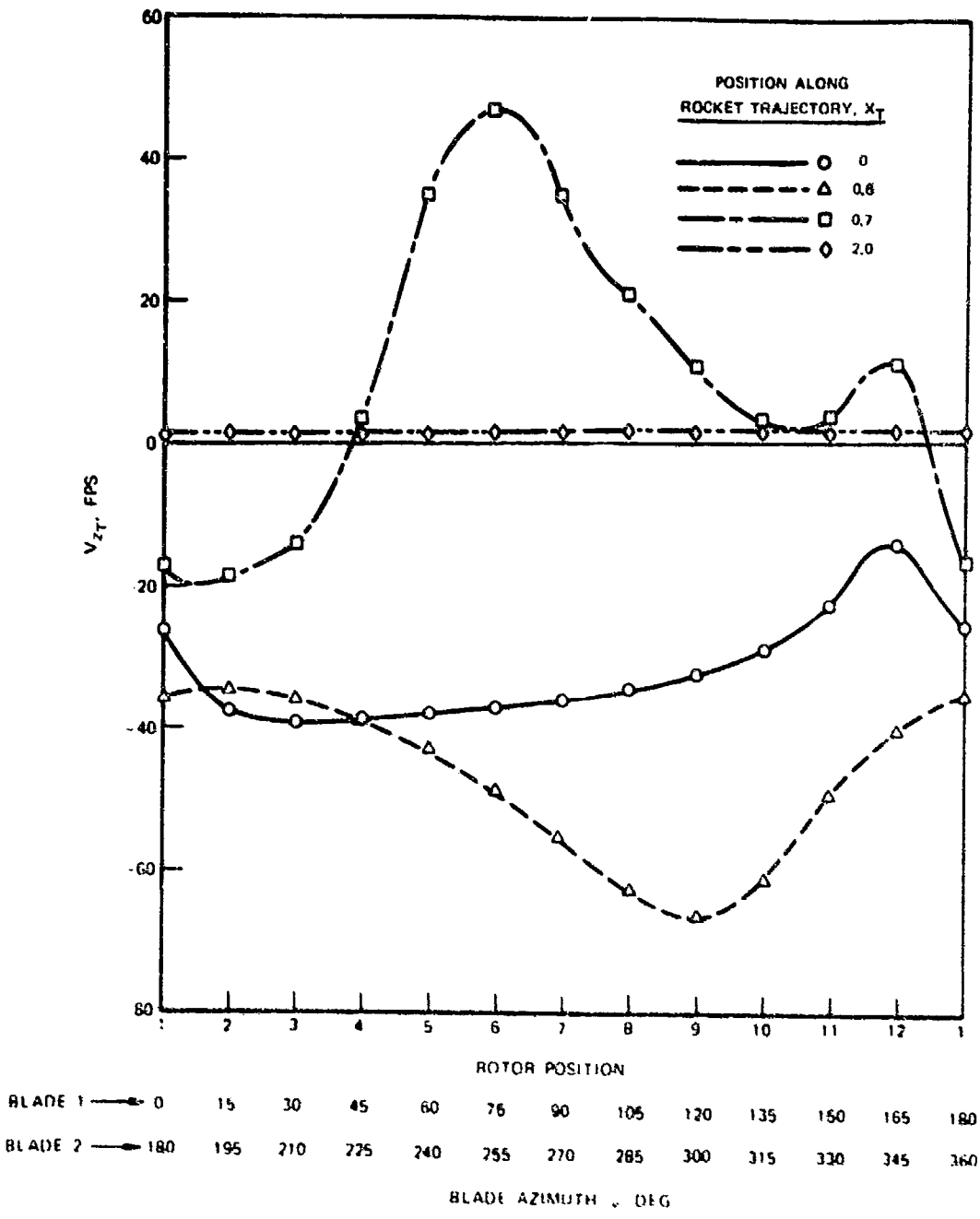

Figure 38. Variation of Instantaneous v_{z_T} Velocity Component With Rotor Position for Selected Points on One Rocket Trajectory -- 15 Kt, Undistorted Wake, Rocket No. 4 (y_T = 0.22).

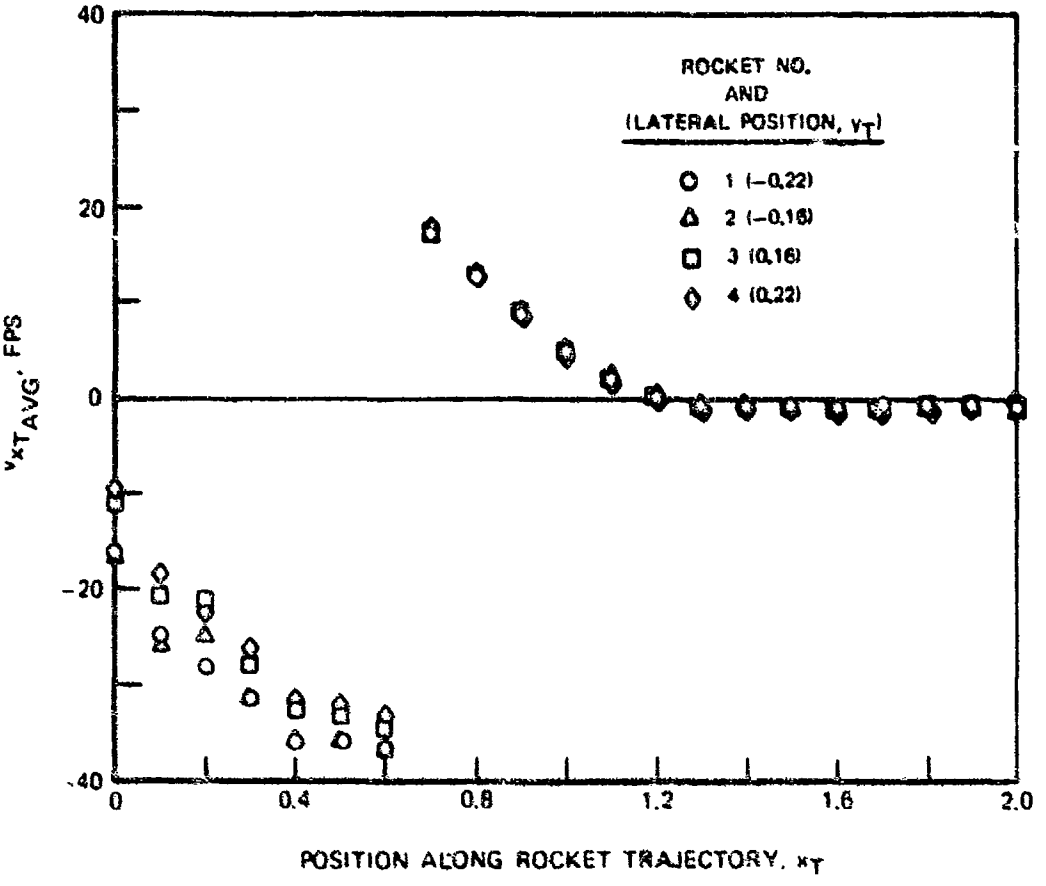

Figure 39. Variation of Time-Averaged v_{x_T} Velocity Component Along the Four Rocket Trajectories -- 15 Kt, Undistorted Wake.

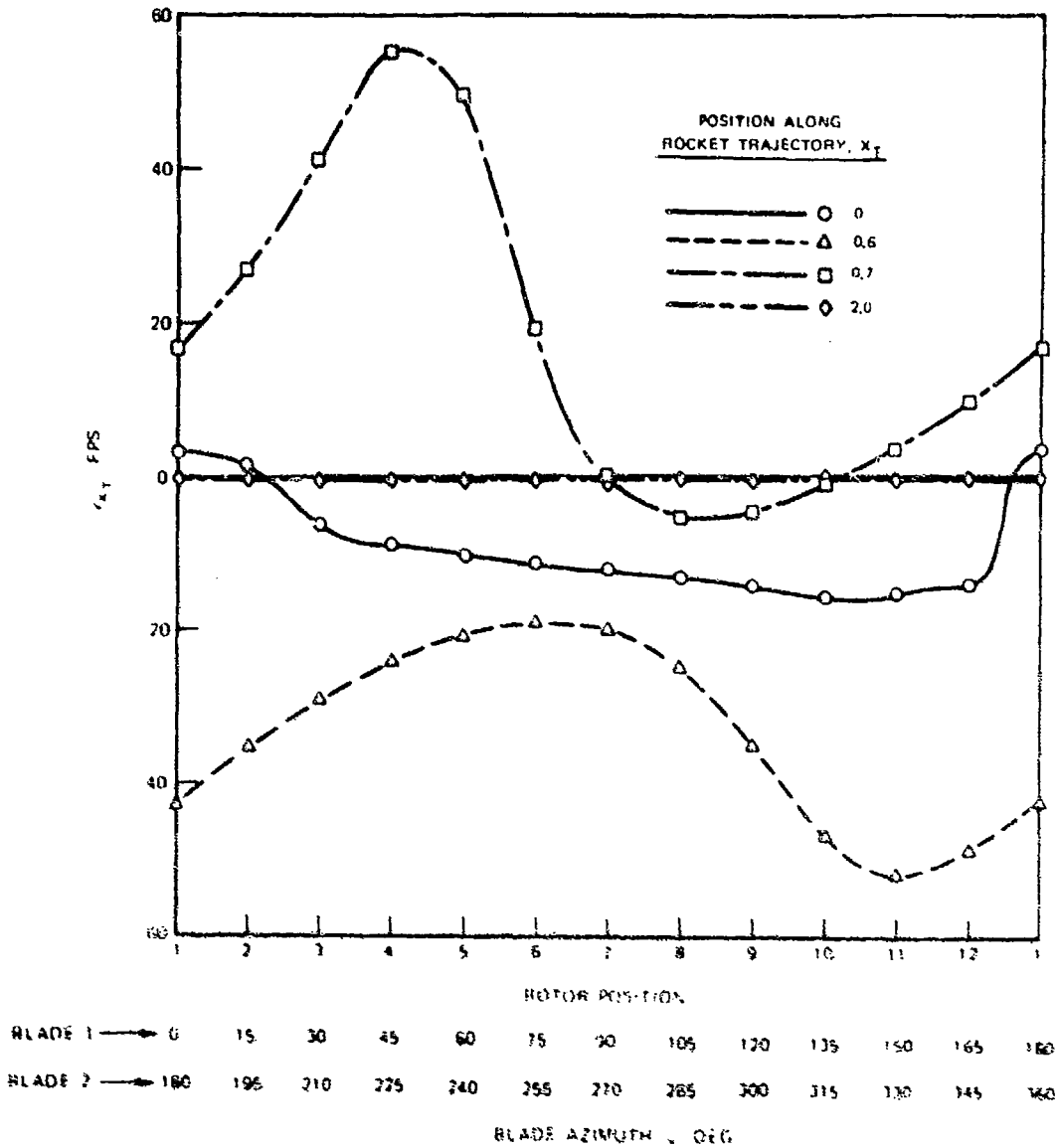

Figure 40. Variation of Instantaneous v_{x_T} Velocity Components With Rotor Position for Selected Points on One Rocket Trajectory -- 15 Kt, Undistorted Wake, Rocket No. 4 ($y_T = 0.22$).

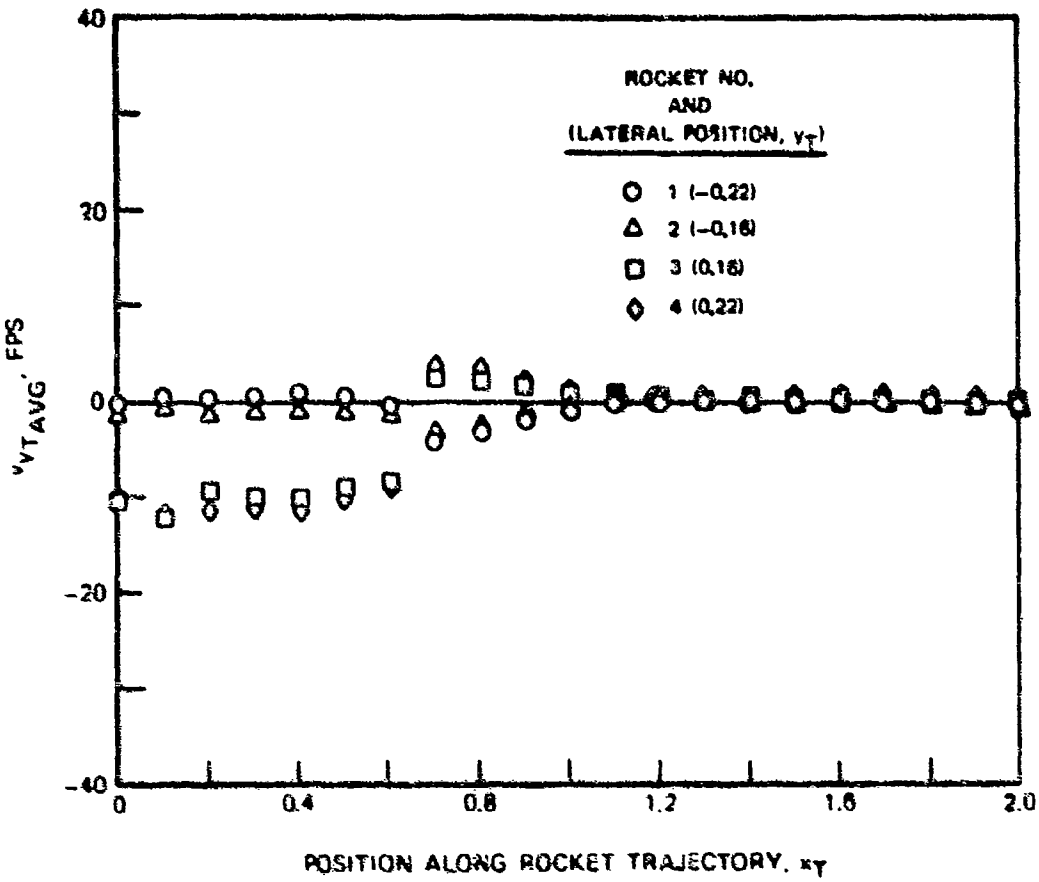

Figure 41. Variation of Time-Averaged v_{y_T} Velocity Component Along the Four Rocket Trajectories -- 15 Kt, Undistorted Wake.

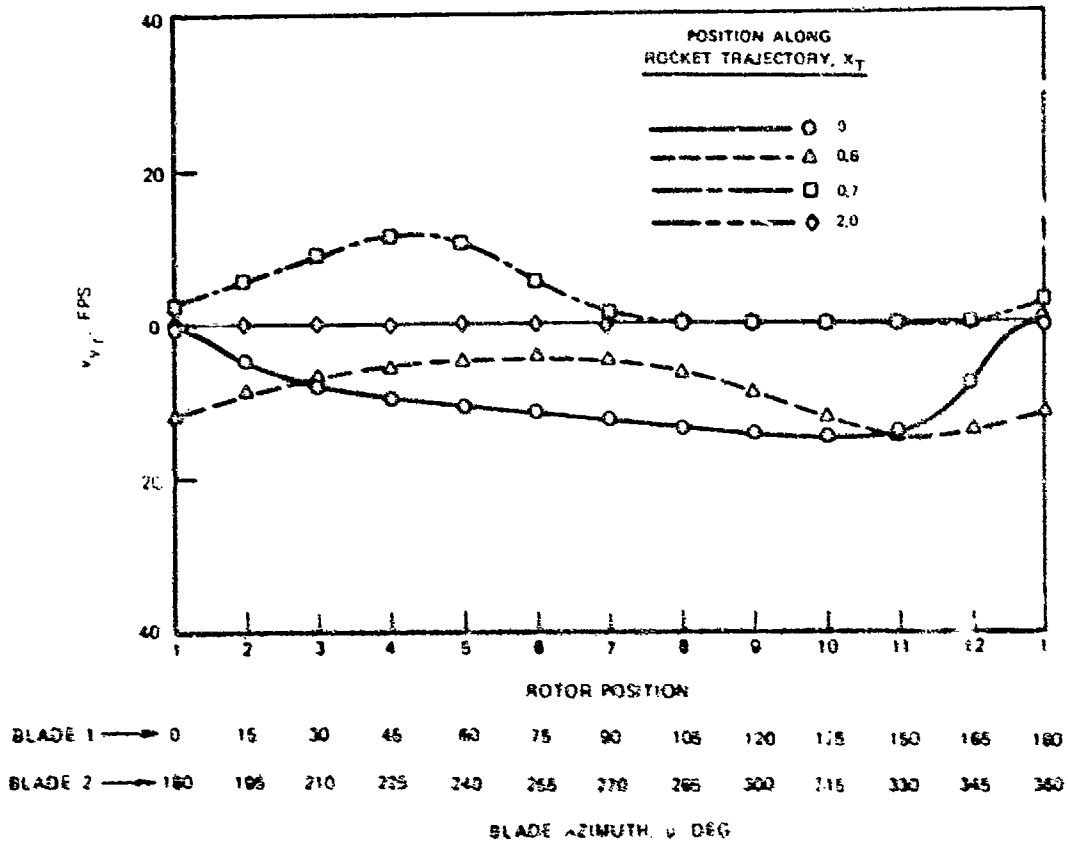

Figure 42. Variation of Instantaneous v_{y_T} Velocity Component With Rotor Position for Selected Points on One Rocket Trajectory -- 15 Kt, Undistorted Wake, Rocket No. 4 ($\bar{y}_T$ = 0.72).

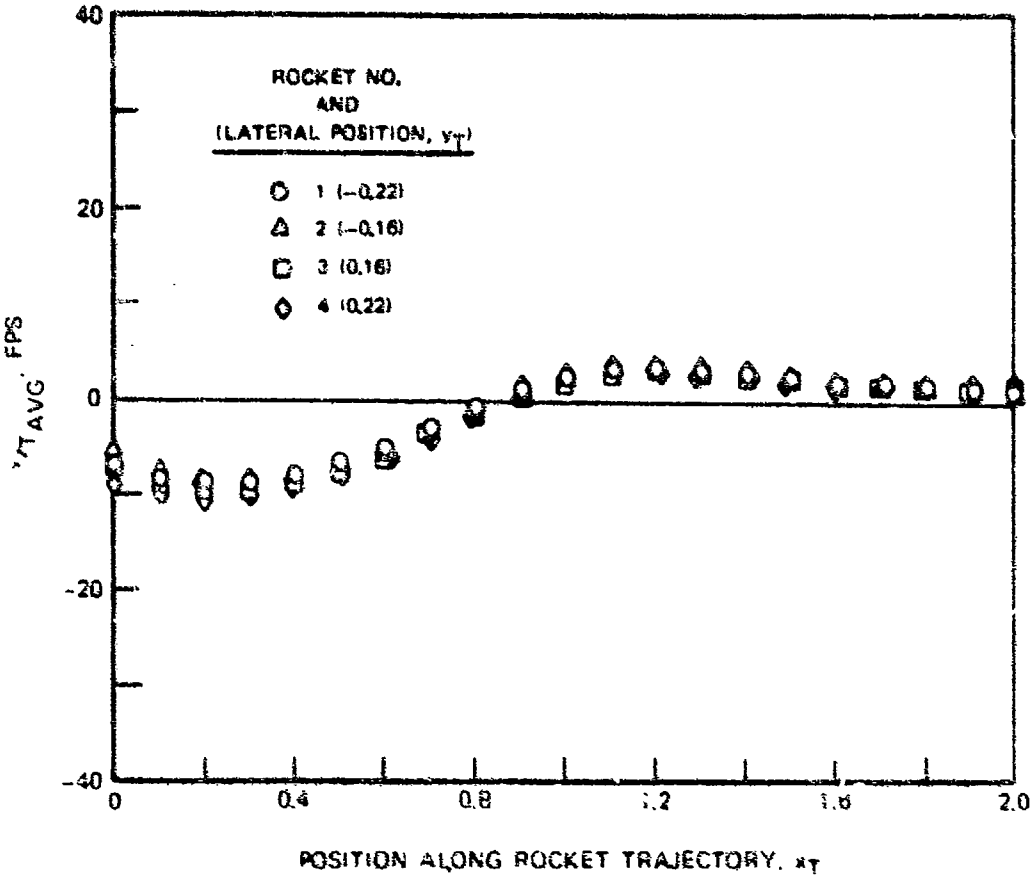

Figure 43. Variation of Time-Averaged v_T Velocity Component Along the Four Rocket Trajectories -- 30 Kt, Distorted Wake.

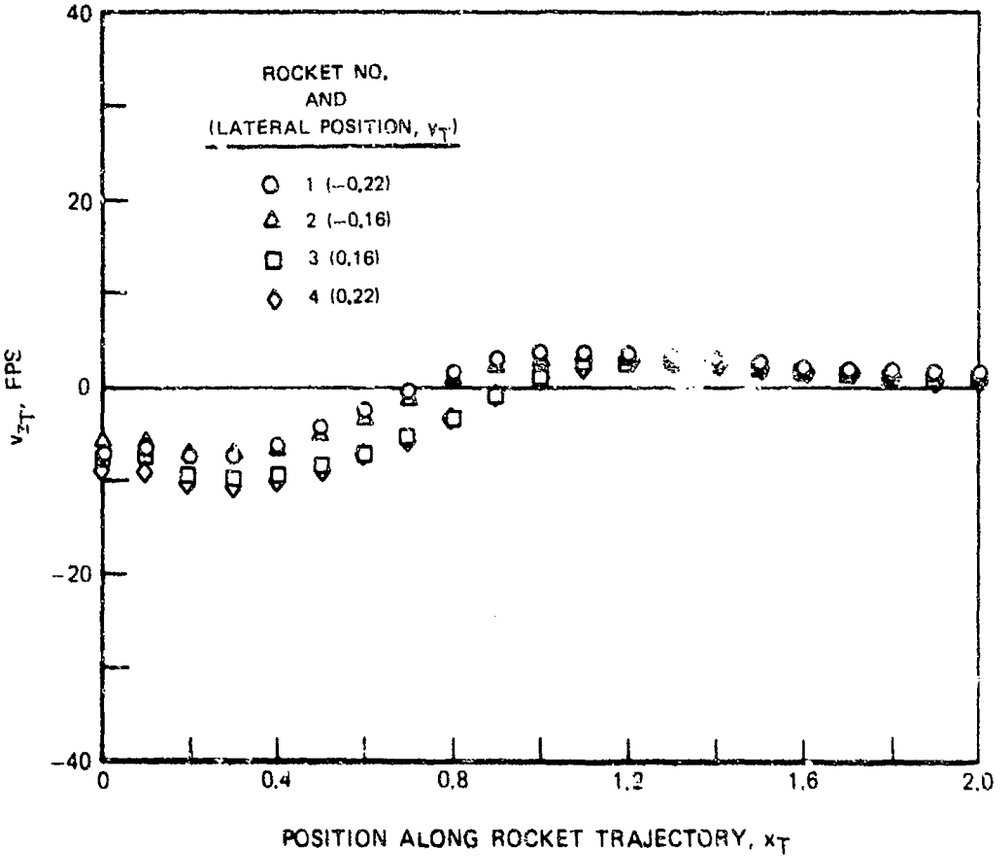

Figure 44. Variation of Instantaneous v_{z_T} Velocity Component Along the Four Rocket Trajectories for One Rotor Position -- 30 Kt, Distorted Wake, Rotor Position 1 (Ψ = 0, 180 Deg).

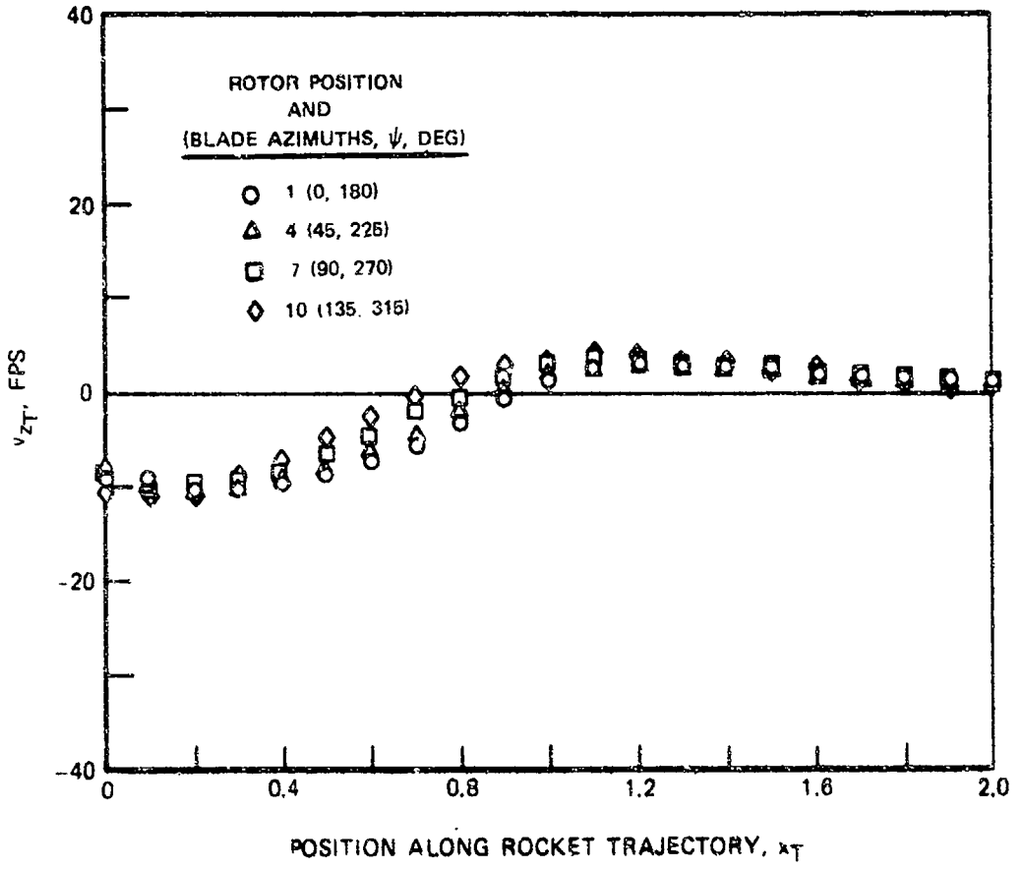

Figure 45. Variation of Instantaneous v_{z_T} Velocity Component Along One Rocket Trajectory for Selected Rotor Positions -- 30 Kt, Distorted Wake, Rocket No. 4 (y_T = 0.22).

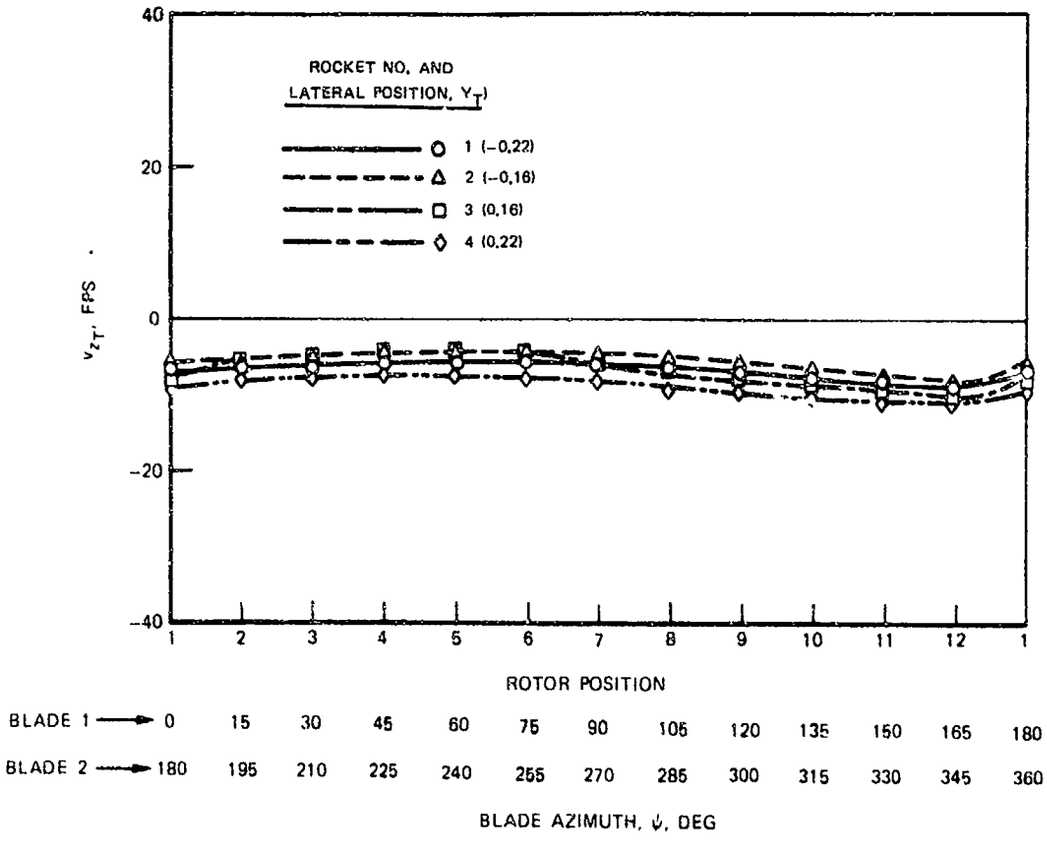

Figure 46. Variation of Instantaneous v_{z_T} Velocity Component With Rotor Position for the Four Rocket Launch Points (x_T = 0) -- 30 Kt, Distorted Wake.

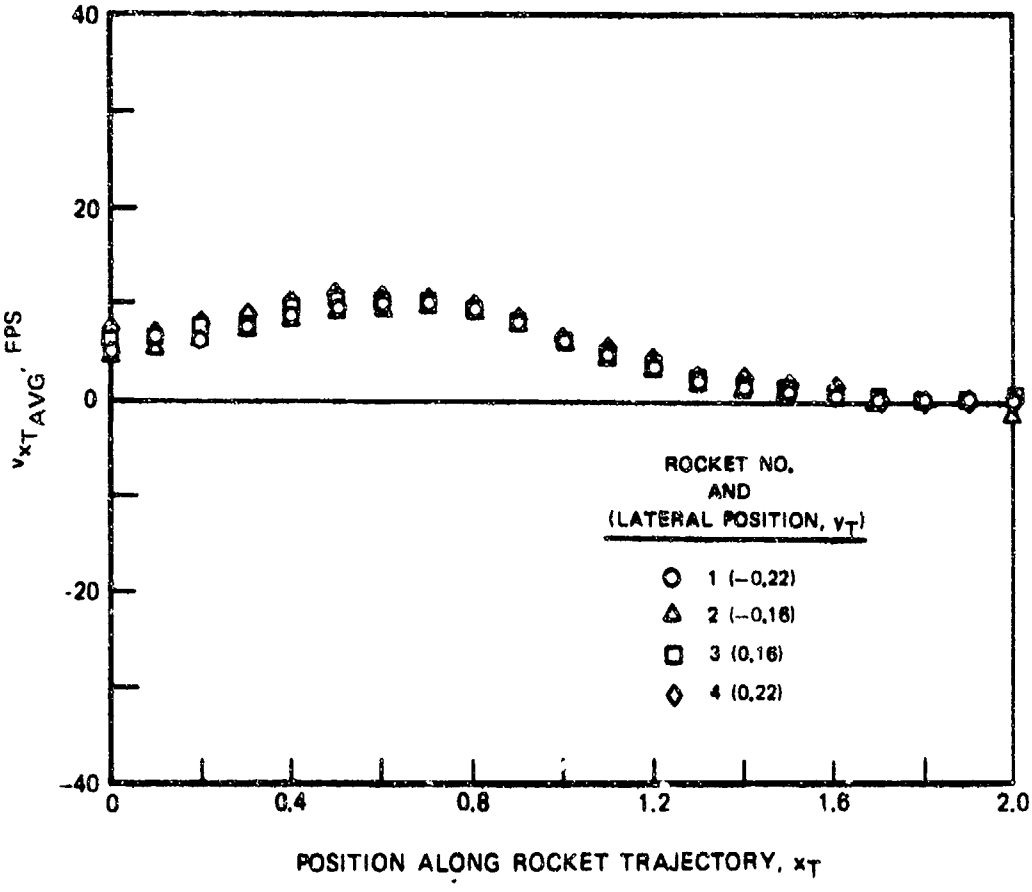

Figure 47. Variation of Time-Averaged v_{x_T} Velocity Component Along the Four Rocket Trajectories -- 30 Kt, Distorted Wake.

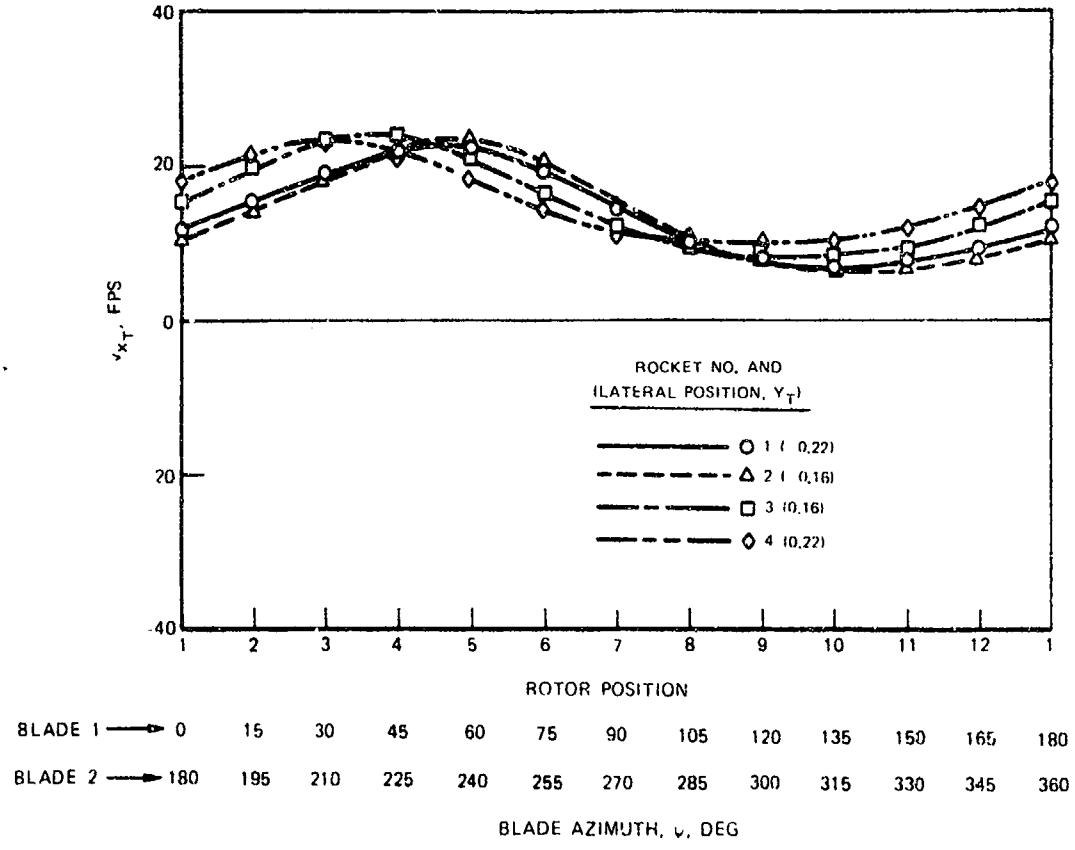

Figure 48. Variation of Instantaneous v_{x_T} Velocity Component With Rotor Position for the Four Rocket Launch Points (x_T = 0) -- 30 Kt, Distorted Wake.

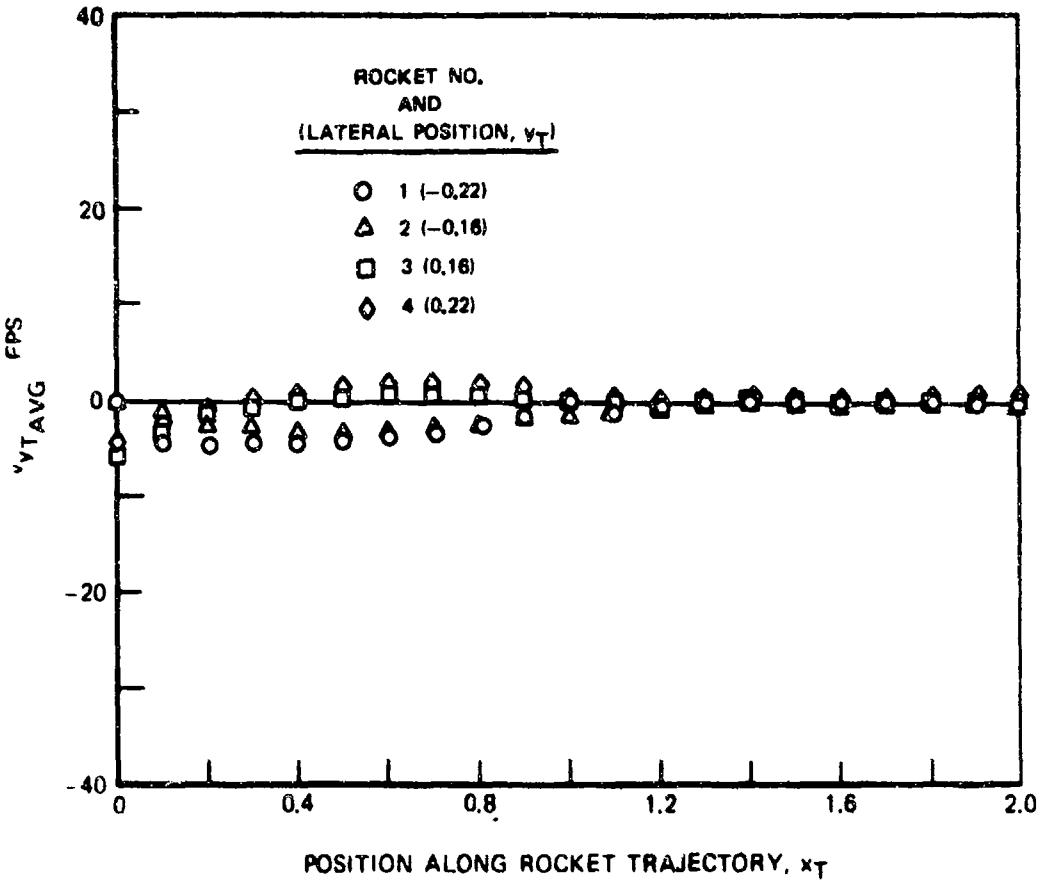

Figure 49. Variation of Time-Averaged v_{y_T} Velocity Component Along the Four Rocket Trajectories -- 30 Kt, Distorted Wake.

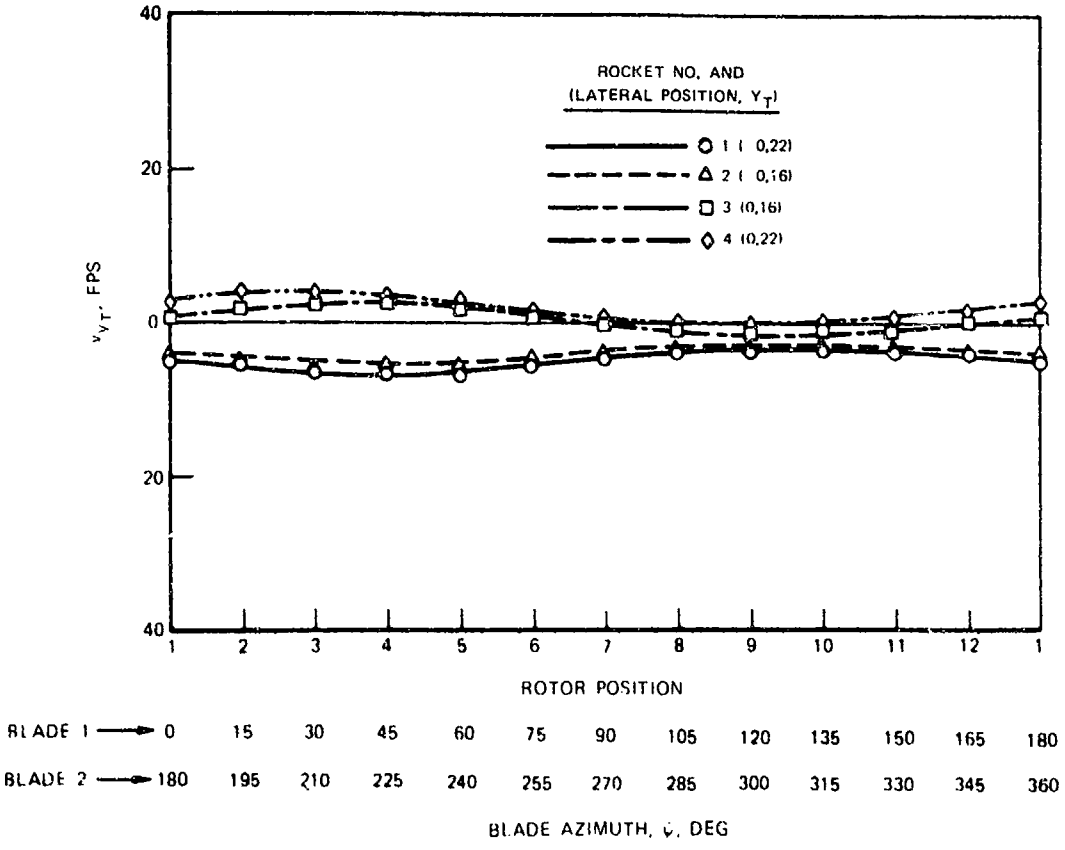

Figure 50. Variation of Instantaneous v_{yT} Velocity Component With Rotor Position for the Four Rocket Launch Points (x_T = 0) -- 30 Kt, Distorted Wake.

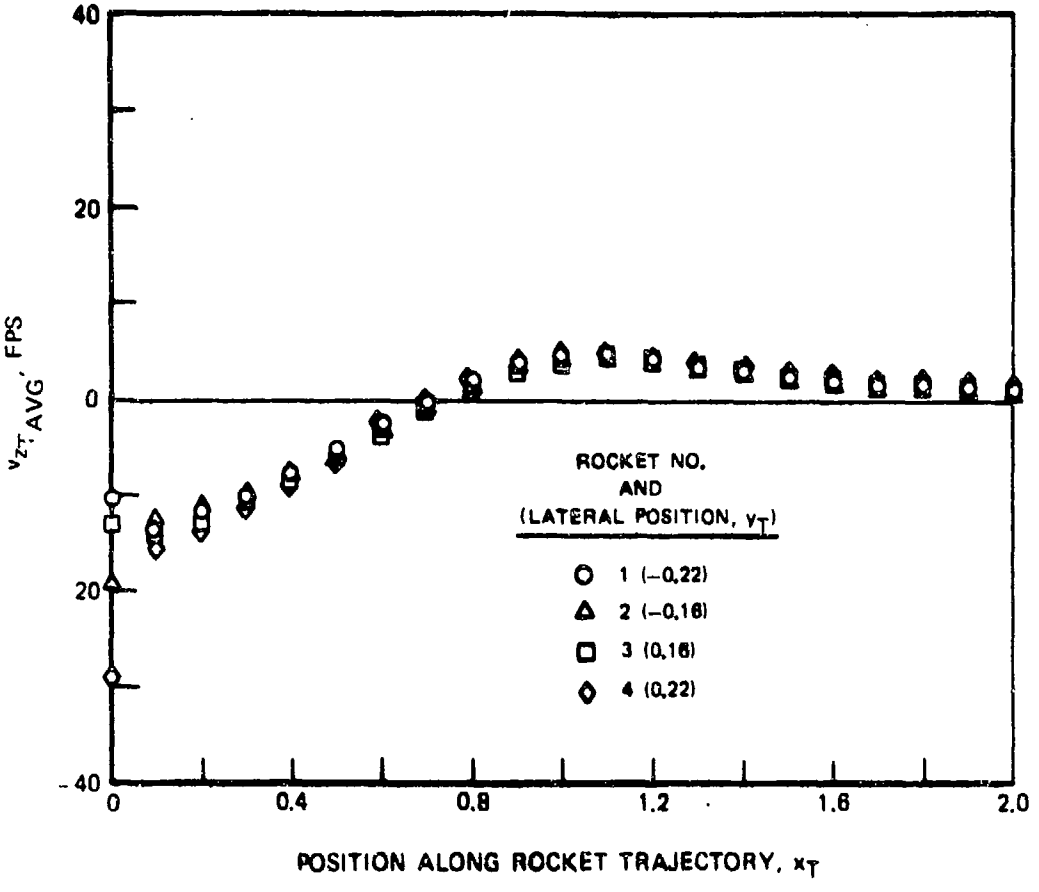

Figure 51. Variation of Time-Averaged v_{z_T} Velocity Component Along the Four Rocket Trajectories -- 30 Kt, Undistorted Wake.

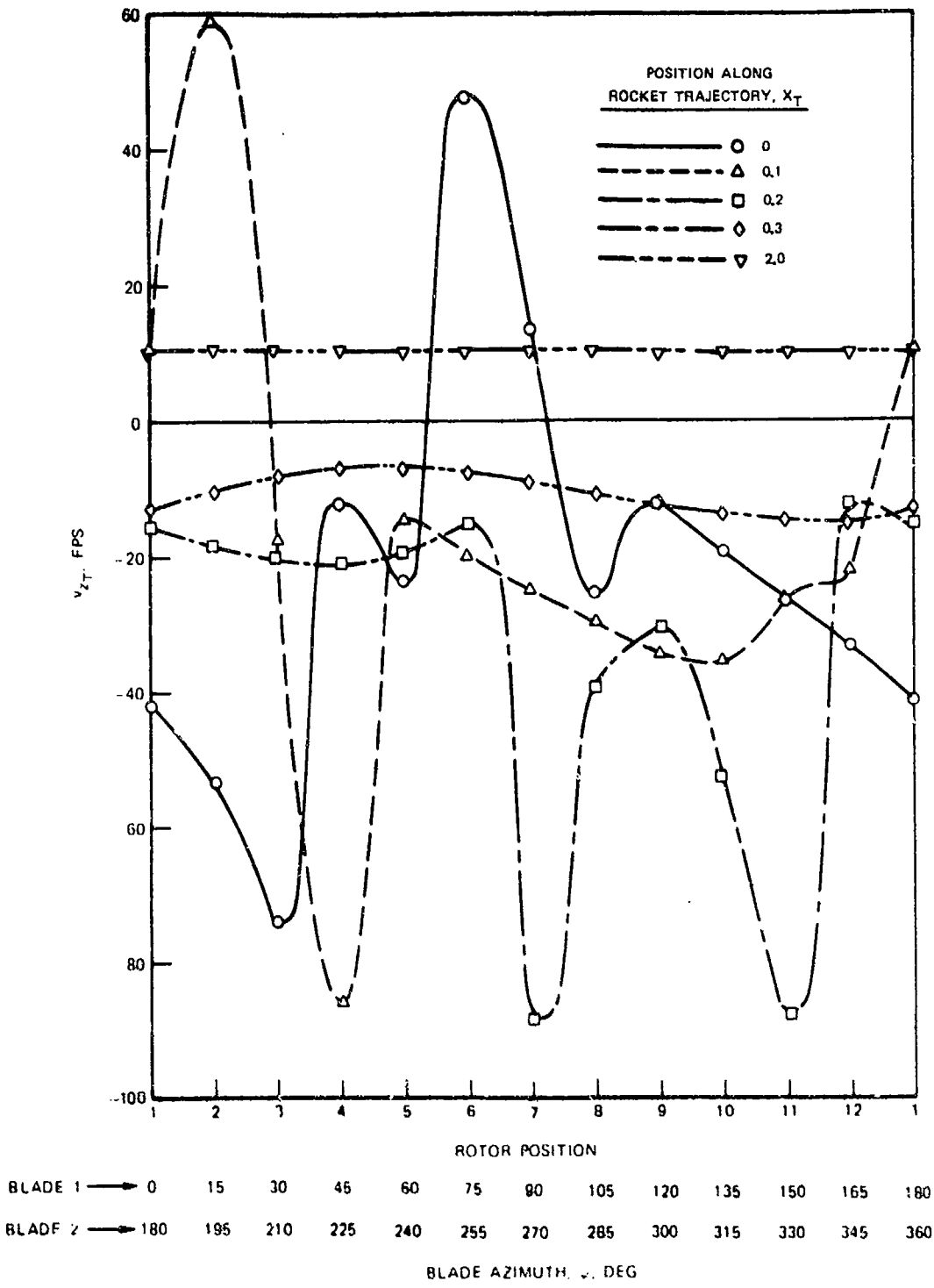

Figure 52. Variation of Instantaneous v_{Z_T} Velocity Component With Rotor Position for Selected Points on One Rocket Trajectory -- 30 Kt, Undistorted Wake, Rocket No. 4 (y_T = 0.22).

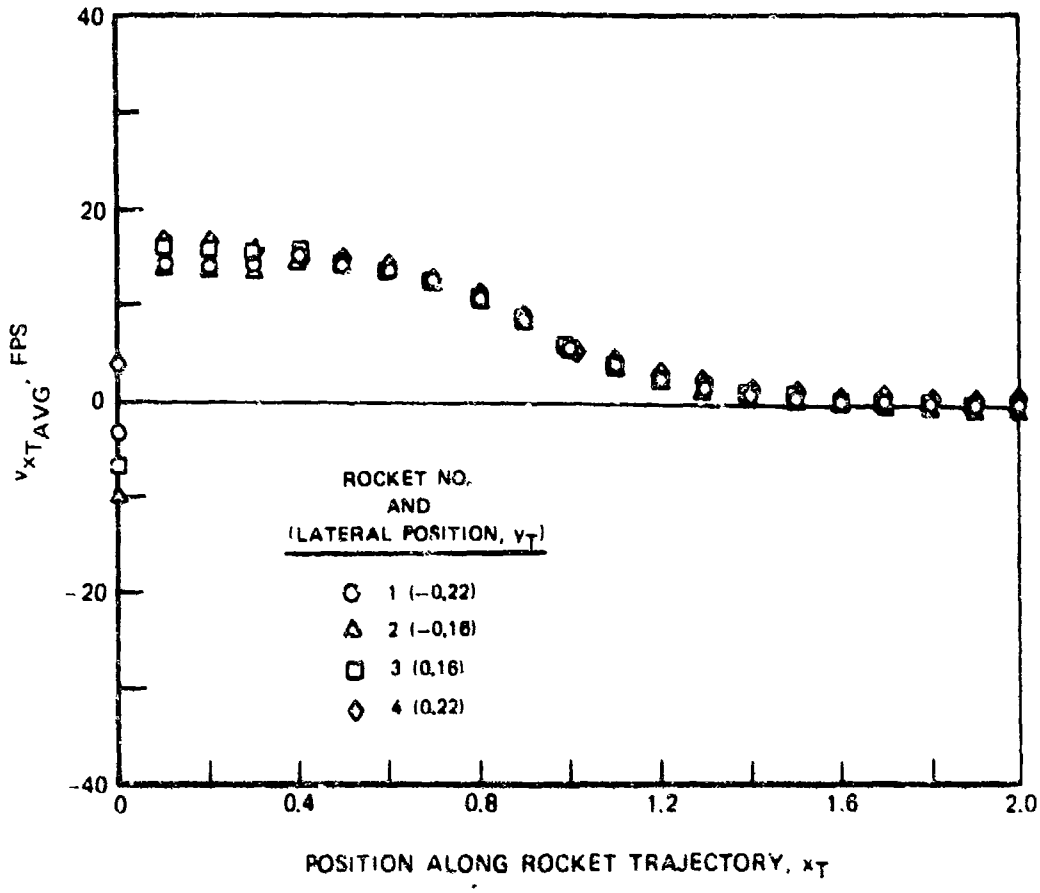

Figure 53. Variation of Time-Averaged v_{XT} Velocity Component Along the Four Rocket Trajectories -- 30 Kt, Undistorted Wake.

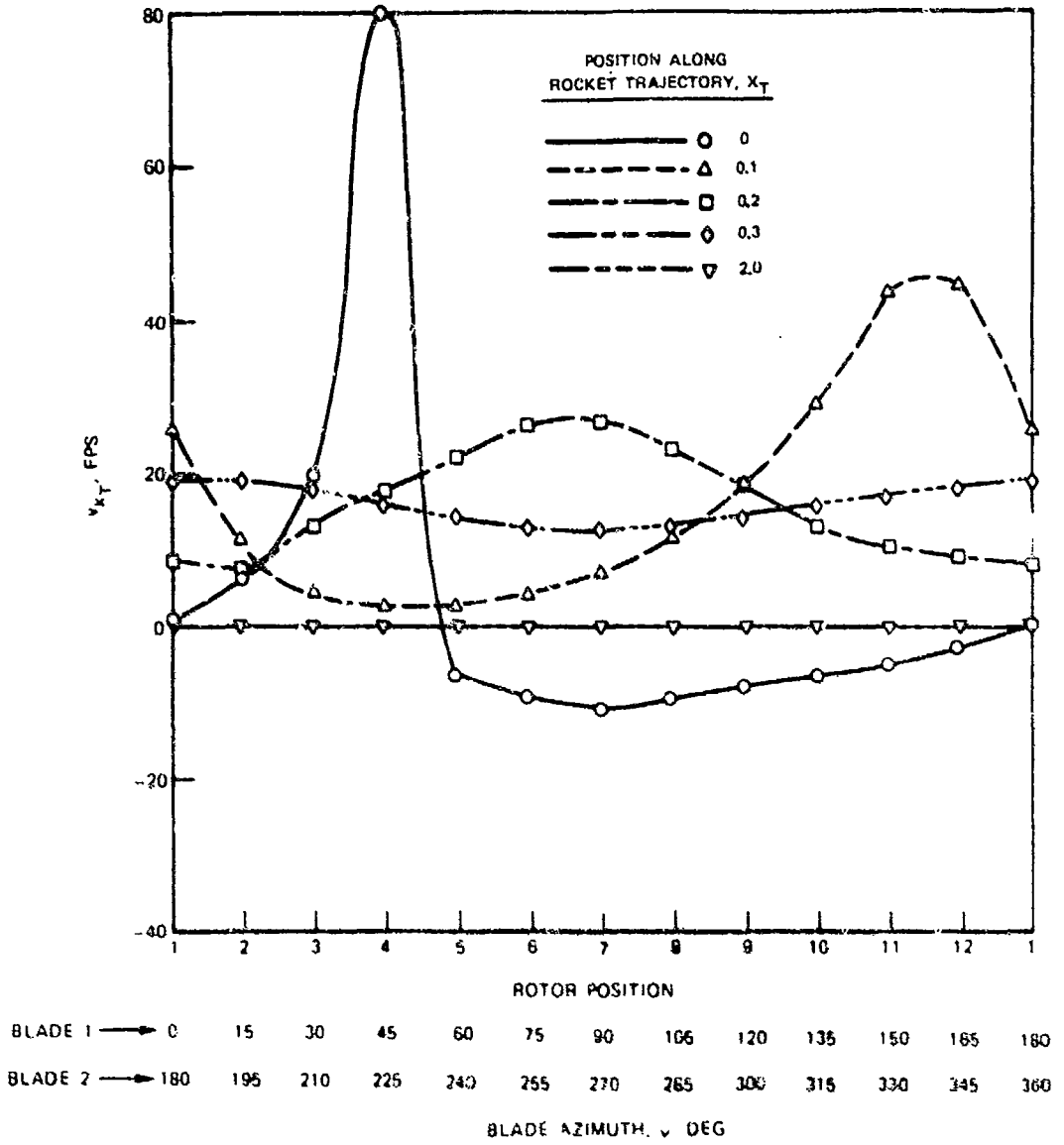

Figure 54. Variation of Instantaneous v_{X_T} Velocity Component With Rotor Position for Selected Points on One Rocket Trajectory -- 30 Kt, Undistorted Wake, Rocket No. 4 (y_T = 0.22).

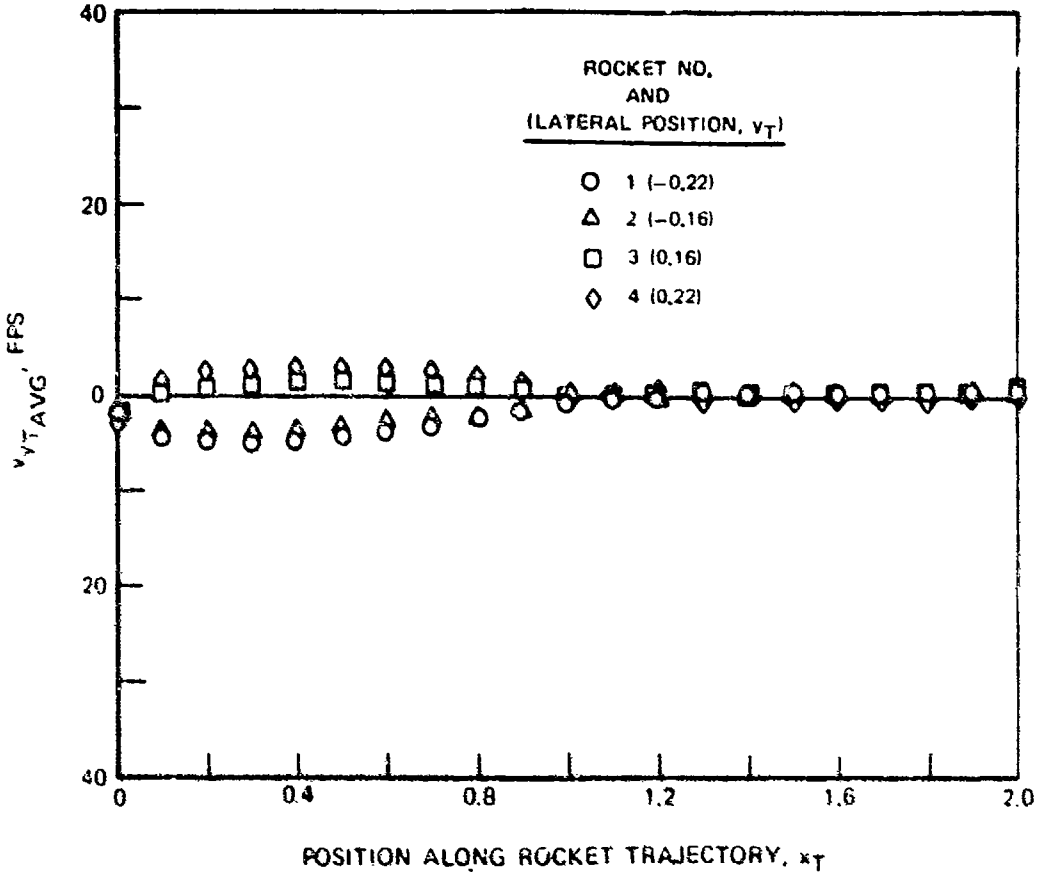

Figure 55. Variation of Time-Averaged v_{x_T} Velocity Component Along the Four Rocket Trajectories -- 30 Kt, Undistorted Wake.

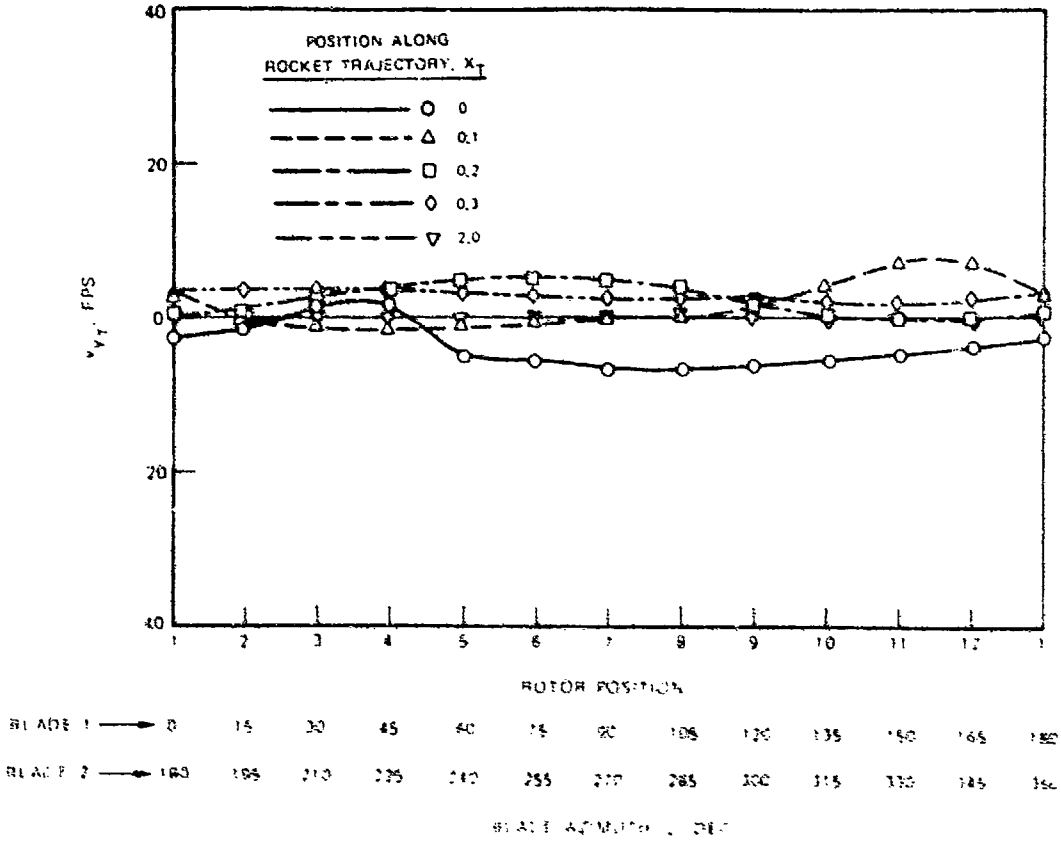

Figure 50. Variation of Instantaneous v_{y_T} Velocity Component With Rotor Position for Selected Points on One Rocket Trajectory -- 30 Kt, Undistorted Wake, Rocket No. 4 ($y_T = 0.22$).

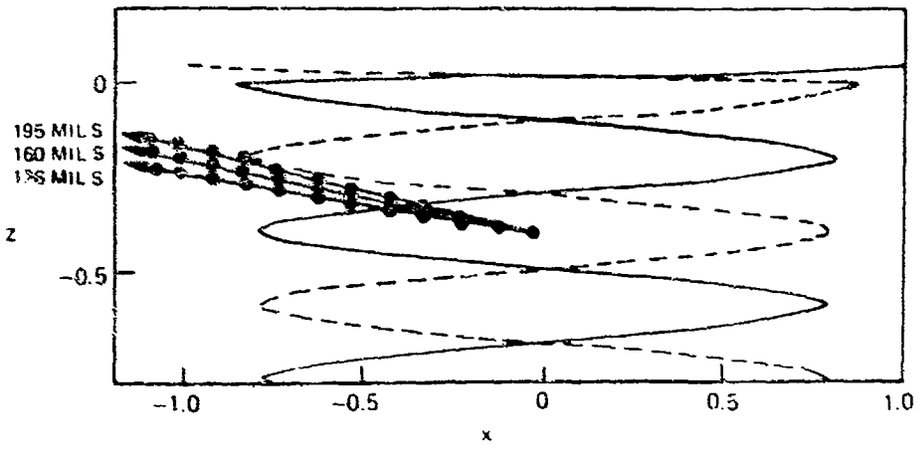

(a) VARIATIONS OF ROCKET LAUNCH ATTITUDE - -
0 KT, DISTORTED WAKE

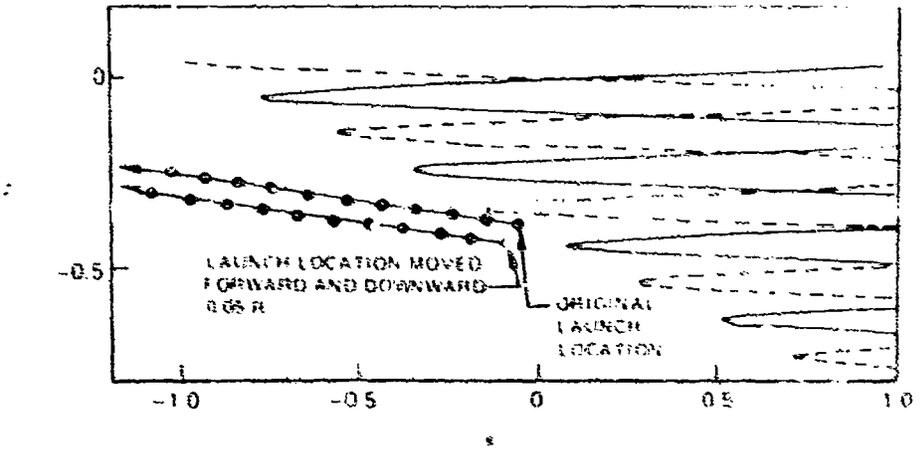

(b) VARIATION OF ROCKET LAUNCH POSITION
30 KT, UNDISTORTED WAKE

Figure 17. Variations of Rocket Launch Attitude and Position.

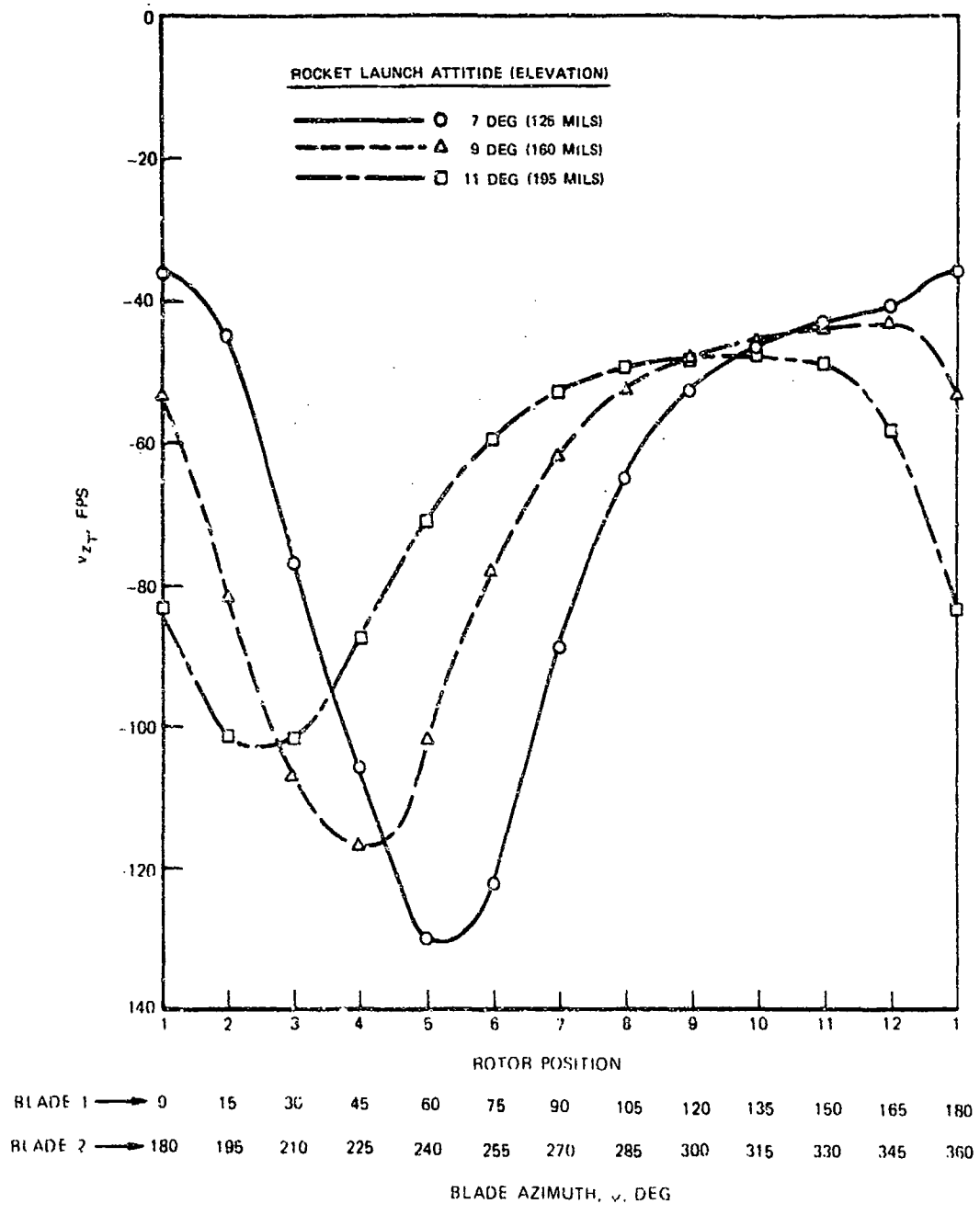

Figure 58. Effect of Variation of Rocket Launch Attitude on Instantaneous v_{z_T} Velocity Component Near the Wake Boundary -- 0 Kt, Distorted Wake, Rocket No. 4 ($x_T = 0.7$).

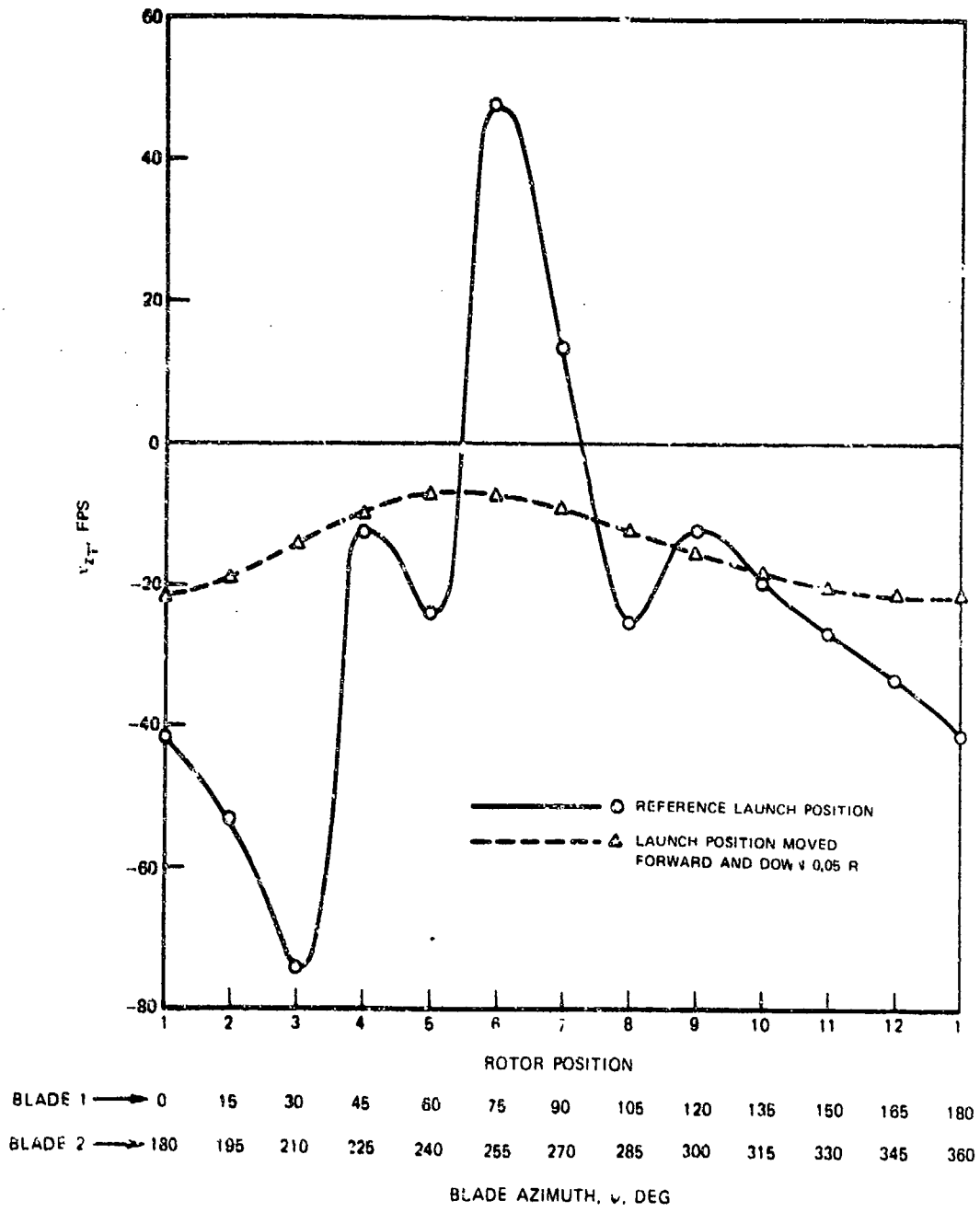

Figure 59. Effect of Variation of Rocket Launch Position on Instantaneous v_{zT} Velocity Component Near the Wake Boundary -- 30 Kt, Undistorted Wake, Rocket No. 4, (x_T = 0).

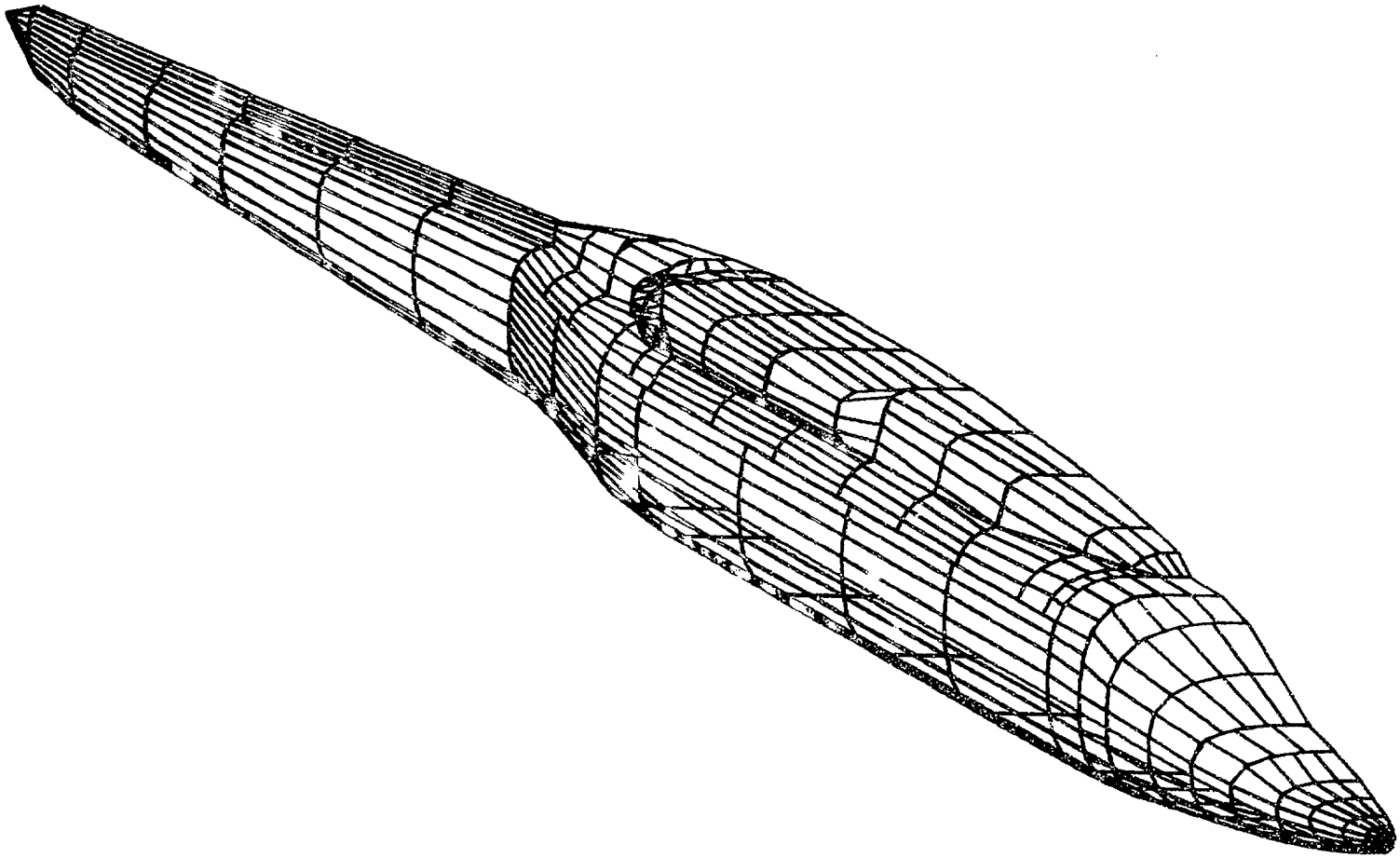

Figure 60. Isometric View of Fuselage Modelled by Computerized Geometry Method.

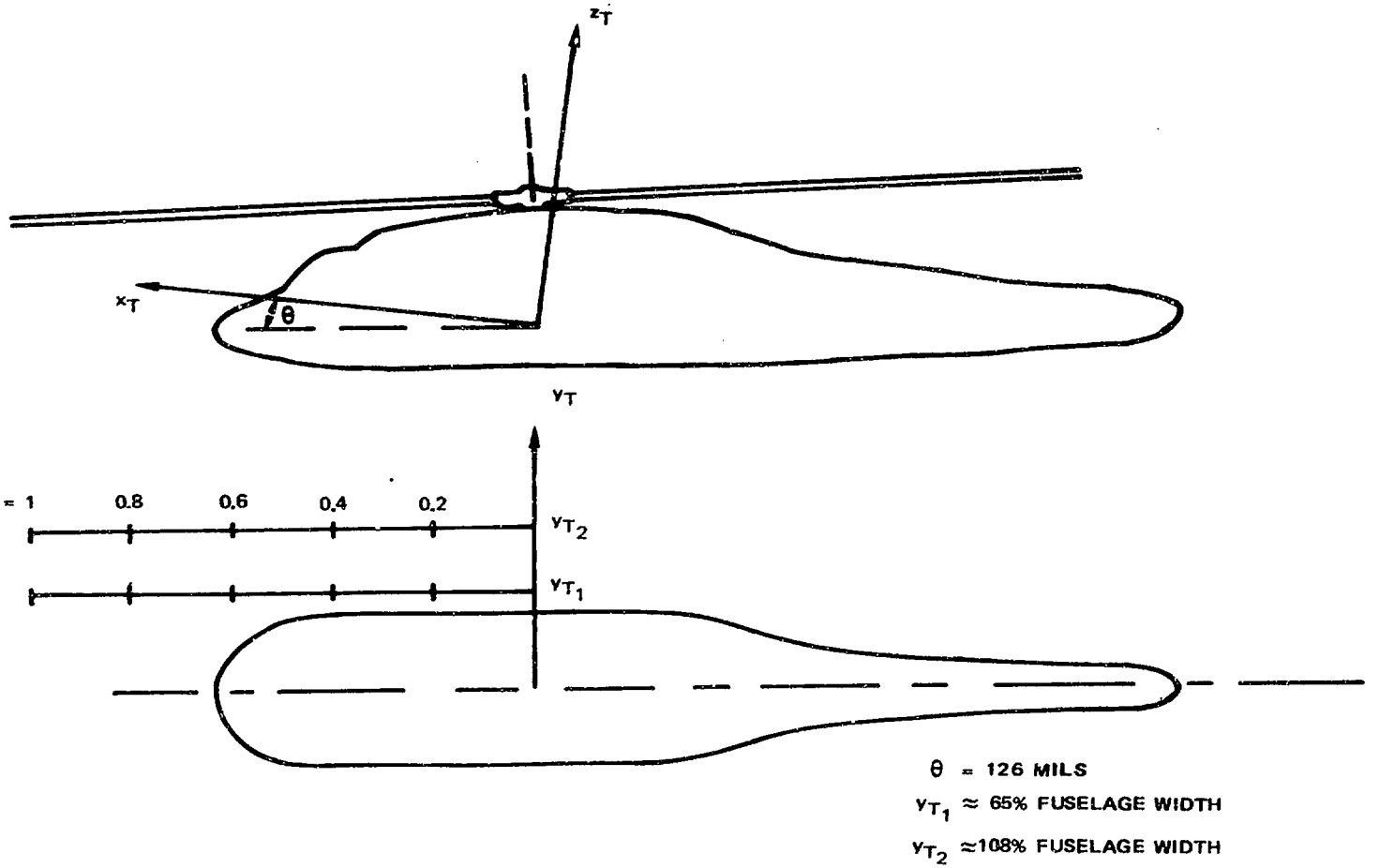

Figure 61. Schematic of Configuration Used to Calculate Fuselage Induced Effects on Rocket Trajectories.

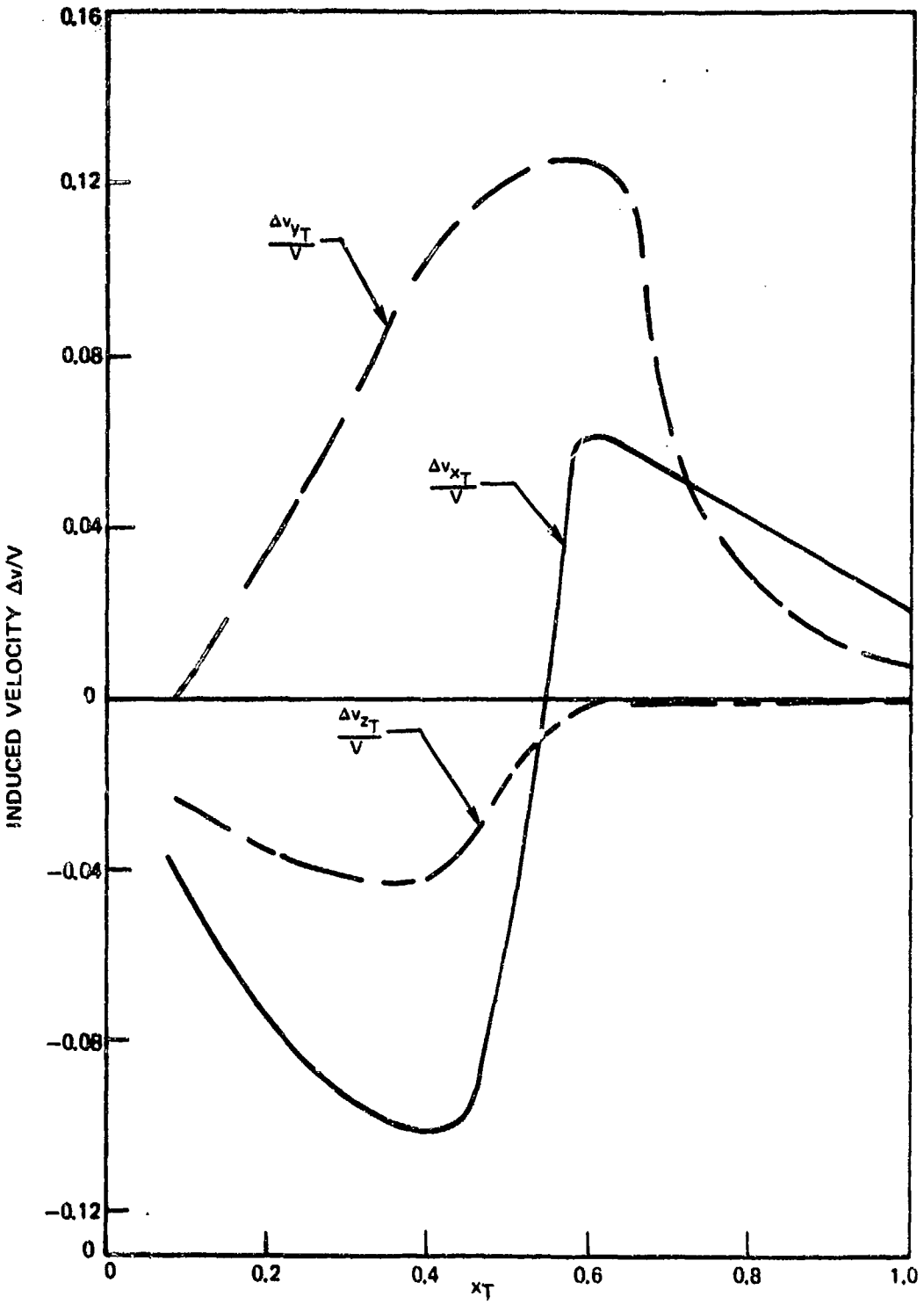

Figure 62. Fuselage Induced Velocities Along Rocket Trajectories -- $\bar{y}_T$ = 65% Fuselage Width.

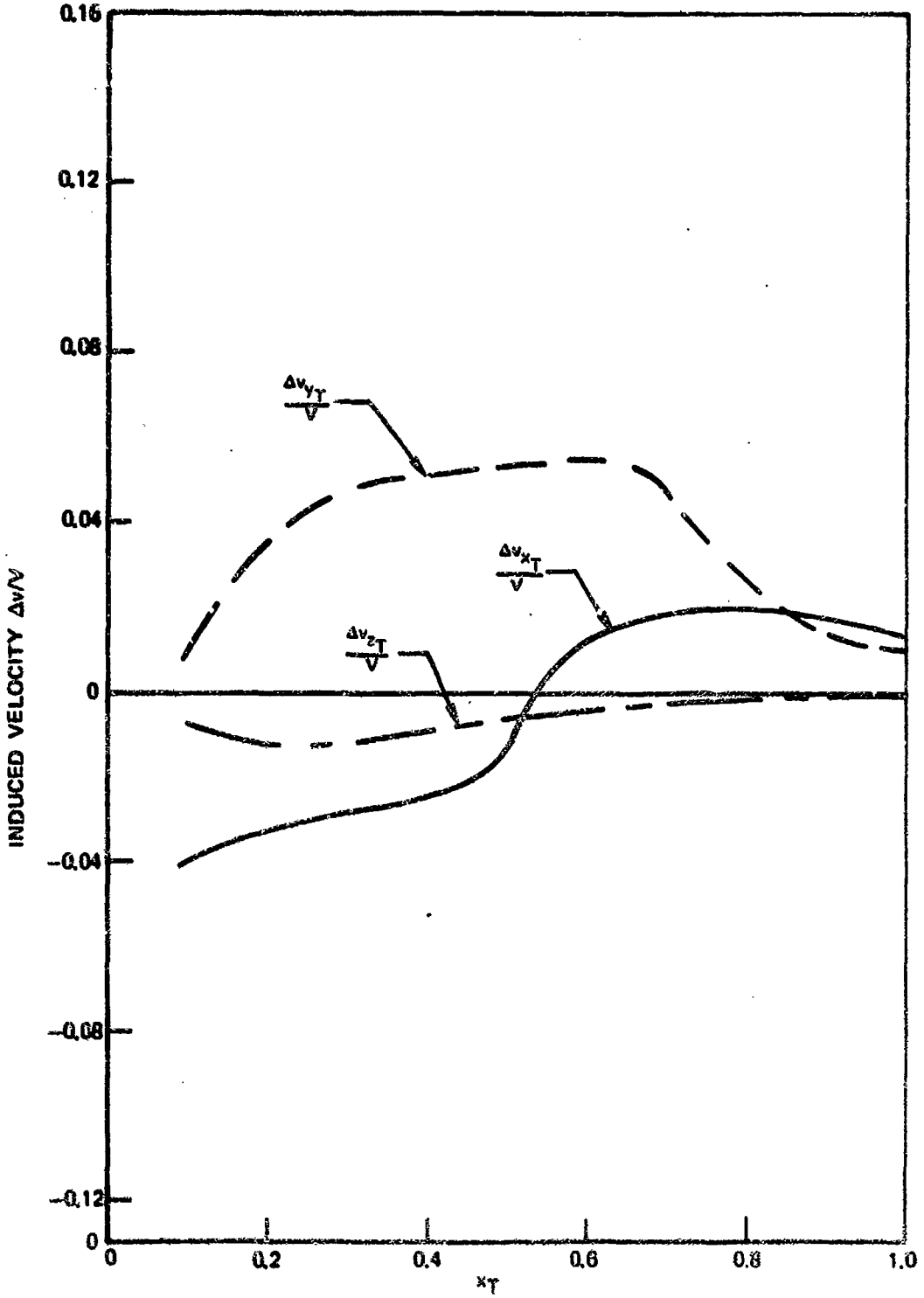

Figure 63. Fuselage Induced Velocities Along Rocket Trajectories -- $\bar{y}_T$ = 108% Fuselage Width.